

Simultaneous Survey of Water and Class I Methanol Masers toward Red MSX Sources

Chang-Hee Kim^{1,2}, Kee-Tae Kim¹, and Yong-Sun Park²

ABSTRACT

We report simultaneous single-dish surveys of 22 GHz H₂O and 44 and 95 GHz class I CH₃OH masers toward 299 Red MSX Sources in the protostellar stage. The detection rates are 45% at 22 GHz, 28% at 44 GHz, and 23% at 95 GHz. There are 15, 53, and 51 new discoveries at 22, 44, and 95 GHz, respectively. We detect high-velocity ($>30 \text{ km s}^{-1}$) features in 27 H₂O maser sources. The 95 GHz maser emission is detected only in 44 GHz maser sources. The two transitions show strong correlations in the peak velocity, peak flux density, and isotropic maser luminosity, indicating that they are likely generated in the same sites by the same mechanisms. The 44 GHz masers have much narrower distributions than 22 GHz masers in the relative peak velocity and velocity range, while 6.7 GHz class II CH₃OH masers have distributions intermediate between the two. The maser luminosity significantly correlates with the parental clump mass, while it correlates well with the bolometric luminosity of the central protostar only when data of the low-mass regime from the literature are added. Comparison with the results of previous maser surveys toward massive star-forming regions suggests that the detection rates of 22 and 44 GHz masers tend to increase as the central objects evolve. This is contrary to the trends found in low- and intermediate-mass star-forming regions. Thus the occurrence of both masers might depend on the surrounding environments as well as on the evolution of the central object.

Subject headings: infrared: ISM — ISM: molecules — masers: ISM — stars: formation

1. Introduction

Interstellar masers of H₂O, CH₃OH, and OH are considered excellent probes of high-mass star formation regions (SFRs). Because at radio frequencies, these masers are quite common, intense, and rarely affected by dust extinction in massive SFRs, they allow us to investigate such regions. The different maser species favor different physical conditions for their production and survival, which has led to the proposition of tracing different evolutionary phases of massive star

¹Korea Astronomy and Space Science Institute, Yuseong-gu, Daejeon 34055, Korea: ktkim@kasi.re.kr

²Department of Physics and Astronomy, Seoul National University, Gwanak-gu, Seoul 08826, Korea: chkim@astro.snu.ac.kr

formation (e.g., Ellingsen et al. 2007; Breen et al. 2010a; Fontani et al. 2010). Since many sources of massive SFRs show emission from multiple maser species or transitions, there must be significant overlap for the evolutionary stage that is traced by the most common types of masers (Breen et al. 2010a). H₂O masers are known to occur in both low- and high-mass SFRs (e.g., Furuya et al. 2003; Szymczak et al. 2005) and are thus an important signpost of ongoing star formation. The evolutionary stage associated with 22 GHz H₂O maser emission has been investigated through extensive single-dish and interferometric observations (e.g., Torrelles et al. 1997; Urquhart et al. 2011), which have indicated that this type of maser is closely associated with high-mass young stellar objects (YSOs) in various evolutionary stages. Although it has been claimed in a few cases that H₂O masers could trace circumstellar disks around (proto)stellar objects (e.g., Torrelles et al. 1997; Seth et al. 2002), connected-array and VLBI observations toward high-mass YSOs have shown that H₂O masers are predominantly associated with jets and outflows (e.g., Torrelles et al. 2001; Codella et al. 2004).

Methanol masers are commonly observed in massive SFRs. They have been empirically classified into two categories: class I and class II. The initial classification was based on the sources toward which the different transitions were detected (Batra et al. 1988; Menten et al. 1991). Class I CH₃OH masers (e.g., the 7₀–6₁ A⁺ and 8₀–7₁ A⁺ at 44 and 95 GHz, respectively) are often observed significantly offset from high-mass YSOs (e.g., Kurtz et al. 2004; Voronkov et al. 2006; Cyganowski et al. 2009). In contrast, class II CH₃OH masers (e.g., the 5₁–6₀ A⁺ and 2₀–3₁ E at 6.7 and 12.2 GHz, respectively) are usually very close to high-mass YSOs (e.g., Cyganowski et al. 2009; Fujisawa et al. 2014). These observational findings were supported by early theoretical models of CH₃OH masers, which suggest that the class I masers are pumped by collisions with molecular hydrogen, while the class II masers are pumped by external far infrared radiation (Cragg et al. 1992). Compared to class II masers, class I CH₃OH masers are relatively poorly studied and understood. There have only been several large surveys of class I masers (mainly at 44 and 95 GHz), primarily undertaken with single-dish telescopes (e.g., Haschick et al. 1990; Bachiller et al. 1990; Slysh et al. 1994; Val’tts et al. 2000; Ellingsen et al. 2005; Chen et al. 2011, 2012, 2013; Gan et al. 2013; Kang et al. 2015, 2016) along with interferometric searches (e.g., Kurtz et al. 2004; Cyganowski et al. 2009; Voronkov et al. 2014; Matsumoto et al. 2014; Jordan et al. 2015; Gómez-Ruiz et al. 2016; Rodríguez-Garza et al. 2017). The catalog from these surveys currently comprises of about 500 class I CH₃OH maser sources (e.g., Bayandina et al. 2012).

Ellingsen et al. (2007) suggested that the common maser species (H₂O, class I and II CH₃OH, and OH masers) may help identify the evolutionary phase of the central objects, and proposed a possible evolutionary sequence of these maser species. This proposed sequence has been improved upon by Breen et al. (2010b) (in their Figure 6). However, there remains significant uncertainty about where in SFRs the different maser species arise and which evolutionary phase they are associated with.

In this study, we performed simultaneous 22 GHz H₂O and 44 and 95 GHz class I CH₃OH maser surveys toward high-mass protostellar objects (HMPOs) using single-dish telescopes. Our

aim is to find new maser sources and to investigate the relationship between the different maser species and between the maser activity and the properties of the central objects and the natal clumps. In Section 2 we describe the source selection and the observations. In Section 3 we present the results of the survey. A discussion of the analyses is given in Section 4, followed by a summary in Section 5.

2. Source Selection and Observations

2.1. Source Selection

Lumsden et al. (2002) identified about 2000 candidates for young massive stars with $21\ \mu\text{m}$ flux densities of $>2.5\ \text{Jy}$ and infrared colors consistent with known massive YSOs, using the color-color plots of the Midcourse Space Experiment (MSX) and Two Micron All Sky Survey (2MASS) data (see also Lumsden et al. 2013). They carried out follow-up observations and incorporated the complementary data from other surveys to distinguish between HMPOs and ultracompact HII regions (UCHIIs) (e.g., Urquhart et al. 2014a). From this so-called Red MSX Source (RMS) catalog¹, we selected 299 HMPO candidates at the beginning of this study in 2011 with two criteria: bolometric luminosities of $> 10^3 L_{\odot}$ and declinations of $> -30^{\circ}$. These sources are very likely under active accretion and so have not yet developed detectable UCHIIs. As of 2018 February, however, the online catalog contains 353 HMPOs satisfying the criteria. Fifty eight sources have been added because they were re-classified as HMPOs with new data, while four sources were re-classified as UCHII regions and so now are excluded. Table 1 lists their information as extracted from the RMS catalog, including their RMS ID, MSX name, equatorial coordinates, source type, distance, bolometric luminosity, and systemic velocity. The 4 UCHIIs are marked by daggers in the table.

2.2. Observations

We surveyed the 299 RMS sources in three maser transitions: $\text{H}_2\text{O}\ 6_{16} - 5_{23}$ (22.235080 GHz, Lovas et al. 2004), $\text{CH}_3\text{OH}\ 7_0 - 6_1\ \text{A}^+$ (44.069430 GHz, Pickett et al. 1998), and $8_0 - 7_1\ \text{A}^+$ (95.169463 GHz, Müller et al. 2004). The observations were undertaken using the Korean VLBI Network (KVN) 21 m telescopes from 2011 April to 2014 May. The telescopes were equipped with multi-frequency receiving systems which made it possible to observe in the 22, 43, 86, and 129 GHz bands simultaneously (Han et al. 2008). The first-epoch observations were made only at 22 and 44 GHz in 2011 because the 86 and 129 GHz receivers were not then installed, while the second-epoch observations were conducted at 22, 44, and 95 GHz in 2012. Supplementary observations were performed toward 15 sources in 2013 April and May and 2015 May to confirm their detections. We observed dual polarization both at 22 and 44 GHz in the first epoch, and single polarization at

¹<http://rms.leeds.ac.uk/cgi-bin/public/RMS.DATABASE.cgi>.

22 and 44 GHz and dual polarization at 95 GHz in the second epoch. The backend was a digital spectrometer that provided 4096 channels and 64 MHz bandwidth for each stream. The velocity coverage and the spectral resolution for each transition are summarized in Table 2. The central velocity of each source was taken from the RMS catalog (see also Table 1)

The full widths at half maximum (FWHMs) of the telescopes were about 130'' at 22 GHz, 65'' at 44 GHz, and 32'' at 95 GHz. The telescope pointing and focus were checked every ~ 2 hr by observing strong SiO maser sources at 43 or 86 GHz. The pointing accuracy was better than 5''. Each spectrum was obtained in position-switching mode usually with an offset of +2 minutes in the right ascension. The total (ON+OFF) integration time was 30 minutes for each source, which yielded typical 1σ noise levels of about 0.6 Jy, 0.7 Jy, and 0.8 Jy at about 0.2 km s^{-1} resolution after smoothing for 22, 44, and 95 GHz, respectively. The data were calibrated with the standard chopper wheel method to provide the line intensity on the T_{A}^* scale, which were converted to flux density using the conversion factors in Table 2. The KVN telescopes are of shaped Cassegrain type and hence have quite high first-sidelobe levels of ~ 14 dB (4%) at ~ 1.5 times FWHM away from the pointing center (Kim et al. 2011; Lee et al. 2011). We thus mapped each detected source at the same frequency to investigate contamination from nearby bright maser sources. The mapping area was $1.5\text{ FWHM} \times 1.5\text{ FWHM}$ around a source with half-beam spacing at each frequency. The typical rms noise level was 5 Jy at 0.2 km s^{-1} . Seven and four sources turned out to be detected by the first sidelobe at 22 and 44 GHz, respectively (see Table 1). They were not counted as detected sources except RMS 3308 and 3555 for which maser emission was detected not only by the sidelobe but also by the main beam at different velocities.

We also surveyed 10 sources in our sample in the $^{13}\text{CO J=1-0}$ and $\text{HCO}^+ \text{ J=1-0}$ lines in 2013 June. The ^{13}CO line observations were conducted with the Taeduk Radio Astronomy Observatory (TRAO) 14 m telescope, while the HCO^+ line observations were made with the KVN telescope at the Tamna station. The observed sources were H_2O maser sources with maser features largely offset from the systemic velocities (see Section 3.3.1). These observations aimed to search for dense molecular cores associated with those features. The TRAO telescope was equipped with the 15-beam receiver, QUARRY (QUabbin ARRaY) (Erickson et al. 1992). The backends were autocorrelators, each of which had 427 channels and a bandwidth of 100 MHz. We utilized the position switching mode. Table 2 summarizes the observational details. All the spectral data were reduced and analyzed with the GILDAS/CLASS package.

3. Result

3.1. Detection Statistics

Our search toward the 299 RMS sources resulted in the detection of 151 (51%) sources at least in one of the three maser transitions. Table 1 presents the detection summary: detection (y), nondetection (n), and new detection (Y). All the detected maser lines were limited to signals

stronger than the 3σ rms noise levels, which were typically 1.8, 2.1, and 2.4 Jy for 22, 44, and 95 GHz, respectively. Table 3 lists the numbers of observed and detected sources and the corresponding detection rates for each transition and epoch (see also Figure 1). We detected 22, 44, and 95 GHz maser emission in 135 (45%), 83 (28%), and 68 (23%) sources, respectively. The detection rates (42% and 37%) of H₂O maser emission are a little different in the first and second epochs, although the difference is not statistically significant, while those (25% and 27%) of 44 GHz CH₃OH maser emission are practically the same. All detected maser spectra are shown in Figures 2–6: sources detected in all three masers in Figure 2; sources detected in 22 and 44 GHz masers in Figure 3; sources detected in 44 and 95 GHz masers in Figure 4; sources detected only in 22 GHz maser in Figure 5; sources detected only in 44 GHz maser in Figure 6.

There are several maser surveys of HMPO candidates with various sensitivities. Sridharan et al. (2002) detected 22 GHz H₂O maser emission toward 42 % of 69 HMPOs at a rms noise level of ~ 0.4 Jy. Urquhart et al. (2011) searched for H₂O maser emission toward 597 RMS sources with a detection rate of $\sim 52\%$ for 275 HMPOs. The survey had a mean rms noise level of ~ 0.12 Jy at a velocity resolution of ~ 0.33 km s⁻¹. If it had had sensitivity similar to ours, ~ 0.6 Jy, neglecting the difference in the velocity resolution, the detection rate would be 42%. Fontani et al. (2010) surveyed 88 HMPOs in the 44 GHz CH₃OH maser with a twice better sensitivity to ours, and obtained a detection rate of 31 %. Gan et al. (2013) detected 95 GHz maser emission in 22% (62) of 288 outflow sources. Val'tts et al. (2007) also found that 24 % of the outflow sources are associated with class I CH₃OH maser sources, including 36, 44, and 95 GHz masers, within 2'. Thus the detection rates of the three masers in this study seem to be comparable to those of the previous surveys. On the other hand, Chen et al. (2011) and Chen et al. (2013) detected 95 GHz maser emission toward 55% of 192 and 71% of 52 extended green objects (EGOs), respectively, at comparable detection limit (1.6 Jy) with ours. Because EGOs are known to trace shocked gas in high-mass protostellar outflows, which are closely associated with class I CH₃OH masers, the high detection rates may be due to selection effects.

One hundred seventy sources in our sample are distributed in the Methanol Multibeam (MMB) survey area of 6.7 GHz class II CH₃OH maser with the Parkes 64 m telescope (Green et al. 2010, 2012; Breen et al. 2015). Among them, 54 (32%), 51 (30%), and 45 (26%) sources are associated with 22, 44, and 95 GHz masers, respectively. We found that 38 of the 170 corresponds to 6.7 GHz maser sources. Here we used a matching radius of 2'', because the 6.7 GHz CH₃OH maser spots are spread typically within 2'' (Caswell 2009) and the astrometric accuracy of RMS sources is better than about 2'' (Lumsden et al. 2013). Of the 38 sources, 16 (42%), 14 (37%), and 11 (29%) are related to 22, 44, and 95 GHz masers, respectively. For comparison, Kang et al. (2015) searched 22, 44, and 95 GHz masers toward seventy seven 6.7 GHz maser sources at similar detection limits to this survey using the same telescopes, and achieved detection rates of 51%, 32%, and 25% for 22, 44, and 95 GHz masers, respectively. Szymczak et al. (2005) surveyed only H₂O maser emission toward seventy nine 6.7 GHz maser sources at a comparable detection limit of ~ 1.5 Jy with the Effelsberg 100 m (FWHM $\simeq 40''$). The detection rate was 52%. Titmarsh et al. (2014, 2016)

conducted interferometric observations (the synthesized beam size $\simeq 10''$) of H_2O maser emission toward 323 6.7 GHz maser sources found in the MMB survey with detection limits of ~ 0.2 Jy at 0.5 km s^{-1} resolution, and obtained a detection of 48%. Despite much higher sensitivity, this detection rate similar to those of the aforementioned single-dish surveys may be in part due to their much smaller matching radius of $3''$.

3.2. New Detections

We compared our results with the previous surveys of H_2O and class I CH_3OH masers to identify newly detected sources. In this comparison we used a search radius of a HWHM at each frequency. For 22 GHz H_2O masers, we examined the catalogs of Han et al. (1995), Han et al. (1998), Valdettaro et al. (2001), Sunada et al. (2007), Urquhart et al. (2009), Breen et al. (2011), Urquhart et al. (2011), and Titmarsh et al. (2014). In particular, Urquhart et al. (2011) observed ~ 600 RMS sources using the Green Bank Telescope (GBT) in 2009 and 2010 and detected 308 sources ($\sim 50\%$). Their sample contains 257 sources in common with our sample, 145 (56%) of which were detected. There are 110 common detections with this survey. Fifteen and thirty five sources were detected only in this survey and Urquhart et al. (2011), respectively (see Table 1). We identified 15, 53, and 51 new maser sources at 22, 44, and 95 GHz, respectively. All of the new 22 GHz maser sources have been observed but not detected by Urquhart et al. (2009) (2) and Urquhart et al. (2011) (13) with better sensitivities of 0.1 and 0.25 Jy (1σ), respectively. Thus these non-detections were very likely to be due to significant variability in flux density. Two of the new 95 GHz maser sources have previously been searched for emission in this transition. RMS 2996 was observed by Ellingsen et al. (2005) at a detection limit of 4.2 Jy (3σ) using the Mopra 22 m. Considering the measured peak flux density of 7.9 Jy, their non-detection could be caused by flux variability. RMS 3314 was observed by Chen et al. (2011) at a detection limit of 1.7 Jy (3σ) using the same telescope, which has a FWHM of $36''$. The observed position was about $40''$ away from RMS 3314. Since the measured flux density is 3.4 Jy, their non-detection might be due to the large positional offset.

3.3. Maser Properties

We determined the line parameters of the observed maser spectra, including the peak velocity, the peak flux density, the integrated flux density, and the minimum and maximum values of the velocity range over which the maser lines are distributed. Table 4 summarizes the measurements. Table 5 presents the mean, median, minimum, and maximum values of the peak flux density (S_p), the relative peak velocity with respect to the systemic velocity (V_{rel}), and the velocity range (V_{range}) of 22, 44, and 95 GHz masers for the detected sources. The mean and median values of 44 and 95 GHz CH_3OH masers are very similar for all the three parameters, while they are much lower than those of the 22 GHz H_2O masers (see also Figure 7).

The isotropic luminosity of maser emission can be estimated from the integrated flux density using the following equations:

$$L_{22} = 2.30 \times 10^{-8} L_{\odot} \left(\frac{\int S_{22} dv}{\text{Jy km s}^{-1}} \right) \left(\frac{D}{\text{kpc}} \right)^2, \quad (1)$$

$$L_{44} = 4.60 \times 10^{-8} L_{\odot} \left(\frac{\int S_{44} dv}{\text{Jy km s}^{-1}} \right) \left(\frac{D}{\text{kpc}} \right)^2, \quad (2)$$

$$L_{95} = 9.92 \times 10^{-8} L_{\odot} \left(\frac{\int S_{95} dv}{\text{Jy km s}^{-1}} \right) \left(\frac{D}{\text{kpc}} \right)^2. \quad (3)$$

$$L_{6.7} = 6.95 \times 10^{-9} L_{\odot} \left(\frac{\int S_{6.7} dv}{\text{Jy km s}^{-1}} \right) \left(\frac{D}{\text{kpc}} \right)^2, \quad (4)$$

where D is the distance to the source. We adopted the distances from Urquhart et al. (2014a), who gathered well-determined distances from the literature or derived kinematic distances using available molecular and HI line data for the individual sources. The integrated flux densities given by Breen et al. (2015) were used for 6.7 GHz CH₃OH masers. The derived isotropic maser luminosities are listed in the 11th column of Table 4.

3.3.1. H₂O maser

We detected 22 GHz H₂O maser emission toward 135 sources in our sample: 126 in the first epoch and 112 in the second epoch. The median of the peak flux densities is 15.5 Jy with the minimum and maximum values of 0.8 and 4552 Jy, respectively. The vast majority (78%) of the detected sources have velocity ranges smaller than 20 km s⁻¹. RMS 3555 exhibits the largest velocity range, 230 km s⁻¹. Twenty seven sources (19%) have one or more high-velocity features, which are defined to be offset from the systemic velocity by more than 30 km s⁻¹ as in Breen et al. (2010a). These high-velocity sources fall into three categories: eighteen with only blueshifted features, three with both blue- and redshifted ones, and six with only redshifted ones. For comparison, Breen et al. (2010a) detected high-velocity features toward 33% (77) of 223 detected H₂O maser sources in their sample. This higher detection rate might be due to their sensitivity, which is nearly six times better than ours. The median value of V_{rel} is slightly blueshifted, -0.9 km s⁻¹, for all the 135 sources.

Caswell & Phillips (2008) reported four so-called dominant blueshifted H₂O maser sources, which show blueshifted high-velocity maser features with no or very weak features around the systemic velocities, and suggested that the features can be generated by pole-on jets. We found 9 blue and 2 red dominant H₂O maser source candidates. To examine whether the dominant blueshifted maser feature candidates are associated with other YSOs in the same lines of sight, we

observed 10 of them in the ^{13}CO J=1–0 line and found that 3 of them have weak ^{13}CO lines around the candidate features. For the remaining one (RMS 3936), no ^{13}CO J=2–1 line emission near the candidate feature was confirmed using the JCMT archive. We observed the 3 candidates in the HCO^+ J=1–0 line, which is known to be a good tracer of massive star-forming cores (Purcell et al. 2006), and detected the line emission toward 2 of them (RMS 2716, 3360). Thus these two appear to originate from YSOs other than the target source which happen to lie along a nearby line of sight, although we cannot exclude the possibility that they are related to high-velocity outflows from targets. The remaining 9 are very likely to be dominant shifted H_2O maser sources. Table 6 summarizes the survey results and Figure 8 shows the detected molecular spectra together with the 22 and 44 GHz maser spectra. Urquhart et al. (2011) also observed 8 of the 9 candidates and detected H_2O maser emission in 7 sources. However, only two (RMS 2547, 2584) of them showed dominant blueshifted features with similar velocity offsets. The others (RMS 3158, 3587, 3766, 3911, 3936) showed maser emission only around the systemic velocities except RMS 3911, which showed high-velocity features, as well. Most of these sources are discussed in more detail in Section 3.4.

3.3.2. Class I CH_3OH maser

We detected 44 and 95 GHz class I CH_3OH maser emission toward 83 and 68 sources, respectively, in the two epochs. It should be noted that 95 GHz maser emission was detected only in 44 GHz maser sources (Figure. 1). The peak flux densities range from 1.1 to 253 Jy at 44 GHz and between 1.1 and 147 Jy at 95 GHz. The peak velocities are always very close to the systemic velocities within $\pm 5 \text{ km s}^{-1}$ (Figure 9). The medians of the relative peak velocities are between -0.1 and 0.1 km s^{-1} for both masers (Table 5). The measured velocity ranges limited by 3σ noise levels are $0.2\text{--}15.5 \text{ km s}^{-1}$ at 44 GHz and $0.2\text{--}13.4 \text{ km s}^{-1}$ at 95 GHz. The median values are 2.3 and 2.4 km s^{-1} for 44 and 95 GHz masers, respectively. With the same criterion (FWHM = 1 km s^{-1}) as in Ellingsen et al. (2005), we found by Gaussian fitting to the spectrum that the broad emission features appear in 48% and 56% of detected 44 and 95 GHz maser sources. Such features have been reported by previous surveys of class I CH_3OH masers (e.g., Ellingsen et al. 2005; Chen et al. 2011). They might include quasi-thermal emission, which means maser emission that is blended with the thermal component.

Figure 9 compares 44 GHz transition with 95 GHz transition in the relative peak velocity, the peak flux density, and the isotropic maser luminosity. There appear to be strong correlations between the two transitions. The least-squares fitting results are as follows:

$$V_{\text{rel},95} = (0.98 \pm 0.05) (V_{\text{rel},44}) - (0.01 \pm 0.10) \quad (\rho = 0.73), \quad (5)$$

$$\log(S_{\text{p},95}) = (0.98 \pm 0.06) \log(S_{\text{p},44}) - (0.12 \pm 0.07) \quad (\rho = 0.91), \quad (6)$$

$$\log(L_{95}) = (0.96 \pm 0.05) \log(L_{44}) - (0.09 \pm 0.26) \quad (\rho = 0.90). \quad (7)$$

Four sources (RMS 2445, 3963, 3982, and 3998) show differences of $>1 \text{ km s}^{-1}$ between $V_{\text{rel},44}$ and $V_{\text{rel},95}$. They all have two or more velocity components and/or broad emission features. Thus the peak velocity measurements could be affected by the combination of the positional offsets from the pointing center and the different beam sizes at 44 and 95 GHz. If the four are excluded, the correlation between $V_{\text{rel},44}$ and $V_{\text{rel},95}$ becomes stronger with a correlation coefficient of 0.96. Val'tts et al. (2000) and Jordan et al. (2015) estimated the peak flux density ratio of 44 and 95 GHz transitions ($S_{\text{p},95}/S_{\text{p},44}$) to be 0.31–0.32, while Kang et al. (2015) recently derived the ratio to be about 0.71 ± 0.08 . Our result of best fit in linear scale plot is $S_{\text{p},95} = (0.56 \pm 0.08) \times S_{\text{p},44} + (2.16 \pm 0.91)$ ($\rho = 0.89$) (Figure 10), and this is consistent with the estimate of Kang et al. (2015). It is worth noting that the former two studies established datasets using different telescopes in epochs separated by several years while this study and Kang et al. (2015) utilized the datasets simultaneously taken from the same telescopes at the same velocity resolution. We also found a strong correlation between L_{44} and L_{95} . However, there is no correlation in the isotropic maser luminosity between 44 GHz masers and 22 GHz H_2O or 6.7 GHz class II CH_3OH masers.

We compared the first-epoch spectrum with the second-epoch one for each of seventy four 44 GHz CH_3OH maser sources that were detected in both epochs. Using a simple equation of $S_{\text{p},2\text{nd}}/S_{\text{p},1\text{st}}$, variability in the peak flux density was quantitatively examined for each source. The values range between 0.35 and 2.1 with a mean of 0.92 ± 0.28 . We also compared the peak velocities of the first- and second-epoch spectra and found the differences range from -0.85 to 0.64 km s^{-1} with a mean of $0.03 \pm 0.18 \text{ km s}^{-1}$. There is a trend that weaker sources are more variable in the peak flux density. If we focus on bright sources, i.e., 30 sources with signal-to-noise ratios >10 , the variations significantly decrease both in the peak flux and velocity: 0.53 to 1.24 with a mean of 0.91 ± 0.17 and -0.02 to 0.42 km s^{-1} with a mean of 0.03 ± 0.09 . The first- and second-epoch spectra show very similar line profiles for almost all sources.

3.3.3. Class II CH_3OH maser

As mentioned in § 3.1, 38 of the 170 sources in the MMB survey area are associated with 6.7 GHz class II CH_3OH maser emission. Green et al. (2010, 2012) and Breen et al. (2015) measured the line parameters of the 6.7 GHz maser spectra. The peak flux densities range from 0.9 to 517 Jy. Table 5 presents the mean, median, minimum, and maximum values of S_{p} , V_{rel} , and V_{range} of four maser species for the maser-detected sources in the MMB survey area. The median value of S_{p} of 6.7 GHz masers is comparable to that of 22 GHz masers, while the two are (2–3) times larger than those of 44 and 95 GHz masers. The median values of V_{rel} and V_{range} for 6.7 GHz masers are in the middle of the values of 22 and 44 (or 95) GHz masers. These trends are well displayed in Figure 7. We could *not* find any correlation in the isotropic maser luminosity between 6.7 GHz masers and the other maser species.

3.4. Comments on Individual Sources of Interest

RMS 121. Strong H₂O maser emissions were detected in the first and second epochs with peak flux densities of 53 and 25 Jy, respectively. During the observing period of 2 years, the peak velocity changed from redshifted (7.2 km s⁻¹) to blueshifted (-3.1 km s⁻¹) relative to the systemic velocity (3.1 km s⁻¹). While there is a considerable variation in the H₂O maser line, the 44 GHz CH₃OH maser lines are invariable in peak flux density and peak velocity.

RMS 145. As noted in § 3.3.1, this new H₂O maser source can be classified as a dominant redshifted source (Table 6; Figure 8). A high-velocity feature appears at 125 km s⁻¹ without any feature near the systemic velocity, 46.6 km s⁻¹. Both ¹³CO (1–0) and HCO⁺ (1–0) lines were detected only around the systemic velocity. The peak flux density practically remained constant, ~8 Jy, between the two epochs. Neither 44 GHz nor 95 GHz CH₃OH maser emission was detected toward this object.

RMS 2490. This is located in the W33A massive star-forming region. H₂O maser lines were detected near the systemic velocity of 35.8 km s⁻¹ in both epochs. The peak flux density of them increased from 11.4 Jy in the first epoch to 15.6 Jy in the second epoch. A high-velocity maser feature was also detected at -7.9 km s⁻¹ in the second epoch. The peak flux was 15.8 Jy. Urquhart et al. (2011) detected only maser features around the systemic velocity.

RMS 2547. This is a dominant blueshifted H₂O maser source (Table 6; Figure 8). High-velocity features were detected at -70.9 and -65.5 km s⁻¹ in the first and second epochs, respectively, with no emission around the systemic velocity of 20.9 km s⁻¹. Urquhart et al. (2011) also detected this source in 2009–2010. The peak flux density rapidly increased from 13.5 Jy in 2009–2010 to 128 Jy in 2011 April and 945 Jy in 2012 June, while the velocity range remained very similar over the three epochs. Weak 44 GHz CH₃OH maser emission was detected near the systemic velocity in both epochs.

RMS 2584. This source showed strong dominant blue-shifted H₂O maser features in both epochs (Table 6; Figure 8). Urquhart et al. (2011) also detected them. The peak flux density rapidly faded out from 165 Jy in 2009–2010 to 75 Jy in 2011 March and 5 Jy in 2012 June, while the velocity range appeared similar in three epochs.

RMS 3236. Two weak 44 GHz CH₃OH maser features were detected toward this source. One is at the systemic velocity, while the other is offset by -29 km s⁻¹. From the Galactic Ring Survey (GRS) ¹³CO J=1–0 line data archive (Jackson et al. 2006), we examined whether there are ¹³CO lines associated with both maser features or not. As a result, we found that the latter feature in the offset is related to another YSO in the same line of sight.

RMS 3546. This source was observed in both epochs with the same OFF position, i.e., +1^m offset in R.A., (19:24:26.61, 14:40:16.9). An absorption feature was detected at ~57 km s⁻¹ only in the second epoch (Figure 5). It can be explained by the appearance of H₂O maser source, which did not appear in the first epoch, at the OFF position in the second epoch. This source is located

in the active star-forming complex W51. Kang et al. (2009) identified 737 YSO candidates from the Spitzer data, and several of them lie within $60''$ of the OFF position, including No. 608 that is $15''$ away. One of them might emit H_2O maser emission in the second epoch, although there is no previous report of the maser detection toward the position.

RMS 3555. This source is located within G49.5–0.4 in the W51 A complex. H_2O maser emission toward this is the broadest (188 and 230 km s^{-1}) in velocity range at each epoch. The peak flux density was about 3600 Jy at 57.0 km s^{-1} in the second epoch. The emission of CH_3OH maser was detected near the systemic velocity (60.1 km s^{-1}) at 44 and 95 GHz . Interestingly, weak 44 GHz maser emission was also detected at 50 km s^{-1} far from the systemic velocity in both epochs. The grid mapping result suggests that this emission may result from W51 IRS 1 in a sidelobe.

RMS 3587. In the first epoch, H_2O maser emission showed dominant blueshifted features (Table 6; Figure 8). High-velocity features were detected around -44 km s^{-1} in both epochs, although the peak flux density decreased from 4.2 Jy in 2011 March to 2.2 Jy in 2012 May by a factor of 2. The H_2O maser emission near the systemic velocity (16.1 km s^{-1}) emerged in the second epoch with a peak flux of 6.7 Jy . Urquhart et al. (2011) detected multiple features only near the systemic velocity.

RMS 3735. The emission of CH_3OH maser was marginally detected only at 44 GHz in the second epoch, with a peak flux density of 1.4 Jy near the systemic velocity. As for the H_2O maser, a single velocity component was detected in both epochs, and the peak flux density increased by a factor of 6 in a period of two years : from 5 Jy in 2011 April to 30 Jy in 2013 April. There is no significant change in velocity position of peak flux density.

RMS 3749. The emission of H_2O maser was detected in both epochs. The peak flux density varied from 73 Jy in 2011 April to 266 Jy in 2012 October. Also, the velocity of peak flux density moved from blueshifted (1.7 km s^{-1}) to redshifted (15.6 km s^{-1}) relative to the systemic velocity (7.9 km s^{-1}). Urquhart et al. (2011) detected a peak flux density of 175 Jy at -2.4 km s^{-1} .

RMS 3766. A dominant blueshifted H_2O maser feature with a peak flux of 5.0 Jy was detected at -25.7 km s^{-1} in the first epoch (Table 6; Figure 8), while a 1.2 Jy feature solely appeared around the systemic velocity of 5.6 km s^{-1} in the second epoch. In both epochs 44 GHz CH_3OH maser emission ($\sim 2 \text{ Jy}$) was detected near the systemic velocity.

RMS 3846. In both epochs, 44 GHz CH_3OH maser spectra consisted mainly of two strong features of about 25 Jy at -5.2 km s^{-1} and -3.1 km s^{-1} . These lines appeared to have a symmetrical profile with respect to the systemic velocity (-4.4 km s^{-1}). Contrasting with the 44 GHz CH_3OH maser, 95 GHz maser spectrum showed a red-skewed profile in a similar velocity range of 44 GHz maser.

RMS 3911. A dominant high-velocity H_2O maser feature was detected at -75.0 km s^{-1} and -65.8 km s^{-1} in the first and second epochs, respectively (Table 6; Figure 8). The peak flux density

decreased by a factor of 2 from 6.4 Jy to 3.2 Jy. In comparison, Urquhart et al. (2011) detected multiple features with a peak flux density of 5.8 Jy around the systemic velocity, -46.6 km s^{-1} , as well as a high-velocity feature around -75.0 km s^{-1} .

RMS 3936 Weak H_2O maser features were detected between -75 and -55 km s^{-1} in the first epoch, while a dominant redshifted feature was detected at -10.1 km s^{-1} with a peak flux of 3.2 Jy in the second epoch (Table 6; Figure 8). Urquhart et al. (2011) detected the peak flux density of ~ 19 Jy at the systemic velocity (-87.5 km s^{-1}) and multiple high-velocity features from -88.6 to -27.6 km s^{-1} . No class I CH_3OH maser emission was detected in our survey.

RMS 3958. Dominant blueshifted H_2O maser features were detected around -96.4 km s^{-1} without any feature near the systemic velocity (-51.2 km s^{-1}) in the first epoch, while no maser emission was detected in the second epoch (Table 6; Figure 8). The peak flux density was 11.7 Jy. Urquhart et al. (2011) detected H_2O maser features only near the systemic velocity. The 44 GHz and 95 GHz CH_3OH maser emission were detected at the systemic velocity.

4. Analysis and Discussion

4.1. Masers and the Central Objects

In Figure 11, the isotropic luminosities of four maser species are plotted against the bolometric luminosity (L_{bol}) of the central protostar. In our sample, as marked in Table 1, 62 sources have one or two additional RMS sources within $20''$ of each of them. By considering the FWHMs of the KVN telescopes, we integrated the bolometric luminosities of the individual members and use the total luminosity for this comparison. The total bolometric luminosity is less than 5 times larger than the luminosity of a target source for 90% of them. Thus this integration may not significantly affect the derived relationship here. The maser luminosity tends to increase with the bolometric luminosity for all maser species, although the correlations seem to be weak. Linear least-square fittings result in the following relations with correlation coefficients of 0.27–0.50:

$$\log(L_{22}) = (1.40 \pm 0.11) \log(L_{\text{bol}}) - (11.00 \pm 0.46) \quad (\rho = 0.50), \quad (8)$$

$$\log(L_{44}) = (1.25 \pm 0.10) \log(L_{\text{bol}}) - (10.31 \pm 0.41) \quad (\rho = 0.40), \quad (9)$$

$$\log(L_{95}) = (1.17 \pm 0.10) \log(L_{\text{bol}}) - (9.70 \pm 0.39) \quad (\rho = 0.34), \quad (10)$$

$$\log(L_{6.7}) = (1.27 \pm 0.18) \log(L_{\text{bol}}) - (11.06 \pm 0.84) \quad (\rho = 0.27). \quad (11)$$

The relationship between the isotropic maser luminosity and the bolometric luminosity has been investigated in several previous studies of H_2O and CH_3OH masers in SFRs. For H_2O masers, the correlation between $L_{\text{H}_2\text{O}}$ and L_{bol} has been proposed by Furuya et al. (2003) for low-mass YSOs ($L_{\text{bol}} \sim 0.1 - 10^2 L_{\odot}$), Bae et al. (2011) for intermediate-mass YSOs ($L_{\text{bol}} \sim 10^2 - 10^4 L_{\odot}$), and Felli et al. (1992) for low- to high-mass YSOs ($L_{\text{bol}} \sim 10 - 10^6 L_{\odot}$). The slopes of their fit lines are close to 1 (0.81 – 1.02). For comparison, we plot our data together with H_2O maser data

of low- and intermediate-mass YSOs from Furuya et al. (2003) and Bae et al. (2011). We obtain a relation of $\log(L_{22}) = (1.07 \pm 0.05) \times \log(L_{\text{bol}}) - (9.21 \pm 0.20)$ with a much higher correlation coefficient ($\rho = 0.76$), which is consistent with previous studies (Figure 12a).

In the case of 44 CH₃OH masers, the relation between $L_{\text{CH}_3\text{OH}}$ and L_{bol} has been investigated by Kalenskii et al. (2013) for low-mass YSOs ($L_{\text{FIR}} \sim 0.1 - 10^2 L_{\odot}$) and Bae et al. (2011) for intermediate-mass YSOs ($L_{\text{bol}} \sim 10^2 - 10^3 L_{\odot}$). We combine our data with the data of Kalenskii et al. (2013) and Bae et al. (2011) to widen the range of L_{bol} . The best-fit line of 44 GHz data is $\log(L_{44}) = (1.12 \pm 0.07) \times \log(L_{\text{bol}}) - (9.77 \pm 0.27)$ ($\rho = 0.71$) (Figure 12b). For the 95 GHz CH₃OH masers, Gan et al. (2013) presented a relation of $\log(L_{95}) = (0.51 \pm 0.08) \times \log(L_{\text{bol}}) - (7.77 \pm 0.33)$ ($\rho = 0.66$) from low to high-mass YSOs ($L_{\text{bol}} \sim 10^1 - 10^6 L_{\odot}$).

4.2. Masers and the Parental Clumps

We search for dust clumps associated with our target sources using the 870 μm continuum data of the APEX Telescope Large Area Survey of the Galaxy (ATLASGAL) (Schuller et al. 2009; Contreras et al. 2013). We find that 135 sources are located in the survey area and that 116 (86%) of them are associated with the ATLASGAL clumps within a search radius of 30'', in which $\sim 90\%$ of ATLASGAL–RMS matches are distributed (Urquhart et al. 2014b). The maser detection rates of the 116 sources are 35%, 36%, and 31% at 22, 44, and 95 GHz, respectively, in the second epoch. These values are higher than the maser detection rates of the remaining 19 sources: 26%, 26%, and 10%. Assuming that dust emission is optically thin at 870 μm , we derive the clump mass in a similar way to Urquhart et al. (2014b) using the following equation

$$M_{\text{clump}} = \frac{S_{\text{int}} D^2}{k_{\nu} B_{\nu}(T_{\text{d}}) R_{\text{d}}}. \quad (12)$$

Here S_{int} is the integrated flux density, D is the distance to the source, k_{ν} is the mass absorption coefficient per unit mass of dust, $B_{\nu}(T)$ is the Planck function, T_{d} is the dust temperature, and R_{d} is the dust–to–gas mass ratio. We take S_{int} from the ATLASGAL catalog and adopt $k_{\nu} = 1.85 \text{ cm}^2 \text{ g}^{-1}$, $T_{\text{d}} = 20 \text{ K}$, and $R_{\text{d}} = 0.01$ as in Urquhart et al. (2014b). The effective radii of the associated clumps range from 7'' to 154'' with a median of 31''.

Figure 13 shows the maser luminosity versus the estimated clump mass for the detected maser sources. The maser luminosity appears to correlate with the clump mass for all four maser species, especially 44 and 95 GHz CH₃OH masers. Linear least-squares fittings result in the following relations with correlation coefficients of 0.57 to 0.77.

$$\log(L_{22}) = (1.66 \pm 0.25) \log(M_{\text{clump}}) - (10.11 \pm 0.81) \quad (\rho = 0.57), \quad (13)$$

$$\log(L_{44}) = (1.30 \pm 0.10) \log(M_{\text{clump}}) - (9.16 \pm 0.36) \quad (\rho = 0.69), \quad (14)$$

$$\log(L_{95}) = (1.38 \pm 0.13) \log(M_{\text{clump}}) - (9.10 \pm 0.44) \quad (\rho = 0.77), \quad (15)$$

$$\log(L_{6.7}) = (1.63 \pm 0.27) \log(M_{\text{clump}}) - (10.67 \pm 0.92) \quad (\rho = 0.58). \quad (16)$$

Chen et al. (2012) also found a strong ($\rho=0.84$) correlation between L_{95} and the clump mass for the Bolocam Galactic Plane Survey (BGPS) sources. However, the slope was much lower, 0.81. Chen et al. (2011) and Gan et al. (2013) obtained even lower (0.5–0.6) slopes of the best linear fits between L_{95} and M_{clump} for the BGPS clumps associated with EGOs and molecular outflows, respectively. In our sample, twenty 95 GHz maser sources are associated both with the ATLASGAL clumps and BGPS clumps. After deriving the mass of the BGPS clumps as in Chen et al. (2012), we examine the $M_{\text{clump}}-L_{95}$ relations for the two groups and find no significant difference. The slopes of the best linear fits are 1.3 and 1.2 for the ATLASGAL and BGPS clumps with correlation coefficients of 0.89 and 0.74, respectively.

The peak H_2 column density can be calculated from the peak flux density of each clump using the equation

$$N_{\text{H}_2} = \frac{S_{\text{p}}}{\Omega_{\text{b}} \mu m_{\text{H}} k_{\nu} B_{\nu}(T_{\text{d}}) R_{\text{d}}}, \quad (17)$$

where S_{p} is the peak flux density, Ω_{b} is the beam solid angle, μ is the mean molecular weight, and m_{H} is the mass of hydrogen atom. We adopt $\Omega_{\text{b}}=9.8 \times 10^{-9}$ Sr (Contreras et al. 2013) and $\mu=2.37$. Figure 14 plots the maser luminosity against N_{H_2} for four maser species. No correlation appears for 22 and 6.7 GHz masers while very weak correlations exist with $\rho \simeq 0.3$ for 44 and 95 GHz masers. Figure 15 shows the histograms of N_{H_2} for detected and undetected sources in each maser transition. The median values of N_{H_2} 's are 11.1, 10.7, 11.7, and 6.7 in units of 10^{22} cm^{-2} for 22, 44, 95, and 6.7 GHz maser sources, respectively. The two distributions are significantly different for 22, 44, and 95 GHz masers by Kolmogorov-Smirnov(K-S) test ($p < 10^{-7}$), while they are statistically similar for 6.7 GHz maser ($p = 0.67$). This difference can be caused by different pumping mechanisms of the two groups. The occurrence of 6.7 GHz class II masers, which are radiatively pumped, appears to be less dependent on the ambient physical conditions than H_2O and class I CH_3OH masers that are collisionally pumped (see also Breen et al. 2014).

Figure 16 plots the integrated flux density of each maser ($\int S_{\nu} dv$) versus N_{H_2} . The relationship might be meaningful for the future maser survey because the two parameters are independent of the distance and other intrinsic physical parameters (Chen et al. 2012). We perform least-squares fit and obtain the following relations:

$$\log\left(\int S_{22} dv\right) = (2.00 \pm 0.42) \log(N_{\text{H}_2}) - (44.20 \pm 9.65) \quad (\rho = 0.42), \quad (18)$$

$$\log\left(\int S_{44} dv\right) = (1.69 \pm 0.16) \log(N_{\text{H}_2}) - (37.72 \pm 3.56) \quad (\rho = 0.71), \quad (19)$$

$$\log\left(\int S_{95} dv\right) = (1.80 \pm 0.20) \log(N_{\text{H}_2}) - (40.35 \pm 4.53) \quad (\rho = 0.71), \quad (20)$$

$$\log\left(\int S_{6.7} dv\right) = (1.81 \pm 0.39) \log(N_{\text{H}_2}) - (40.10 \pm 8.93) \quad (\rho = 0.35). \quad (21)$$

The slopes of linear fits are similar (1.7–2.0) for all four maser species. However, there is a significant difference in the correlation coefficient in that 44 and 95 GHz masers show quite high correlation coefficients of 0.71, while 22 and 6.7 GHz masers have considerably lower coefficients of ~ 0.4 . The derived correlation coefficient of 95 GHz masers is consistent with the value (0.69) of Chen et al. (2012), although they used $40''$ beam-averaged column density of the BGPS data.

4.3. NH₃ Line width and Kinetic Temperature

Urquhart et al. (2011) surveyed about 600 RMS sources in the NH₃ as well as 22 GHz H₂O maser lines, and detected the NH₃ line emission toward 479 ($\sim 80\%$) sources. They derived some line and physical parameters using the NH₃ data, including the line width (FWHM) of each transition and the kinetic temperature of gas. As mentioned in Section 3.2, their sample includes 257 sources in our sample. NH₃ line emission was detected in 218 (85%) of them. For these NH₃-detected sources, the line widths range from 0.49 to 8.23 km s⁻¹ with mean and median values of 1.85 and 1.73 km s⁻¹, respectively. The mean and median are similar to those (1.7 and 1.6 km s⁻¹) of infrared dark clouds (IRDCs) measured by Chira et al. (2013) from the NH₃ line observations, while the mean is significantly smaller than that (2.1 km s⁻¹) of UCHIIs measured by Urquhart et al. (2011). We compare the line widths of four subsamples: 99 non-maser, 44 only 22 GHz, 21 only 44 GHz, and 54 both (22 and 44 GHz) maser-detected sources. The median values are 1.5, 1.8, 1.7, and 2.2 km s⁻¹ for non-maser, only 22 GHz, only 44 GHz, and both maser-detected sources, respectively. The line width tends to increase from non-maser to only 22 or 44 GHz to both maser-detected subsamples. This tendency is more clearly displayed in Figure 17, which presents cumulative probabilities of the line width for the four subsamples. The difference between non-maser and both maser-detected subsamples seems to be distinct. We perform a K-S test for combinations of the four subsamples in order to examine the statistical difference in their distributions. The K-S test shows that both maser-detected subsample has a significantly different distribution from the other three subsamples, namely, the p-values being 1.2×10^{-10} , 0.001, and 0.02 for non-maser, only 22 GHz, and only 44 GHz maser-detected subsamples, respectively.

The estimated kinetic temperatures are in the range of 12–45 K with mean and median values of 21.6 and 21.1 K for the 218 NH₃-detected sources. The mean and median are significantly higher than those (18 and 16 K) of IRDCs (Chira et al. 2013), while the mean is significantly lower than that (24.6 K) of UCHIIs (Urquhart et al. 2011). The median values are 19.2, 23.0, 21.3, and 23.1 K for no masers, only 22 GHz, only 44 GHz, and both maser-detected sources, respectively. The kinetic temperature tends to increase from no masers to only 44 GHz to only 22 GHz and both maser-detected subsamples. Figure 17 shows this tendency. The K-S test also reveals that both maser-detected sources have a different distribution from no masers ($p=1.3 \times 10^{-7}$) and only 44 GHz ($p=0.005$) maser-detected sources. Therefore, non-maser and both maser-detected sources have similar NH₃ line widths and kinetic temperatures to IRDCs and UCHIIs, respectively. This may suggest that both maser-detected sources are more evolved than non-maser sources although

they are all classified as HMPOs.

4.4. The Virial Parameters

We estimate the virial masses of the molecular clumps associated with our RMS sources using the NH₃ line widths. Following Fuller et al. (1992) (see also Urquhart et al. 2015), we first derive the average line width of the total column of gas from the observed NH₃ line width using the equation below

$$\Delta v_{\text{avg}}^2 = \Delta v_{\text{T}}^2 + \Delta v_{\text{NT}}^2 = \Delta v_{\text{corr}}^2 + 8 \ln 2 \frac{k_{\text{b}} T_{\text{kin}}}{m_{\text{H}}} \left(\frac{1}{\mu_{\text{p}}} - \frac{1}{\mu_{\text{NH}_3}} \right). \quad (22)$$

Here Δv_{corr} is the observed line width corrected for the resolution of the spectrometer, k_{b} is the Boltzmann constant, T_{kin} is the kinetic temperature of gas, taken from ammonia analysis in Section 4.3, μ_{p} and μ_{NH_3} are the mean molecular weights of hydrogen and ammonia molecules taken as 2.37 and 17, respectively.

Assuming the associated clumps are self-gravitating, we calculate the virial mass from

$$M_{\text{vir}} = \frac{5}{8 \ln 2 G} \frac{R_{\text{eff}} \Delta v_{\text{avg}}^2}{a_1 a_2} = 210 M_{\odot} \frac{(R_{\text{eff}}/\text{pc})(\Delta v_{\text{avg}}/\text{kms}^{-1})^2}{a_1 a_2}, \quad (23)$$

$$a_1 = \frac{1 - p/3}{1 - 2p/5} \text{ for } p < 2.5, \quad a_2 = y \frac{\text{arcsinh}(y^2 - 1)^{\frac{1}{2}}}{(y^2 - 1)^{\frac{1}{2}}}, \quad (24)$$

where R_{eff} is the effective radius of the clump, G is the gravitational constant, a_1 is the correction for the power-law density distribution $\rho(r) \sim r^{-p}$, a_2 accounts for the effect of the clump ellipticity, and y is the aspect ratio of the clump (Bertoldi et al. 1992). We adopt the mean power value determined by Mueller et al. (2002), $\langle p \rangle = 1.8$ (i.e. $a_1 = 1.43$), from modeling the 350 μm continuum emission maps of 31 massive star-forming clumps, and the mean aspect ratio of the 116 associated ATLASGAL clumps, $y = 1.55$ (i.e., $a_2 \sim 1.3$).

Figure 18 shows the virial parameter α ($\equiv M_{\text{vir}}/M_{\text{clump}}$) versus M_{clump} for the clumps with and without maser emission. The virial parameter tends to decrease with increasing clump mass. This implies that more massive clumps are more gravitationally unstable. Linear regression fittings to the clumps with and without maser emission give slopes of about -0.54 ± 0.08 and -0.61 ± 0.07 respectively. These values are similar to the slopes from -0.37 to -0.79 reported by Kauffmann et al. (2013) for 260 other massive star-forming clumps. In addition, the maser-detected clumps appear to have higher α 's than the non-detected clumps with similar masses, which suggests that the former are more stable than the latter. This may be because of more active feedback in the clumps with maser emission.

4.5. Maser Occurrence and Evolutionary Stage

IRDCs are generally believed to be the best candidates of birthplaces for high-mass stars and clusters (e.g., Rathborne et al. 2006). UCHIIs are produced by young massive stars that have reached the main sequence stage. Thus IRDCs, HMPOs, and UCHIIs represent the evolutionary sequence of massive star formation. We investigate how the occurrence rates of H₂O and class I CH₃OH masers vary with the evolution of the central objects. Wang et al. (2006) surveyed H₂O maser emission toward 140 IRDC cores with the Very Large Array (VLA) at a typical rms noise level of ~ 0.1 Jy, and detected the emission in 12% of them. Chambers et al. (2009) also observed the 140 and 50 more IRDC cores using the GBT with a twice lower noise level (~ 0.05 Jy) and obtained a detection rate of 35%. As mentioned earlier, the previous surveys of H₂O maser emission toward HMPOs showed a detection rate of 42% at a similar sensitivity to ours (Sridharan et al. 2002), and a slightly higher rate of $\sim 52\%$ with a better sensitivity (~ 0.12 Jy) (Urquhart et al. 2011). Although Urquhart et al. (2011) obtained the same detection rate of H₂O maser emission toward UCHIIIs as that for HMPOs, other surveys showed significantly higher detection rates for UCHIIIs. Churchwell et al. (1990) surveyed 84 UCHIIIs and detected H₂O maser emission in 67% of them, and Kim et al. (2018) also observed 103 UCHIIIs and obtained a similar detection rate with the KVN telescopes at a similar detection limit to this study. Therefore, the detection rate of H₂O maser emission tends to increase as the central objects evolve.

As for 44 GHz CH₃OH masers, as mentioned in § 3.1, Fontani et al. (2010) detected the emission in 31% of 88 HMPO candidates at a rms noise level of about 0.3 Jy. Kim et al. (2018) observed 103 UCHIIIs in the 44 GHz maser transition at a similar sensitivity to this study, and obtained a significantly higher detection rate of 48%. In actual, Fontani et al. (2010) also acquired the same value for the *high* group of their sample, which has similar *IRAS* colors to UCHIIIs, but a considerably lower detection rate (17%) for the *low* group, which may be in an earlier evolutionary phase than the *high* group. Thus the detection rates of 44 GHz CH₃OH maser emission also appear to increase as the central objects evolve. Moreover, Fontani et al. (2010) found a similar evolutionary trend for 95 GHz masers of which the detection rate increase from the *low* group (6%) to the *high* group (20%), although the number of the detected sources is just 11.

These trends are in contrast to the findings in low- and intermediate-mass star-forming regions. Furuya et al. (2003) found in low-mass YSOs that the detection rate of H₂O masers dramatically decreases from Class 0 to Class I to Class II objects. Bae et al. (2011) also found similar trends in the detection rates of both H₂O and 44 GHz CH₃OH masers toward intermediate-mass YSOs. Bae et al. (2011) suggested that this difference can be caused by the different environments of low- and high-mass star-forming regions. UCHIIIs are still deeply embedded in the natal molecular clouds although the central stars have already reached the main sequence stage. On the contrary, low- and intermediate-mass stars in the pre-main sequence phase are usually visible. Therefore, the occurrence of 22 GHz H₂O and 44 GHz class I CH₃OH masers is closely related to the surrounding environments as well as the evolutionary stage of the central objects. Breen et al. (2014) also suggested from their investigation of H₂O masers associated with 12.2 GHz class II CH₃OH masers

that the occurrence of 22 GHz H₂O masers depends more on the surrounding environments than class II CH₃OH and OH masers, which are produced by radiative pumping.

5. Summary

We have simultaneously surveyed 22 GHz H₂O and 44 and 95 GHz class I CH₃OH masers toward 299 HMPOs in the RMS catalog. The main results are summarized as follows.

1. The overall detection rates are 45%, 28%, and 23% for 22, 44, and 95 GHz masers, respectively. We found 123 new maser sources: 15 at 22 GHz, 56 at 44 GHz, and 51 at 95 GHz. In our sample, 170 sources are distributed in the MMB survey area and 38 of them are associated with 6.7 GHz class II CH₃OH maser emission. We detected high-velocity ($>30 \text{ km s}^{-1}$) features in 27 H₂O maser sources. Nine of them are very likely to be dominant shifted H₂O maser outflow sources, 7 blueshifted and 2 redshifted ones.

2. The 44 and 95 GHz class I CH₃OH masers have very similar properties. The 95 GHz maser emission was detected only in 44 GHz maser sources. The two transitions have strong correlations with each other in the peak velocity, the peak flux density, and the isotropic luminosity. The peak flux density ratio ($S_{p,95}/S_{p,44}$) was estimated to be 0.56. Both of these masers always have the peak velocities within 5 km s^{-1} from the systemic velocities. Therefore, 44 and 95 GHz masers might be produced by the same mechanisms in the same sites. This is consistent with the prediction of some modeling that these two transitions can be maser in similar physical conditions (e.g., McEwen et al. 2014). On the other hand, they show no significant correlation with 22 GHz H₂O or 6.7 GHz class II CH₃OH masers in the isotropic luminosity.

3. The 44 GHz class I CH₃OH masers have much narrower distributions than 22 GHz H₂O masers in the peak velocity relative to the systemic velocity and the velocity range. The 6.7 GHz class II CH₃OH masers have intermediate distributions between the two maser species. As for the peak flux density, 44 GHz masers have a significantly smaller median value than those of 6.7 and 22 GHz masers, which are comparable.

4. We investigated for 22, 44, 95, and 6.7 GHz masers whether the isotropic luminosity of each maser species correlates with the physical properties of the central objects and the parental clumps. The maser luminosity shows significant correlations with the clump mass for all the four maser species, but does *not* correlate with the peak H₂ column density. We found weak correlation between the maser luminosity and the bolometric luminosity only for our sample. However, quite strong correlations appeared between the two parameters for 22 and 44 GHz masers in the case where the data points of low- and intermediate-mass YSOs from the previous studies were added.

5. The line width and kinetic temperature of NH₃ line emission tend to increase from non-maser to only 22 GHz or 44 GHz to both maser-detected sources. This may suggest that both maser-detected sources are more evolved than non-maser sources although they are all classified

as HMPOs. The investigation of the virial mass suggests that the ATLASGAL clumps with any maser emission could be more gravitationally stable than those associated with no maser emission.

6. The detection rates of 22 GHz H₂O and 44 GHz CH₃OH maser emission appear to increase as the central objects evolve in massive star-forming regions. This is contrary to the results of low- and intermediate-mass cases. Therefore, the occurrence of both masers might depend on the encompassing environments as well as on the evolutionary stage of the central objects.

We thank the anonymous referee for many constructive comments and suggestions. We are grateful to all staff members in KVN who helped to operate the array and to correlate the data. The KVN is a facility operated by KASI (Korea Astronomy and Space Science Institute). The KVN operations are supported by KREONET (Korea Research Environment Open NETWORK) which is managed and operated by KISTI (Korea Institute of Science and Technology Information). This paper made use of information from the Red MSX Source survey database at http://rms.leeds.ac.uk/cgi-bin/public/RMS_DATABASE.cgi which was constructed with support from the Science and Technology Facilities Council of the UK.

REFERENCES

- Bachiller, R., Gomez-Gonzalez, J., Barcia, A., et al. 1990, *A&A*, 240, 116
- Bae, J.-H., Kim, K.-T., Youn, S.-Y., et al. 2011, *ApJS*, 196, 21
- Batrla W., Menten K. M. 1988, *ApJ*, 329, L117
- Bayandina O. S., Val'tts I. E., Larionov G. M. 2012, *Arep.*, 56, 553
- Bertoldi, F., & McKee, C. F. 1992, *ApJ*, 395, 140
- Breen, S. L., Caswell, J. L., Ellingsen, S. P., et al. 2010a, *MNRAS*, 406, 1487
- Breen, S. L., Ellingsen, S. P., Caswell, J. L., et al. 2010b, *MNRAS*, 401, 2219
- Breen, S. L., & Ellingsen, S. P. 2011, *MNRAS*, 416, 178
- Breen, S. L., Ellingsen, S. P., Caswell, J. L., et al. 2014, *MNRAS*, 438, 3368
- Breen, S. L., Fuller, G. A., Caswell, J. L., et al. 2015, *MNRAS*, 450, 4109
- Caswell, J. L., & Phillips, C. J. 2008, *MNRAS*, 386, 1521
- Caswell J. L., 2009, *PASA*, 26, 454
- Chambers, E. T., Jackson, J. M., Rathborne, J. M., et al. 2009, *ApJS*, 181, 360
- Chen X., Ellingsen S. P., Shen Z.-Q., et al. 2011, *ApJS*, 196, 9

- Chen, X., Ellingsen, S. P., He, J.-H., et al. 2012, *ApJS*, 200, 5
- Chen, X., Gan, C.-G., Ellingsen, S. P., et al. 2013, *ApJS*, 206, 9
- Chira R.-A., Beuther H., Linz H., et al. 2013, *A&A*, 552, A40
- Churchwell, E., Walmsley, C. M., & Cesaroni, R. 1990, *A&AS*, 83, 119
- Codella C., Lorenzani A., Gallego A. T., et al. 2004, *A&A*, 417, 615
- Contreras, Y., Schuller, F., Urquhart, J. S., et al. 2013, *A&A*, 549, A45
- Cragg, D. M., Johns, K. P., Godfrey, P. D., et al. 1992, *MNRAS*, 259, 203
- Cyganowski, C. J., Brogan, C. L., Hunter, T. R., et al. 2009, *ApJ*, 702, 1615
- Ellingsen, S. P. 2005, *MNRAS*, 359, 1498
- Ellingsen, S. P., Voronkov, M. A., Cragg, D. M., et al. 2007, in *IAU Symp. 242, Astrophysical Masers and their Environments*, ed. J. M. Chapman & W. A. Baan (Cambridge: Cambridge Univ. Press), 213
- Erickson, N. R., Goldsmith, P. F., Novak, G., et al. 1992, *IEEE Trans. Microwave Theory Tech.*, MTT-40, 1
- Felli, M., Palagi, F., & Tofani, G. 1992, *A&A*, 255, 293
- Fontani, F., Cesaroni, R., & Furuya, R. S. 2010, *A&A*, 517, A56
- Fujisawa, K., Sugiyama, K., Motogi, K., et al. 2014, *PASJ*, 66, 31
- Fuller G. A., Myers P. C. 1992, *ApJ*, 384, 523
- Furuya, R. S., Kitamura, Y., Wootten, A., et al. 2003, *ApJS*, 144, 71
- Gan C.-G., Chen X., Shen Z.-Q., et al. 2013, *ApJ*, 763, 2
- Gómez-Ruiz, A. I., Kurtz, S. E., Araya, E. D., et al. 2016, *ApJS*, 222, 18
- Green, J. A., Caswell, J. L., Fuller, G. A., et al. 2010, *MNRAS*, 409, 913
- Green, J. A., Caswell, J. L., Fuller, G. A., et al. 2012, *MNRAS*, 420, 3108
- Han, F., Mao, R. Q., Lei, C. M., et al. 1995, *PPMtO*, 14, 185
- Han, F., Mao, R. Q., Lu, J., et al. 1998, *A&AS*, 127, 181
- Han, S.-T., Lee, J.-W., Kang, J., et al. 2008, *IJIMW*, 29, 69
- Haschick, A. D., Menten, K. M., & Baan, W. A. 1990, *ApJ*, 354, 556

- Jackson, J. M., Rathborne, J. M.; Shah, R. Y., et al. 2006, *ApJS*, 163, 145
- Jordan, C. H., Walsh, A. J., Lowe, V., et al. 2015, *MNRAS*, 448, 2344
- Kalenskii, S. V., Kurtz, S., & Bergman, P. 2013, *AREp*, 57, 120
- Kang, H., Kim, K.-T., Byun, D.-Y., et al. 2015, *ApJS*, 221, 6
- Kang, J.-H., Byun, D.-Y., Kim, K.-T., et al. 2016, *ApJS*, 227, 17
- Kang, M., Biegging, J. H., Povich, M. S., & Lee, Y., 2009, *ApJ*, 706, 83
- Kauffmann, J., Bertoldi, F., Bourke, T. L., et al. 2008, *A&A*, 487, 993
- Kauffmann J., Pillai T., Goldsmith P. F. 2013, *ApJ*, 779, 185
- Kim, K.-T., Byun, D.-Y., Je, D.-H., et al. 2011, *JKAS*, 44, 81
- Kim, W.-J., Kim, K.-T., & Kim, K.-T. 2018, *ApJS*, to be submitted
- Kurtz, S., Hofner, P., & Alvarez, C. V. 2004, *ApJS*, 155, 149
- Lee, S.-S., Byun, D.-Y., Oh, C. S., et al. 2011, *PASP*, 123, 1398
- Lovas, F. J. 2004, *JPCRD*, 33, 177
- Lumsden, S. L., Hoare, M. G., Oudmaijer, R. D., & Richards, D. 2002, *MNRAS*, 336, 621
- Lumsden, S. L., Hoare, M. G., Urquhart, J. S., et al. 2013, *ApJS*, 208, 11
- Matsumoto, N., Hirota, T., Sugiyama, K., et al. 2014, *ApJ*, 789, L1
- McEwen, B. C., Pihlström, Y. M., & Sjouwerman, L. O. 2014, *ApJ*, 793, 133
- Menten K. M., 1991, *ApJ*, 380, L75
- Mueller, K. E., Shirley, Y. L., Evans, N. J., II, et al. 2002, *ApJS*, 143, 469
- Müller H. S. P., Menten K. M., Mäder H., 2004, *A&A*, 428, 1019
- Pickett, H. M., Poynter, R. L., Cohen, E. A., et al. 1998, *JQSRT*, 60, 883
- Purcell, C. R., Balasubramanyam, R., Burton, M. G., et al. 2006, *MNRAS*, 367, 553
- Rodríguez-Garza, C. B., Kurtz, S. E., Gómez-Ruiz, A. I., et al. 2017, *ApJS*, 233, 4
- Rathborne, J. M., Jackson, J. M., & Simon, R. 2006, *ApJ*, 641, 389
- Schuller, F., Menten, K. M., Contreras, Y., et al. 2009, *A&A*, 504, 415
- Seth, A. C., Greenhill, L. J., & Holder, B. P. 2002, *ApJ*, 581, 325

- Slysh V. I., Kalenskii S. V., Val'tts I. E., et al. 1994, MNRAS, 268, 464
- Sridharan T. K., Beuther H., Schilke P., et al. 2002, ApJ, 566, 931
- Sunada, K., Nakazato, T., Ikeda, N., et al. 2007, PASJ, 59, 1185
- Szymczak, M., Pillai, T., & Menten, K. M. 2005, A&A, 434, 613
- Testi, L., Palla, F., & Natta, A. 1998, A&AS, 133, 81
- Titmarsh A. M., Ellingsen S. P., Breen S. L., et al. 2014, MNRAS, 443, 2923
- Titmarsh, A. M., Ellingsen, S. P., Breen, S. L., et al. 2016, MNRAS, 459, 157
- Torrelles, J. M., Gómez, J. F., Rodríguez, L. F., et al. 1997, ApJ, 489, 744
- Torrelles, J. M., Patel, N. A., Gmez, J. F., et al. 2001, ApJ, 560, 853
- Urquhart, J. S., Hoare, M. G., Purcell, C. R., et al. 2009, A&A, 501, 539
- Urquhart, J. S., Morgan, L. K., Figura, C. C., et al. 2011, MNRAS, 418, 1689
- Urquhart J. S., Figura C. C., Moore T. J. T., et al. 2014a, MNRAS, 437, 1791
- Urquhart J. S., Moore, T. J. T., Csengeri, T., et al., 2014b, MNRAS, 443, 1555
- Urquhart, J. S., Moore, T. J. T., Menten, K. M., et al. 2015, MNRAS, 446, 3461
- Valdettaro, R., Palla, F., Brand, J., et al. 2001, A&A, 368, 845
- Val'tts, I. E., Dzyura, A. M., Kalenskii, S. V., et al. 1995, AZh, 72, 22
- Val'tts I. E., Ellingsen S. P., Slysh V. I., et al. 2000, MNRAS, 317, 315
- Val'tts, I. E., & Larionov, G. M. 2007, Astron. Rep., 51, 519
- Voronkov, M. A., Brooks, K. J., Sobolev, A. M., et al. 2006, MNRAS, 373, 411
- Voronkov, M. A., Caswell, J. L., Ellingsen, S. P., et al. 2014, MNRAS, 439, 2584
- Wang, Y., Zhang, Q., Rathborne, J. M., et al. 2006, ApJ, 651, L125

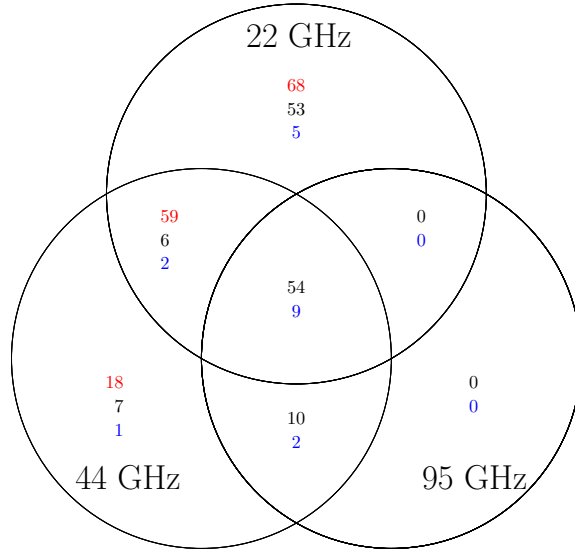


Fig. 1.— Venn diagram showing the numbers of detected 22 GHz H₂O and 44 and 95 GHz class I CH₃OH maser sources in each epoch. The numbers in red and black represent the first and second epochs, respectively. Note that 95 GHz CH₃OH maser was not observed in the first epoch. The numbers in blue are for a subsample of 38 sources with 6.7 GHz class II CH₃OH masers (see Section 3.1 for details).

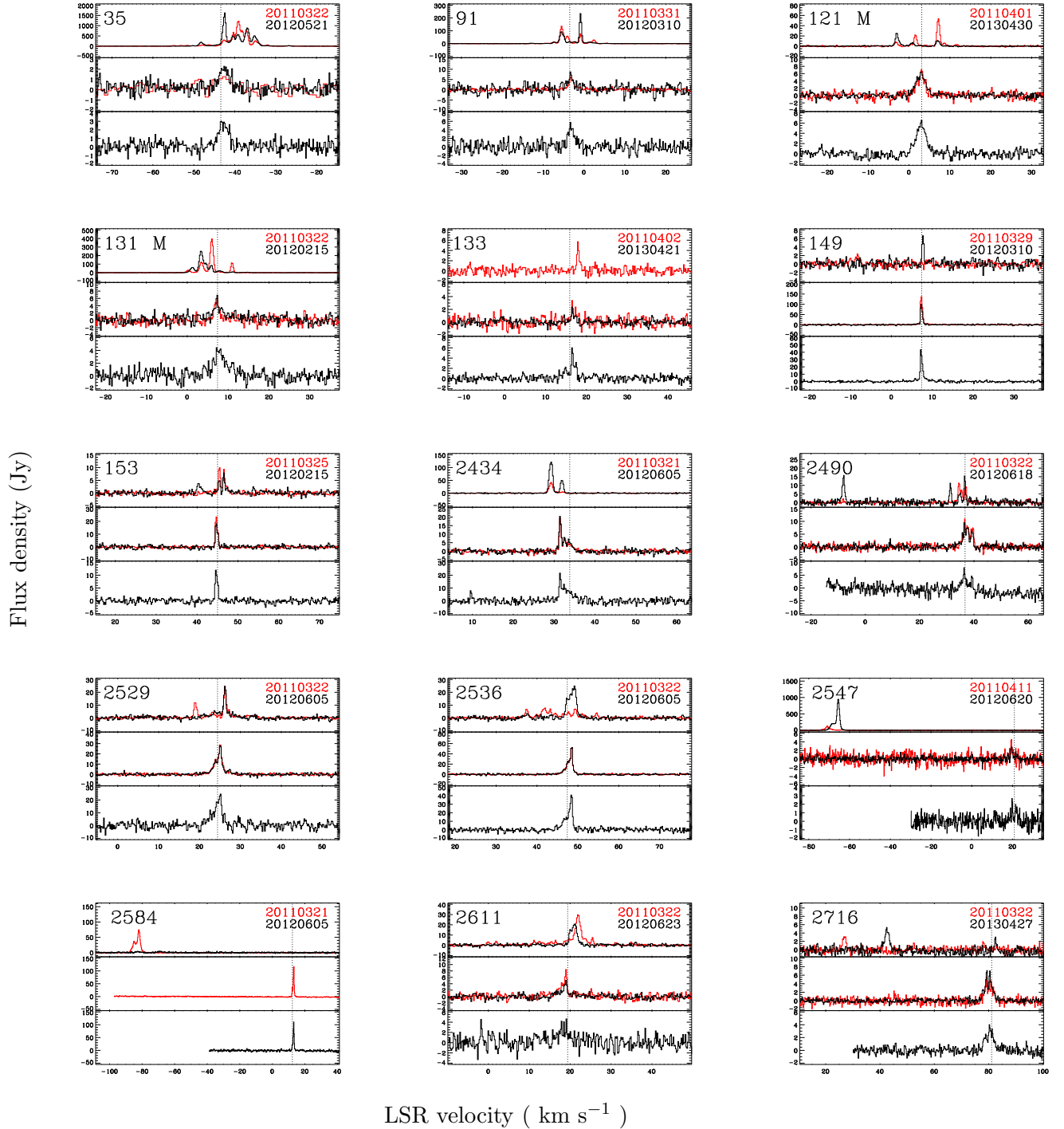


Fig. 2.— (Upper panel) The detected 22 GHz H_2O , (Middle panel) 44 GHz CH_3OH , and (Lower panel) 95 GHz CH_3OH maser spectra of the sources detected in all of 3 transitions. Red and Black colors represent the first and second epochs, respectively. The source name is given in the top-left corner of the upper panel and ‘M’ is attached for the source associated with 6.7 GHz CH_3OH maser emission (see Section 3.1). The observing dates are shown in the top-right corner. The vertical dotted line indicates the systemic velocity, which was mostly determined by the NH_3 line observations (Table 1).

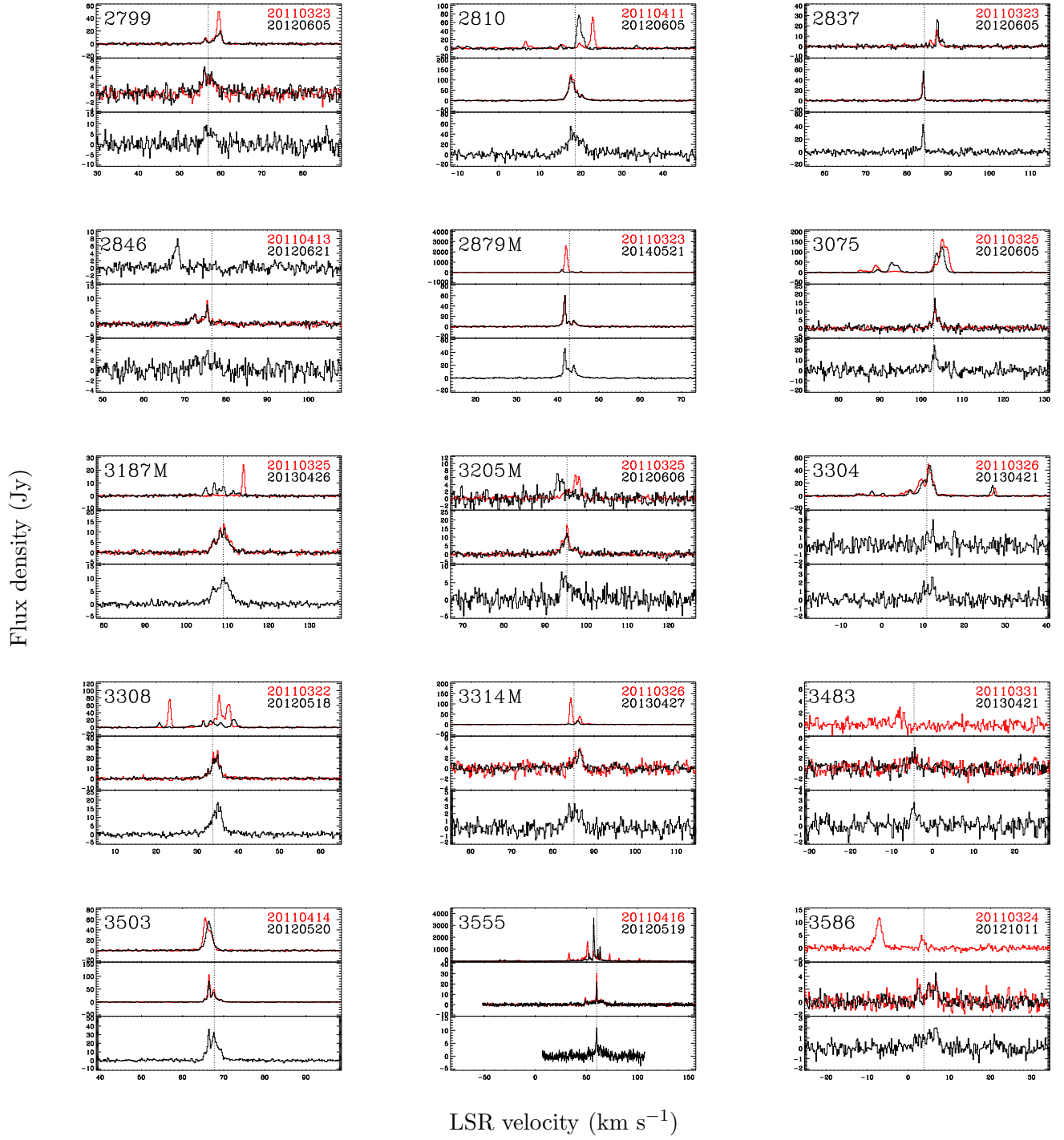


Fig. 2.— Continued

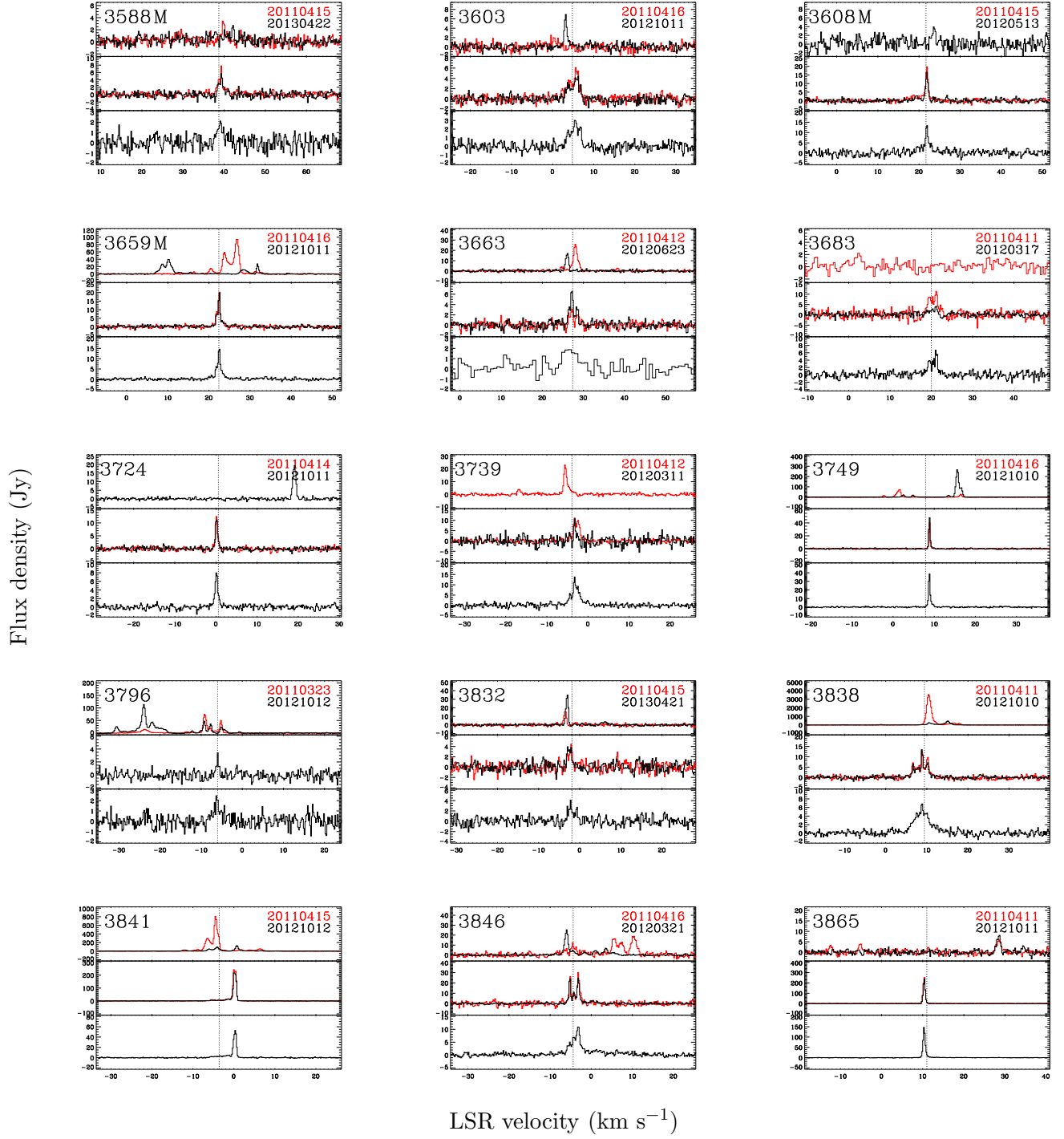


Fig. 2.— Continued

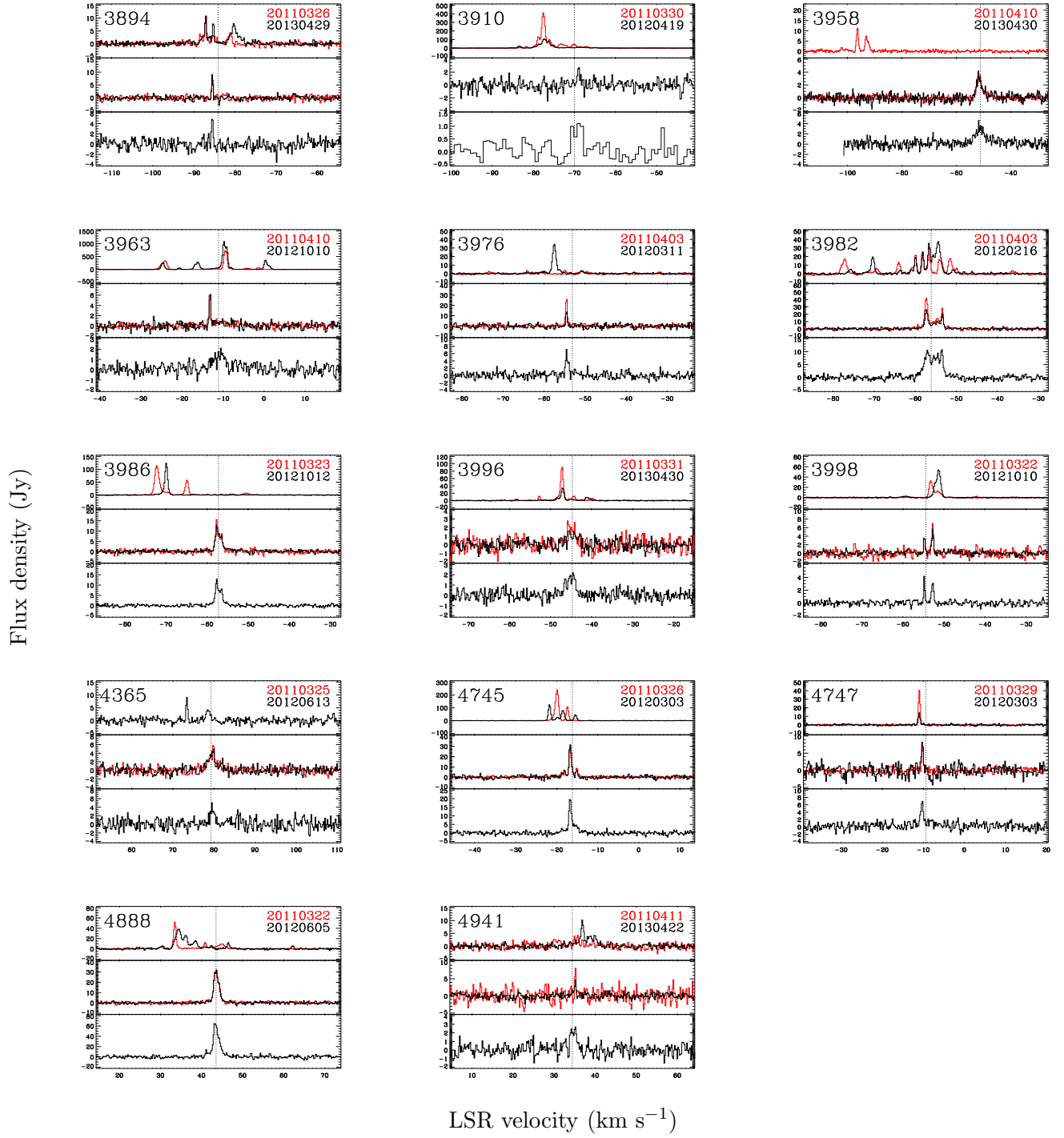


Fig. 2.— Continued

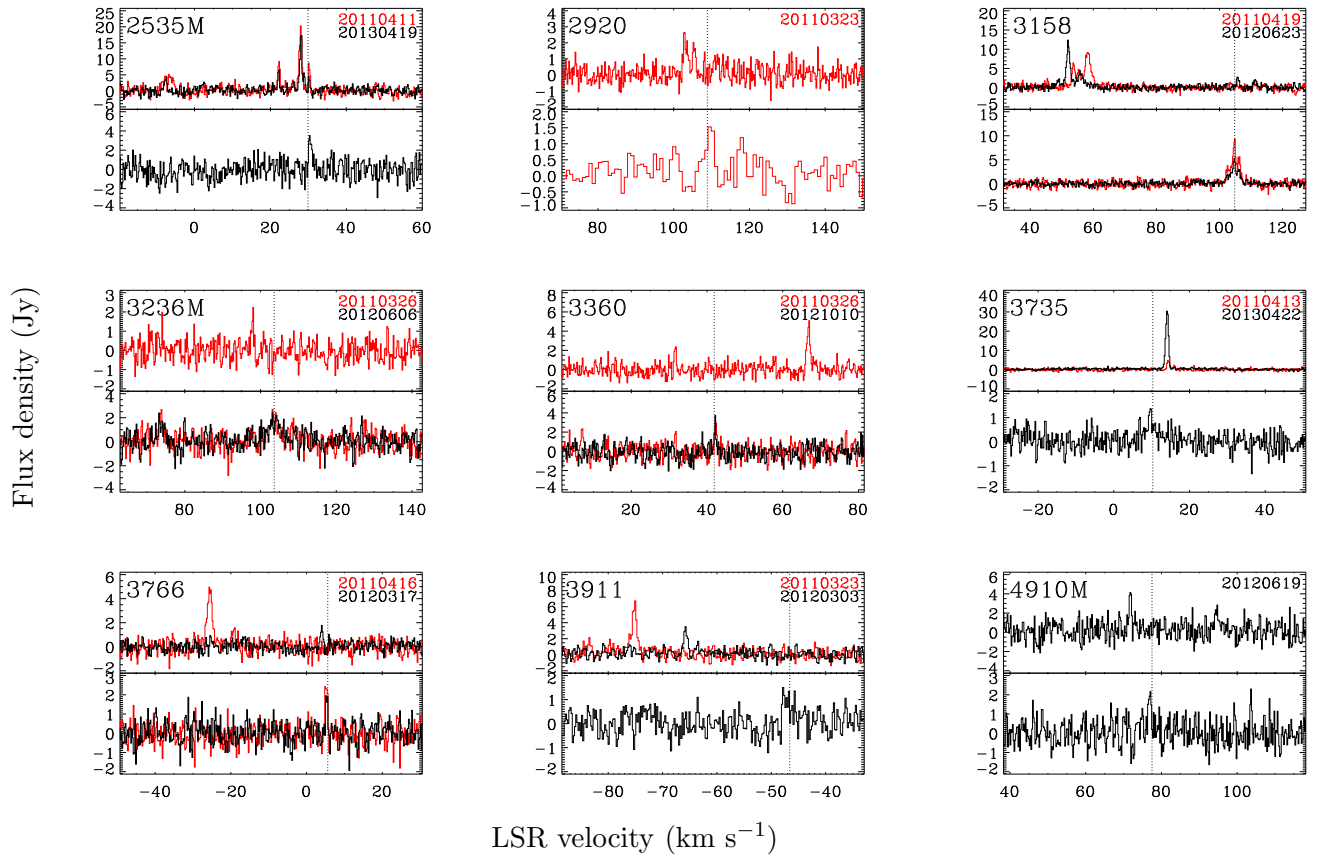


Fig. 3.— Same as in Figure 2 except for the source detected both at (upper panel) 22 GHz and (lower panel) 44 GHz.

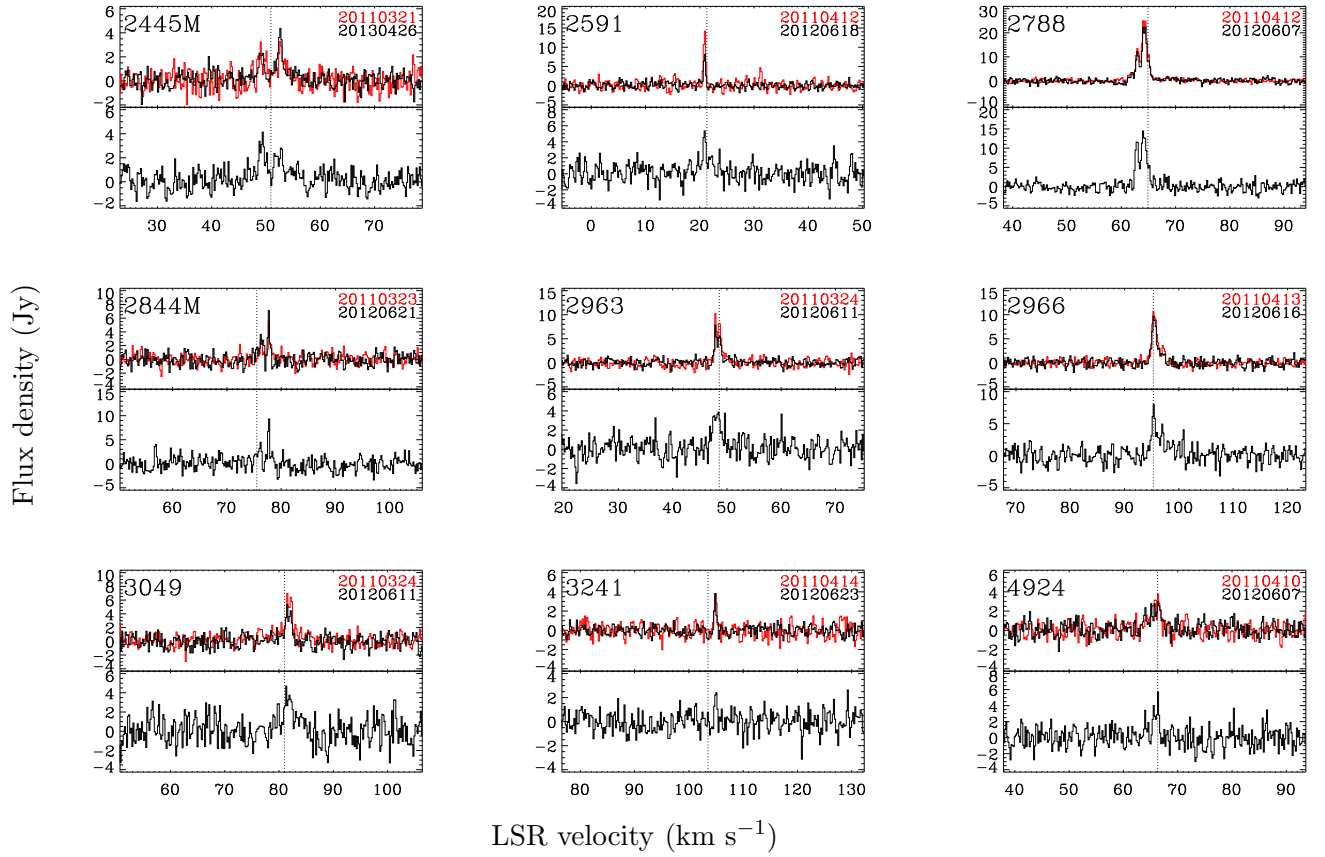


Fig. 4.— Same as in Figure 2 except for the source detected both at (upper panel) 44 GHz and (lower panel) 95 GHz.

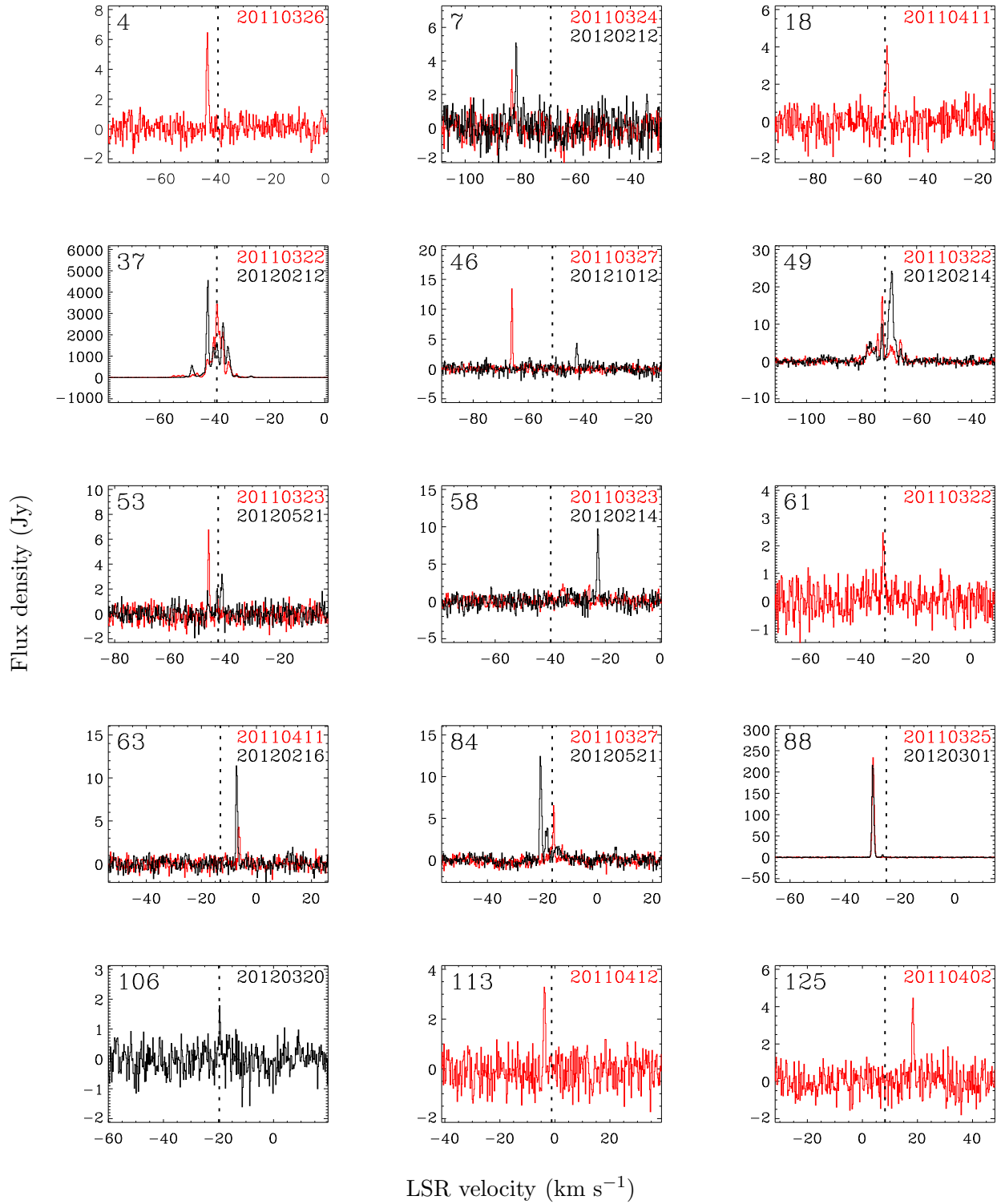


Fig. 5.— Same as in Figure 2 except for the source detected only at 22 GHz.

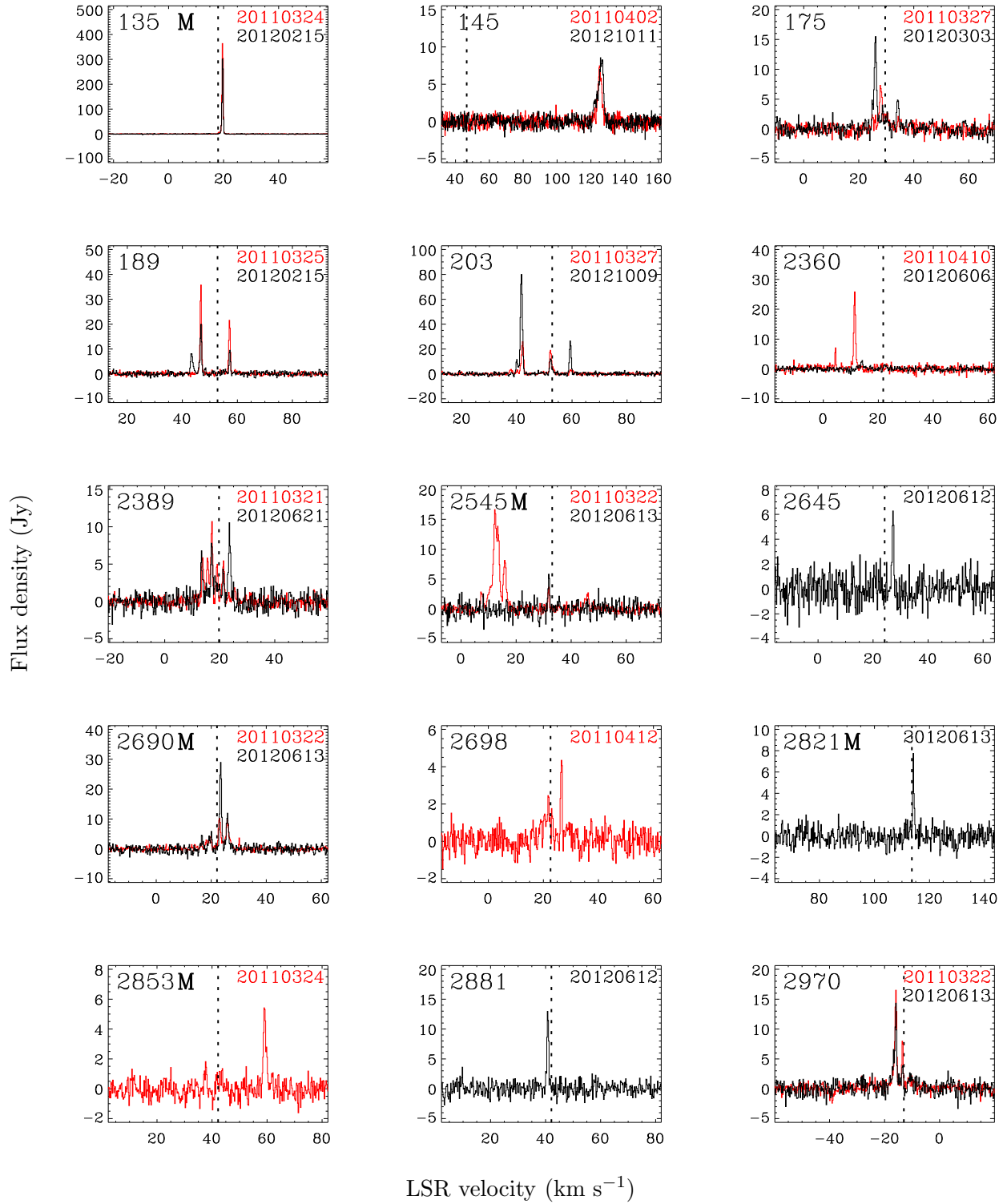


Fig. 5.— Continued

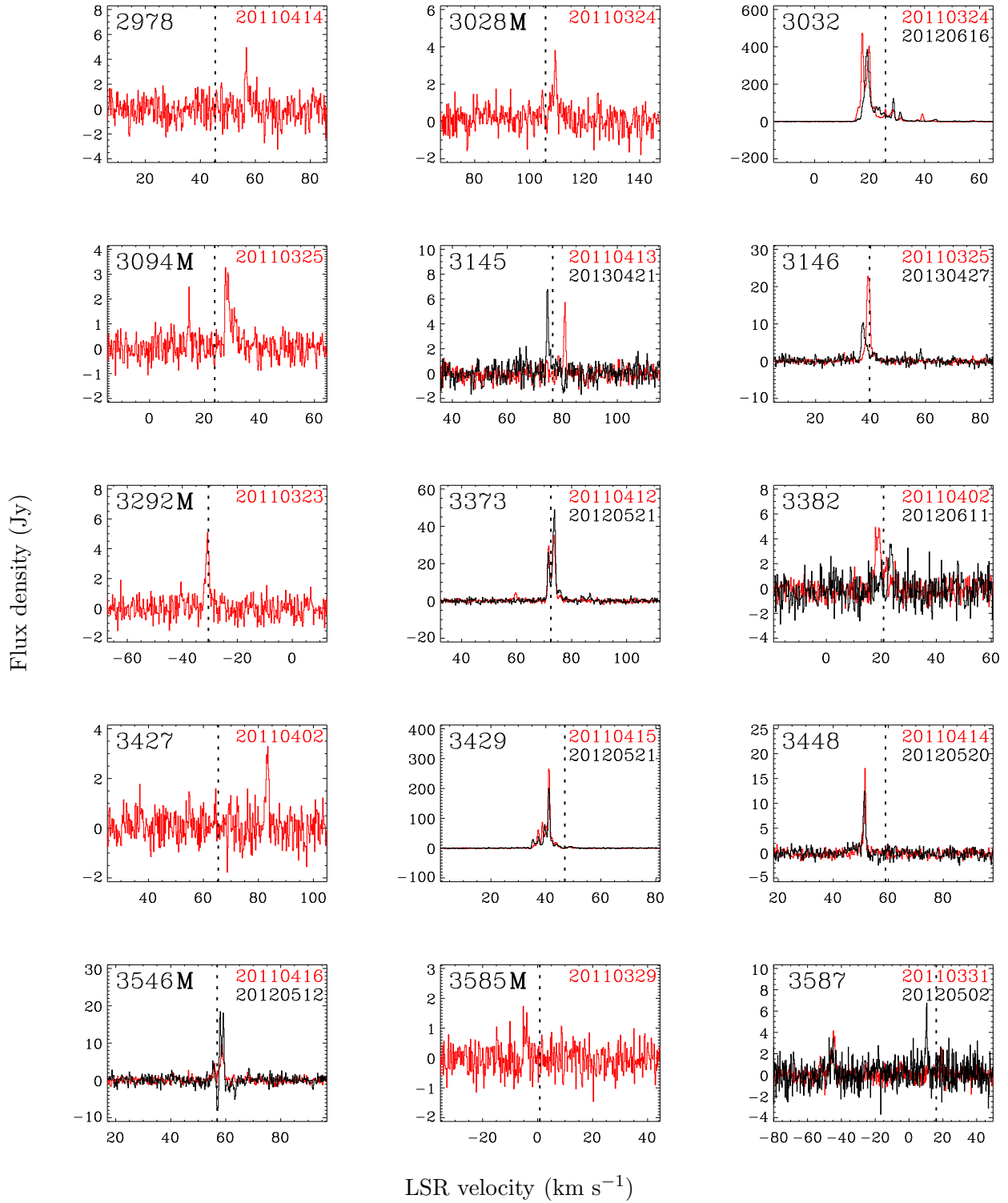


Fig. 5.— Continued

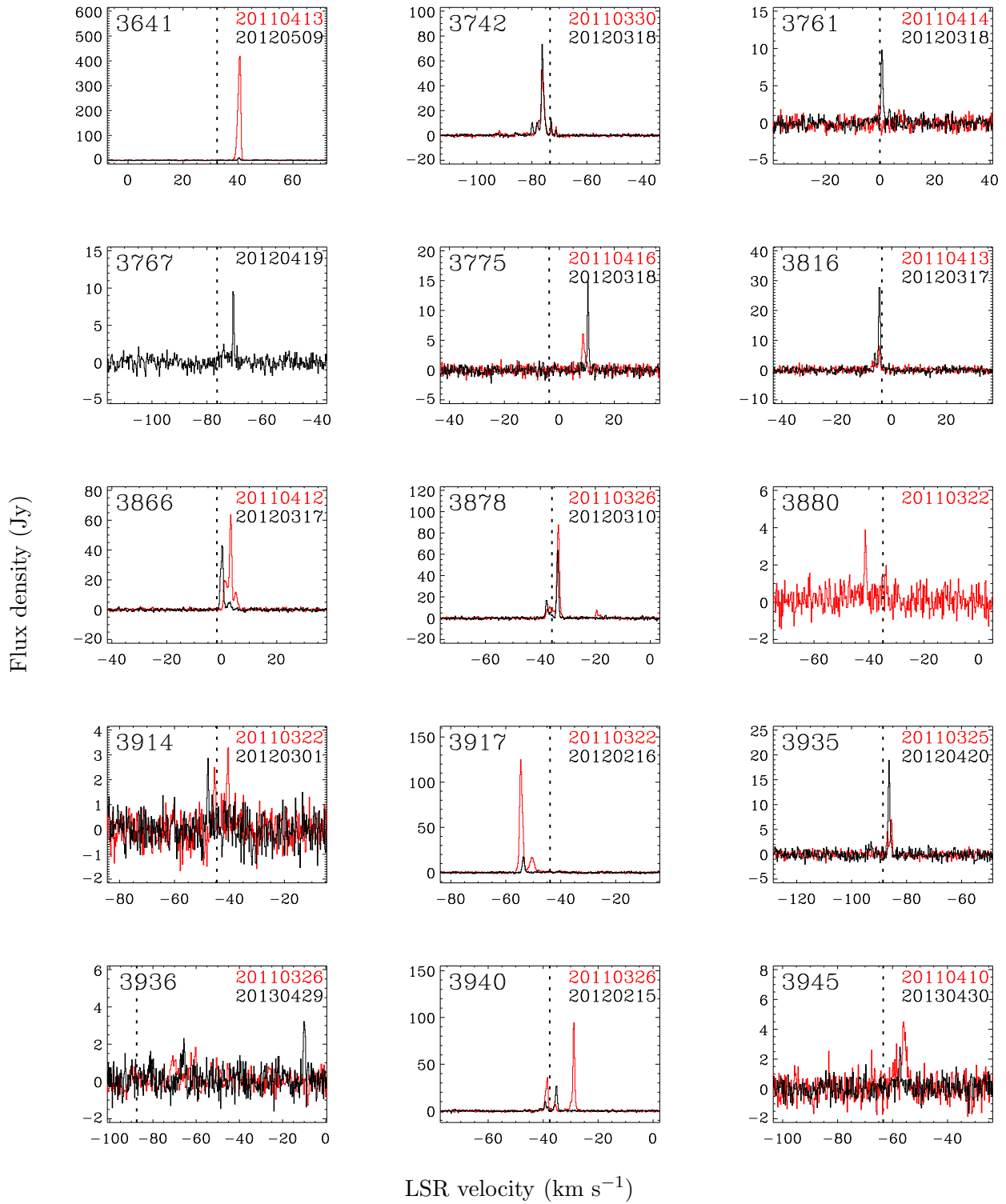


Fig. 5.— Continued

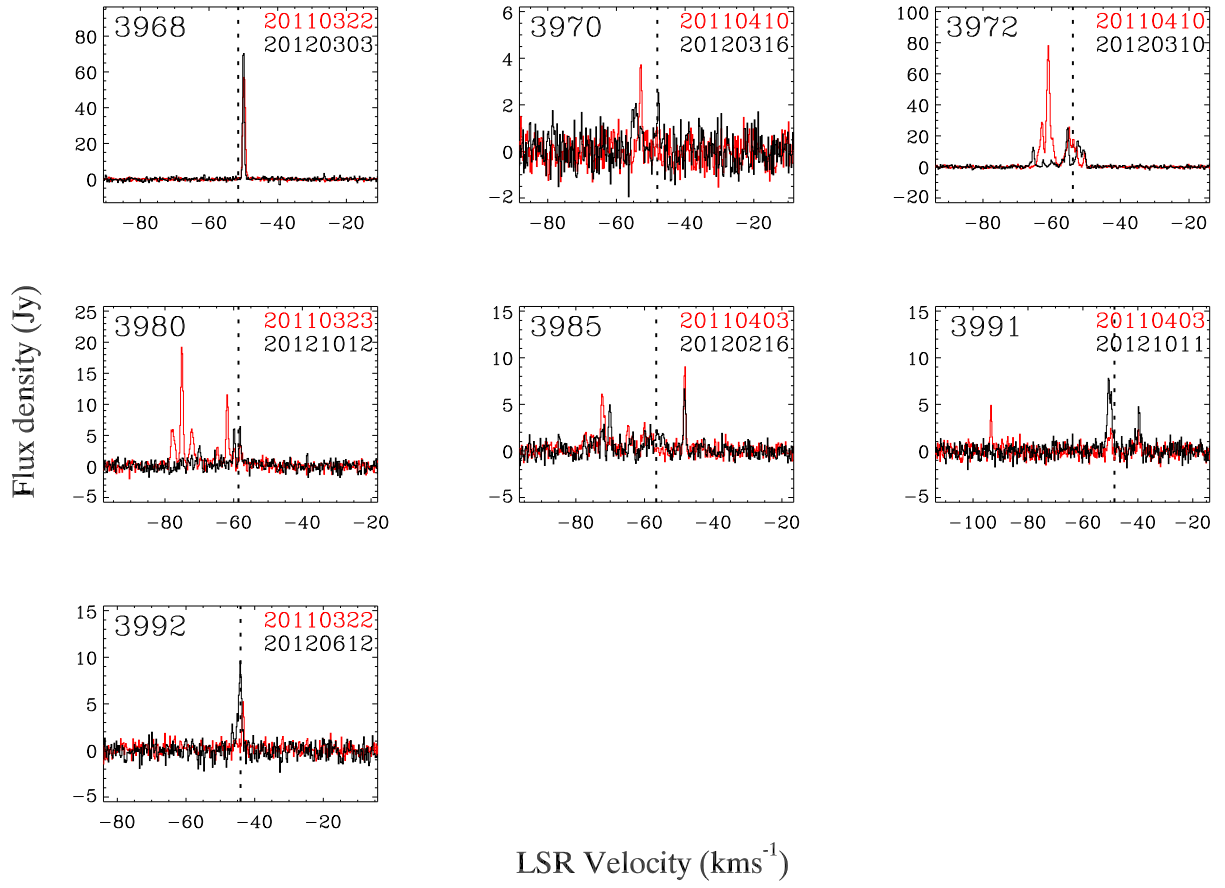


Fig. 5.— Continued

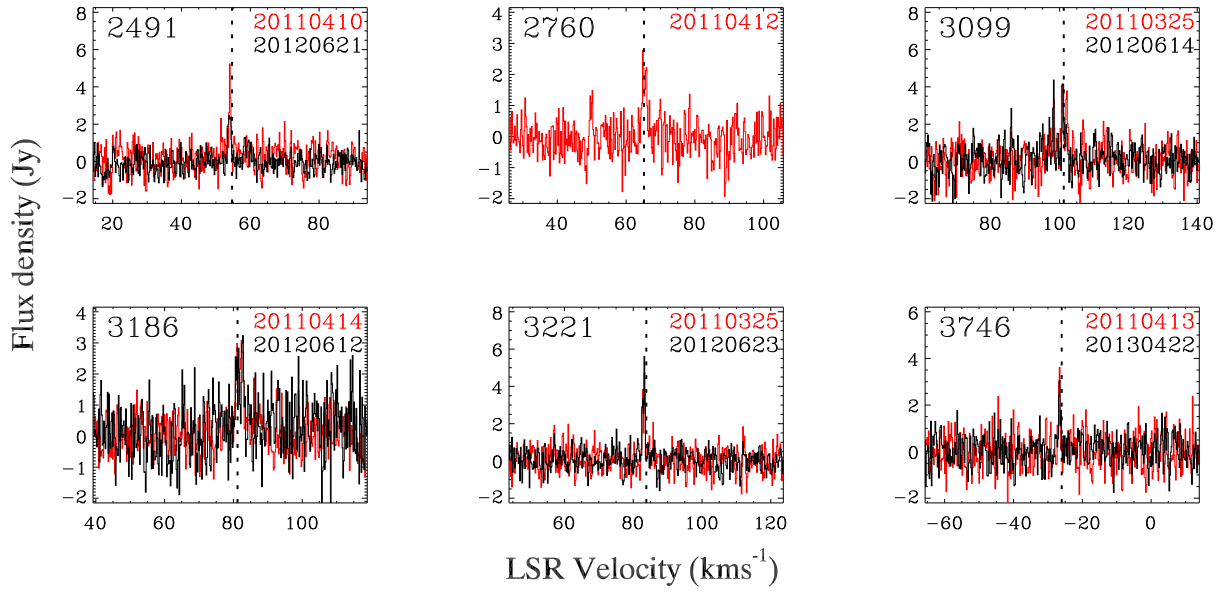


Fig. 6.— Same as in Figure 2 except for the source detected only at 44 GHz.

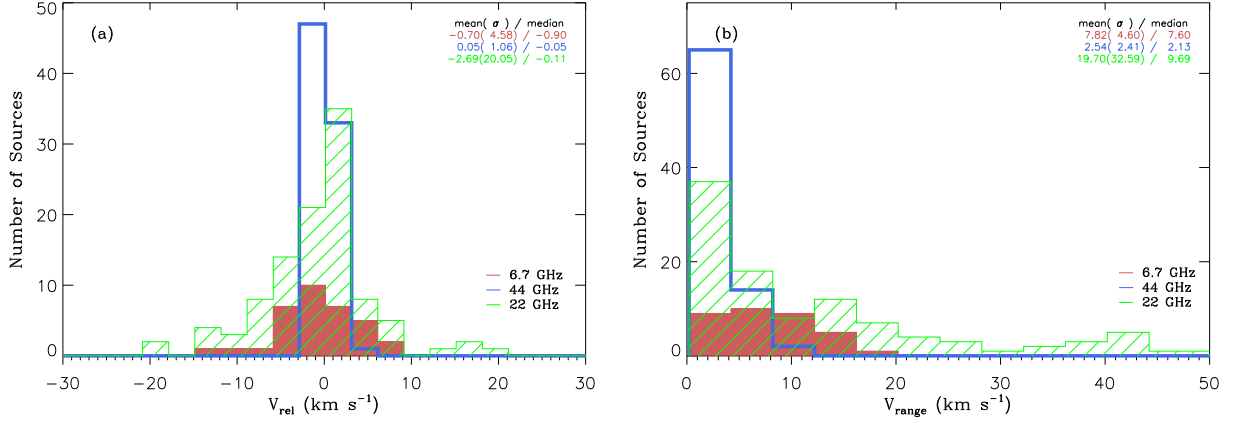


Fig. 7.— (a) Histogram of the relative peak velocities for the 22, 44, and 6.7 GHz maser sources in a bin size of 3 km s⁻¹. Green, blue, and brown colors represent 22, 44, and 6.7 GHz masers, respectively. The 22 and 44 GHz data are from the second-epoch survey of this study, while the 6.7 GHz data are from the MMB survey. The mean and median values of each distribution are listed in the top-right corner of each panel. (b) Same as in (a) except for the velocity ranges in 4 km s⁻¹ bins.

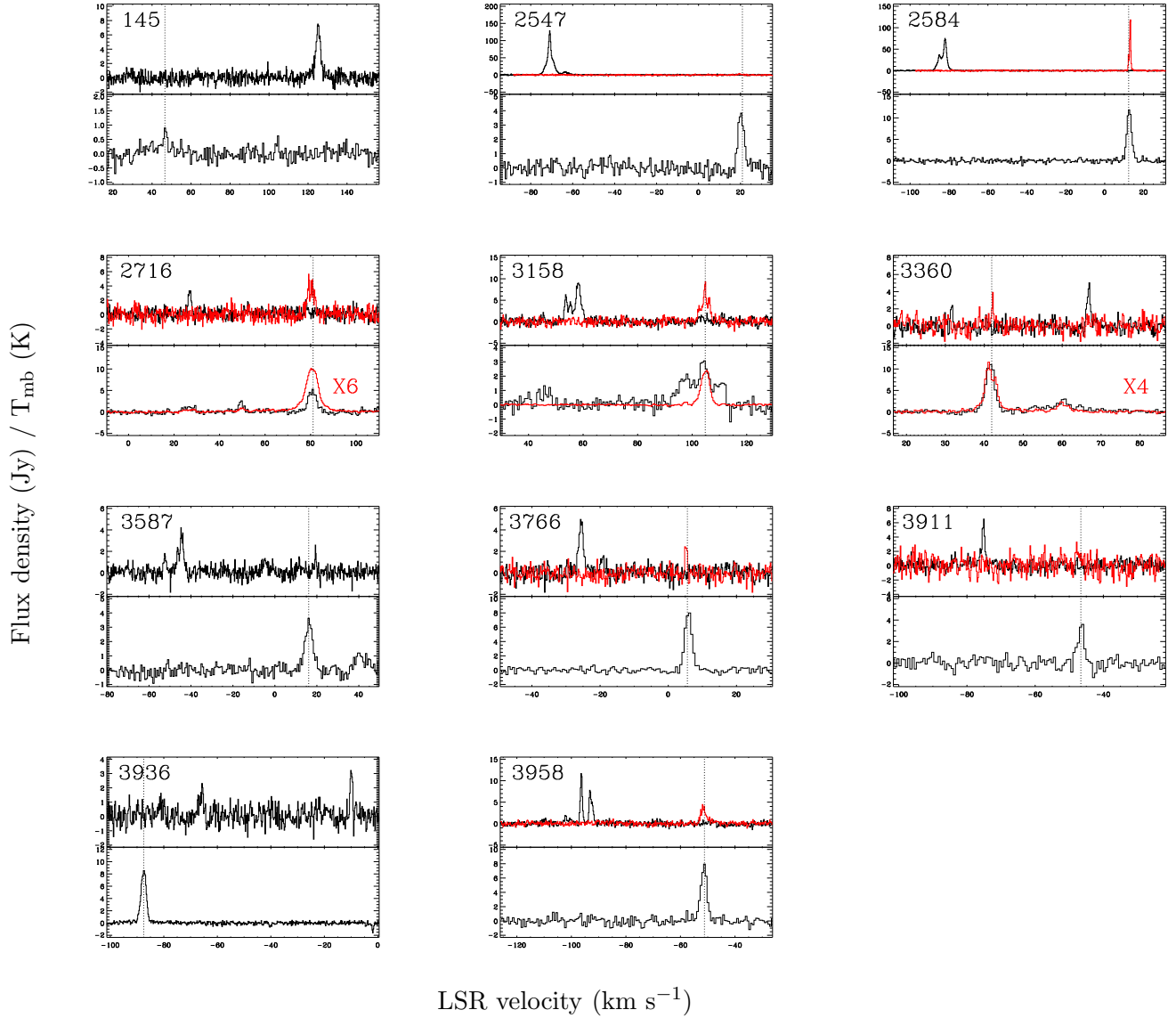


Fig. 8.— (Upper panel) The detected 22 GHz H_2O (*black*) and 44 GHz CH_3OH (*red*) maser spectra and (lower panel) ^{13}CO $J=1-0$ (*black*) and HCO^+ $J=1-0$ (*red*) line spectra of dominant shifted H_2O maser outflow source candidates (^{13}CO $J=2-1$ line spectrum only for RMS 3936). For each source, the source name is presented at the top-left corner of the upper panel and the systemic velocity is indicated by a vertical dotted line.

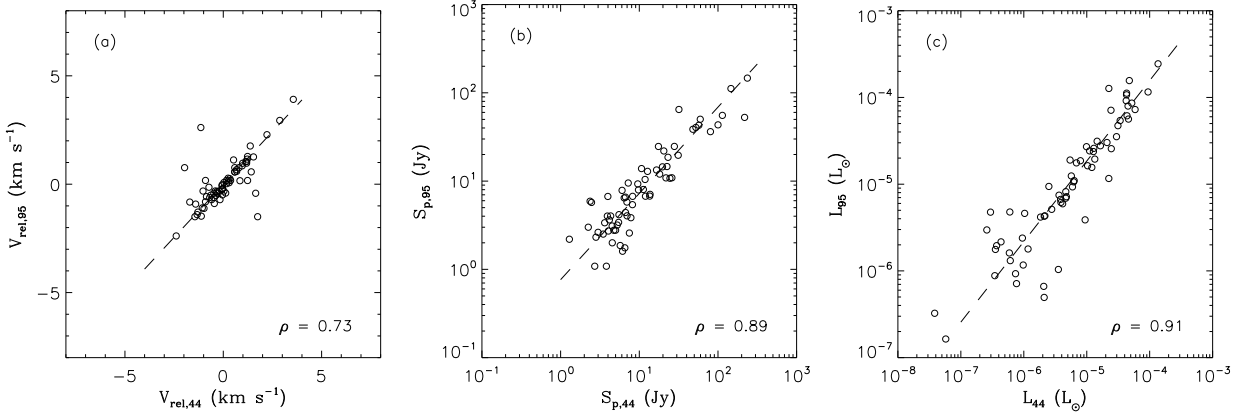


Fig. 9.— Comparison of (a) the relative peak velocities, (b) the peak flux densities, and (c) the isotropic luminosities of the 44 and 95 GHz class I CH₃OH maser sources. In each panel the least-squares fitted relation is displayed by a dashed line with the correlation coefficient in the bottom-right corner.

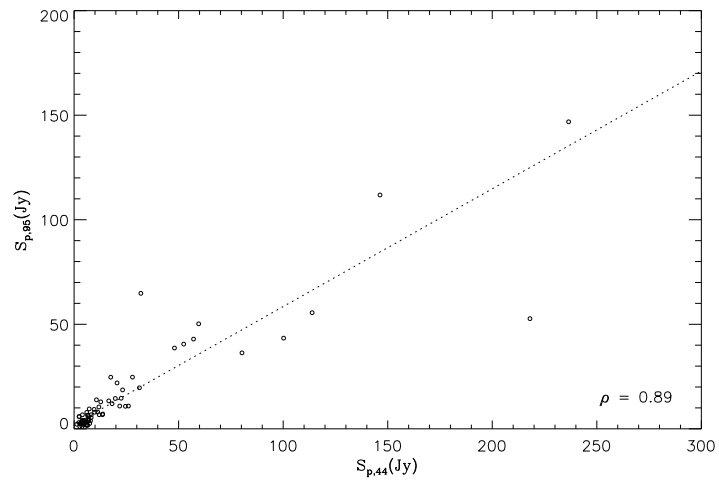


Fig. 10.— Same as in Figure 9 (b) but in linear scale.

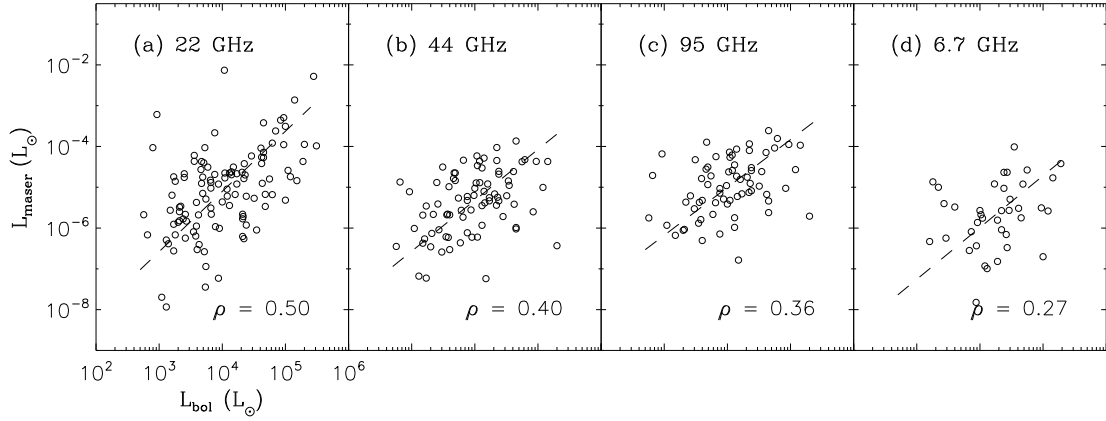


Fig. 11.— Comparison of the isotropic maser luminosity with the bolometric luminosity for (a) the 22 GHz, (b) 44 GHz, (c) 95 GHz, and (d) 6.7 GHz maser sources. The 22, 44, and 95 GHz data are from the second-epoch survey of this study, while the 6.7 GHz data are from the MMB survey (Green et al. 2010, 2012; Breen et al. 2015). The Pearson correlation coefficient is shown in the bottom-right corner of each panel.

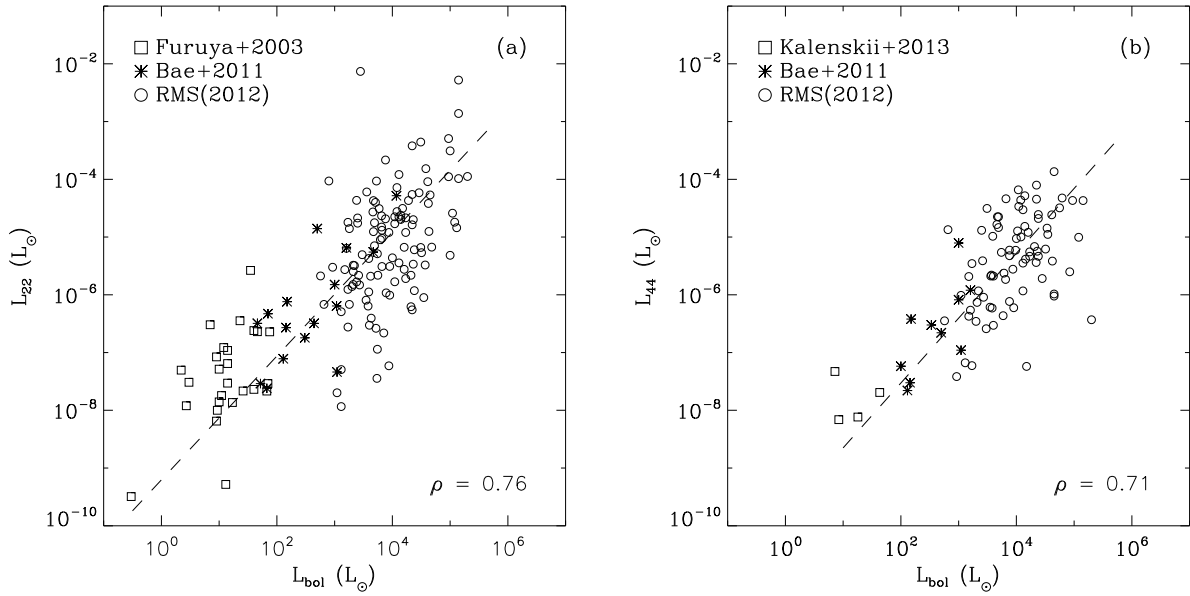


Fig. 12.— Comparison of the isotropic maser luminosity with the bolometric luminosity for (a) the 22 GHz and (b) 44 GHz maser sources. The data points in low- and intermediate-mass regime are added from the literature. In both panels open circles and asterisks are data points of this study in the second epoch and Bae et al. (2011), respectively. Open squares are data points from Furuya et al. (2003) in (a) and Kalenskii et al. (2013) in (b). The least-squares fitted relation is displayed by a dashed line with the correlation coefficient on the bottom-right corner in each panel.

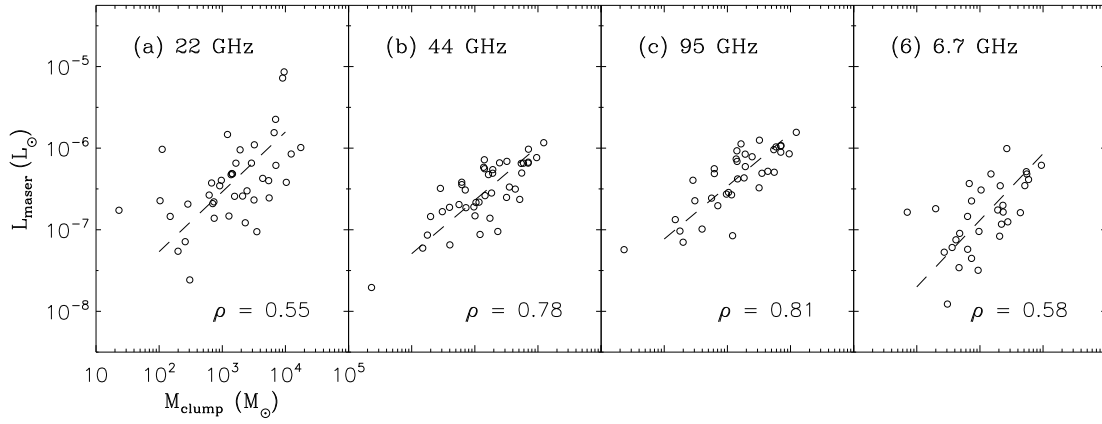


Fig. 13.— Same as in Figure 11 except for the associated ATLASGAL clump mass. In each panel the least-squares fitted relation is shown by a dashed line with the correlation coefficient on the bottom-right corner.

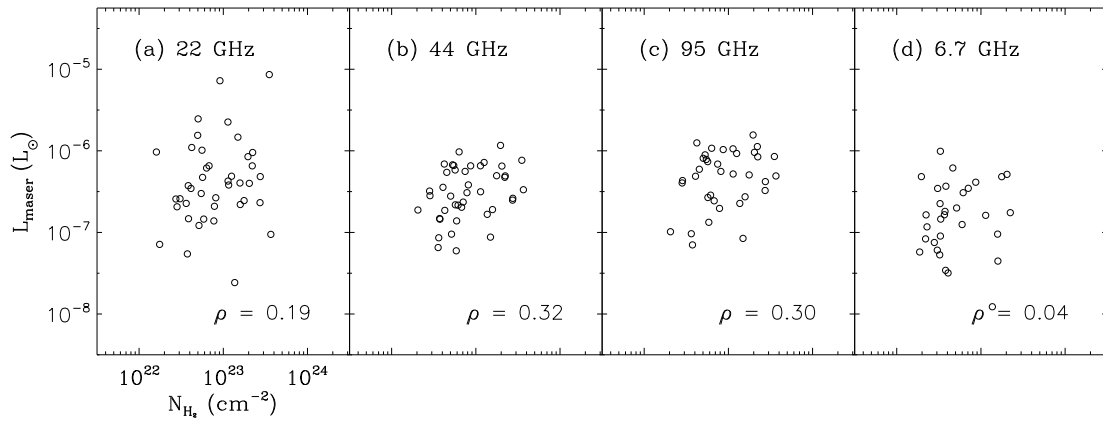


Fig. 14.— Same as in Figure 11 except for the peak H_2 column density.

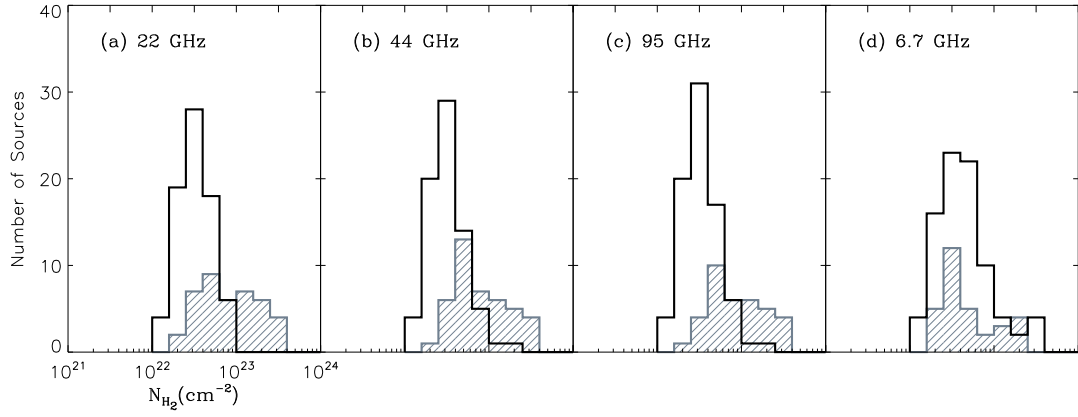


Fig. 15.— The histograms of peak H₂ column density for detected and nondetected sources in each maser transition. The open black and hatched gray lines represent the source with no emission and with emission for each of four masers, respectively. The size of bin is 0.2 dex.

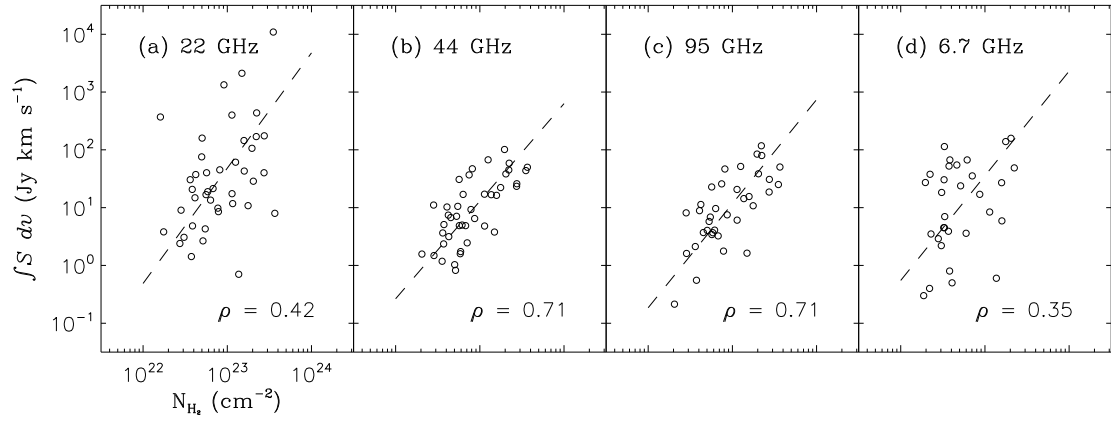


Fig. 16.— The integrated maser flux density versus the peak H₂ column density. In each panel the least-squares fitted relation is shown by a dashed line with the correlation coefficient in the bottom-right corner.

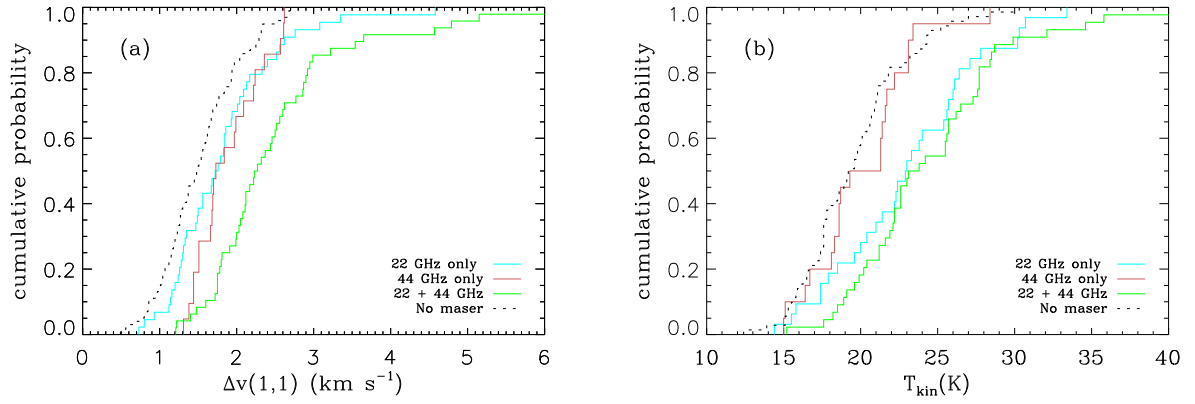


Fig. 17.— Cumulative probability of (a) the NH₃ line width and (b) the kinetic temperature for 4 subsamples, which are divided on the basis of the second-epoch survey results. The subsamples and corresponding colors are displayed on the bottom-right corner in each panel.

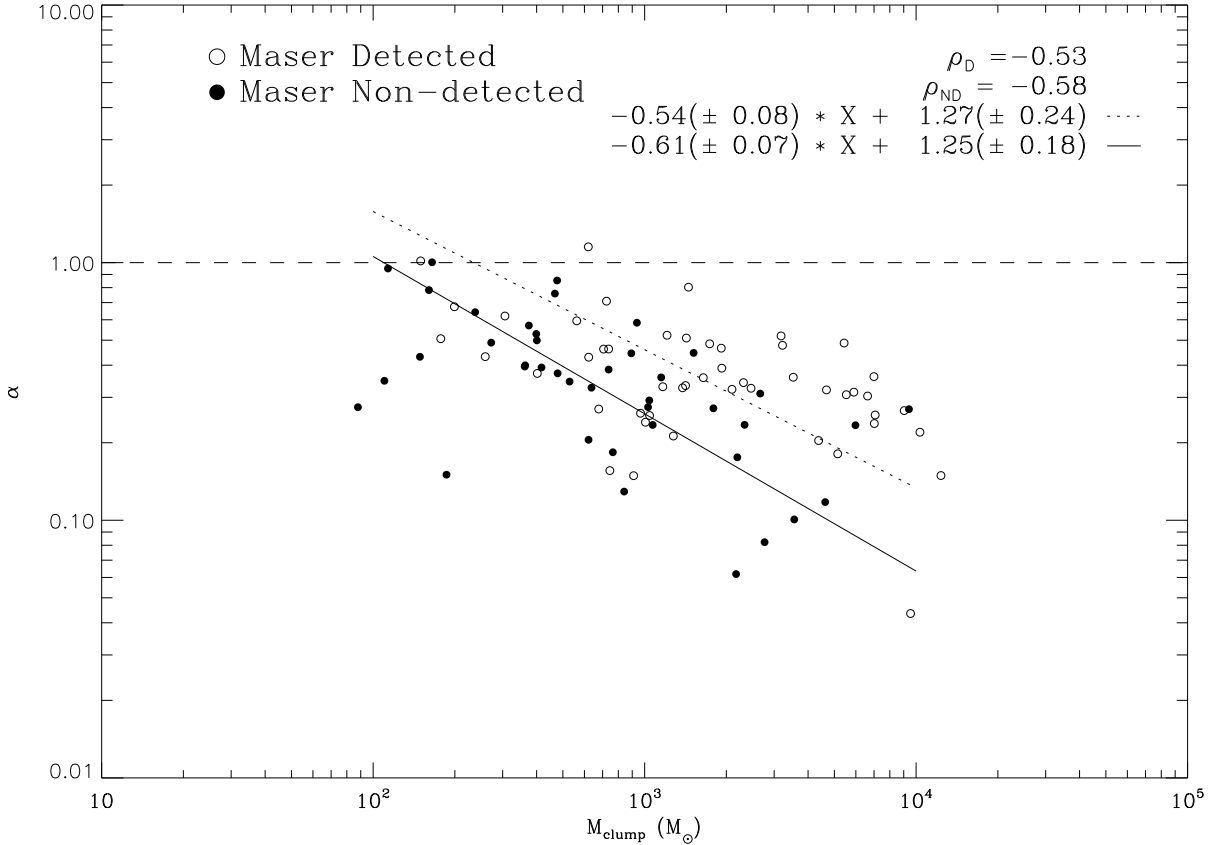


Fig. 18.— The virial parameter (α) versus the clump mass for the associated ATLASGAL clumps. Open and filled circles represent the sources with and without any maser emission, respectively. The dashed line indicates the critical value ($\alpha=1$) for an isothermal sphere in hydrostatic equilibrium without magnetic support. The area of $\alpha < 1$ indicates the region where clumps are gravitationally unstable and likely to be collapsing without additional support from strong magnetic field. The solid and dotted lines show the least-squares fitted relations for the filled and open circles, respectively. The Pearson correlation coefficients are shown in the right upper corner.

Table 1. Summary of Target Sources

RMS ^a ID	MSX name	R.A. (J2000.0)	Decl. (J2000.0)	Distance (kpc)	L_{bol} (L_{\odot})	$V_{\text{sys}}^{\text{b}}$ (km s^{-1})	Detection ^c			MMB Coverage
							22 GHz	44 GHz	95 GHz	
4	G118.6172-01.3312	00:15:27.83	+61:14:18.9	2.8	4900	-39.20	Y ^{11,d}	n	n	...
7	G120.1483+03.3745	00:23:57.04	+66:05:51.5	5.6	21000	-68.90	y ⁴	n	n	...
11	G121.3479-03.3705	00:38:59.37	+59:27:48.2	3.0	1100	-41.90	n	n	n	...
12	G122.4459-00.7815	00:47:17.05	+62:05:09.3	3.1	1600	-42.80	n ^e	n	n	...
14	G123.2836+03.0307	00:54:52.79	+65:53:57.4	4.9	4300	-62.10	n	n	n	...
15	G123.8059-01.7805	00:58:39.99	+61:04:43.0	2.1	2400	-31.90	n	n	n	...
16	G124.0144-00.0267	01:00:55.41	+62:49:30.4	3.1	1800	-43.40	n	n	n	...
18 ^H	G125.6045+02.1038B	01:16:36.21	+64:50:38.4	4.1	8400	-53.70	y ^{4,d}	n	n	...
20	G125.7795+01.7285	01:17:53.03	+64:27:14.3	5.2	5400	-64.50	n	n	n	...
23	G126.7144-00.8220	01:23:33.17	+61:48:48.2	0.7	2600	-13.90	n	n	n	...
35 ^H	G133.6945+01.2166A	02:25:30.99	+62:06:20.9	2.0	45000	-43.40	y ^{4,11}	Y	Y	...
37	G133.7150+01.2155	02:25:40.77	+62:05:52.4	2.0	140000	-39.20	y ^{1,4,6,11}	n	n	...
46	G134.2792+00.8561	02:29:01.93	+61:33:30.5	2.0	5200	-51.20	y ^{1,d}	n	n	...
49	G135.2774+02.7981	02:43:28.64	+62:57:08.7	6.0	29000	-71.50	y ^{4,6,11}	n	n	...
50	G136.3542+00.9543	02:45:10.70	+60:49:38.0	5.5	3700	-61.50	n ^e	n	n	...
53	G136.3833+02.2666	02:50:08.57	+61:59:52.1	3.2	7800	-42.40	y ¹¹	n	n	...
54	G136.5370+02.8934	02:53:43.47	+62:29:23.2	3.9	1200	-48.00	n	n	n	...
56	G138.2957+01.5552	03:01:31.32	+60:29:13.2	2.9	17000	-38.00	n	n	n	...
58 ^H	G139.9091+00.1969A	03:07:24.52	+58:30:43.3	3.2	21000	-39.80	y ^{6,11}	n	n	...
61	G143.8118-01.5699	03:24:50.95	+54:57:32.7	2.4	9200	-31.10	Y ^{11,d}	n	n	...
63	G141.9996+01.8202	03:27:38.76	+58:47:00.1	0.8	5500	-13.10	y ^{1,6,11}	n	n	...
65	G145.1975+02.9870	03:52:27.32	+57:48:31.7	6.5	4500	-58.60	n	n	n	...
66	G148.1201+00.2928	03:56:15.36	+53:52:13.0	3.2	3400	-34.60	n	n	n	...
71	G151.6120-00.4575	04:10:11.86	+50:59:54.4	6.4	61000	-49.70	n ^e	n	n	...
84	G160.1452+03.1559	05:01:39.89	+47:07:21.7	1.9	2100	-16.50	y ^{4,6,11}	n	n	...
88	G168.0627+00.8221	05:17:13.69	+39:22:19.4	2.0	1700	-25.00	y ^{1,4,6,11}	n	n	...
90 [†]	G176.4661-01.6758	05:30:20.82	+31:01:28.7	2.0	1200	-18.90	n ^e	n	n	...
91	G174.1974-00.0763	05:30:46.06	+33:47:54.1	2.0	5900	-3.50	y ^{1,4,6,11}	y ¹²	Y	...
97	G177.7291-00.3358	05:38:47.16	+30:41:18.1	2.0	2300	-16.10	n	n	n	...
106	G173.6339+02.8218	05:41:11.02	+35:50:01.7	2.0	5400	-19.70	Y ^{4,11,d}	n	n	...
110	G178.7540+01.1609	05:47:12.27	+30:36:12.2	2.0	2100	-18.00	n	n	n	...
111	G184.8704-01.7329	05:50:13.89	+23:52:17.7	2.0	2000	2.30	n	n	n	...
113	G188.9696-01.9380	05:58:24.43	+20:13:57.6	2.0	1900	-1.20	y ^{1,3,6}	n	n	y
114	G178.8454+04.2936	06:00:04.99	+32:06:31.8	1.1	2200	0.60	n	n	n	...
119	G189.0307+00.7821	06:08:40.52	+21:31:00.4	2.0	24000	2.50	n	n	n	y
120	G189.0323+00.8092	06:08:46.73	+21:31:44.1	2.0	11000	1.90	n	n	n	y
121	G188.9479+00.8871	06:08:53.40	+21:38:28.1	1.8	2200	3.10	y ^{1,4,6}	Y	Y	y
124	G188.8120+01.0686	06:09:17.90	+21:50:49.9	2.0	664	-0.30	n ^f	n	n	y
125 ^H	G189.8557+00.5011A	06:09:19.82	+20:39:31.5	2.0	1622	8.20	Y ^{6,8}	n	n	y
128	G192.9089-00.6259	06:11:23.74	+17:26:28.5	2.0	1400	22.60	n	n	n	y
131	G192.6005-00.0479	06:12:54.01	+17:59:23.1	2.0	45000	7.40	y ^{1,4,6}	y ^{7,12}	Y	y
133	G194.9349-01.2224	06:13:16.14	+15:22:43.3	2.0	3000	15.90	Y ^{6,8}	y ¹²	Y	y
135	G196.4542-01.6777	06:14:37.06	+13:49:36.4	5.3	94000	18.00	y ^{1,4,6}	n	n	y
136	G196.1620-01.2546	06:15:34.71	+14:17:03.2	1.5	2400	10.80	n	n	n	y
140	G201.3419+00.2914	06:31:06.92	+10:26:04.9	0.8 ^g	1100	-1.40	n	n	n	y
141 ^H	G206.7804-01.9395B	06:33:16.21	+04:34:53.0	1.2	912	14.00	n	n	n	y
145	G212.2344-03.5038	06:37:41.59	-00:58:37.7	5.0	2500	46.60	y ⁴	n	n	...
146	G203.7637+01.2705	06:39:09.95	+08:44:09.7	0.8	483	9.50	n	n	n	y
149	G203.3166+02.0564	06:41:10.15	+09:29:33.6	0.6	1100	7.40	y ^{1,6}	y ^{7,12}	Y	...
151	G211.8957-01.2025	06:45:16.00	+00:22:24.9	4.8	5800	45.00	n	n	n	y

Table 1—Continued

RMS ^a ID	MSX name	R.A. (J2000.0)	Decl. (J2000.0)	Distance (kpc)	L_{bol} (L_{\odot})	$V_{\text{sys}}^{\text{b}}$ (km s^{-1})	Detection ^c			MMB Coverage
							22 GHz	44 GHz	95 GHz	
153	G212.0641-00.7395	06:47:13.36	+00:26:06.5	4.7	16000	45.00	y ^{4,6}	Y	Y	y
154 ^Y	G214.4934-01.8103A	06:47:50.26	-02:12:51.3	2.1	1980	26.80	n	n	n	y
155	G215.8902-02.0094	06:49:40.23	-03:32:52.4	6.1	4100	57.60	n	n	n	...
156	G217.6047-02.6170	06:50:37.41	-05:21:00.9	6.8	4200	63.30	n	n	n	...
157	G211.5350+01.0053	06:52:28.23	+01:42:06.5	4.8	7400	44.80	n	n	n	y
158	G213.9180+00.3786	06:54:35.14	-00:42:17.8	3.9	1200	41.60	n	n	n	y
160	G212.9626+01.2954	06:56:06.32	+00:33:47.7	4.2	1300	42.50	n	n	n	y
167	G217.3020-00.0567	06:59:13.13	-03:54:53.2	1.3	799	26.70	n	n	n	y
172 ^Y	G218.0230-00.3139A	06:59:37.48	-04:40:23.5	1.9	3000	25.70	n	n	n	y
174	G221.9605-01.9926	07:00:50.94	-08:56:30.1	3.2	5500	41.10	n	n	n	y
175	G220.4587-00.6081	07:03:03.06	-06:58:25.9	2.2	2100	29.60	y ^{1,4,11}	n	n	y
176	G224.6065-02.5563	07:03:43.16	-11:33:06.2	0.8	1200	13.80	n	n	n	...
181	G224.6075-01.0063	07:09:20.55	-10:50:28.1	1.0	596	16.20	n ^e	n	n	y
184	G232.0766-02.2767	07:18:59.91	-18:02:41.6	3.0	5000	42.10	n ^e	n	n	...
188	G231.7986-01.9682	07:19:35.93	-17:39:18.0	3.2	5600	43.50	n	n	n	y
189	G229.5711+00.1525	07:23:01.80	-14:41:32.2	4.1	4700	52.80	y ^{4,6,8,11}	n	n	y
193	G233.8306-00.1803	07:30:16.72	-18:35:49.1	3.3	13000	44.60	n	n	n	y
196	G232.6207+00.9959	07:32:09.73	-16:58:13.4	1.7	11000	16.60	n	n	n	y
203 ^Y	G236.8158+01.9821A	07:44:28.02	-20:08:31.2	4.0	3600	52.80	y ^{4,6,8,11}	n	n	y
205	G242.9402-00.4501	07:48:43.25	-26:39:30.9	5.1	3200	63.50	n	n	n	y
2360	G010.5067+02.2285	18:00:34.53	-18:45:17.9	2.9	1700	21.80	y ^{6,8,11}	n	n	...
2384	G011.9019+00.7265	18:08:58.78	-18:16:29.8	2.9	502	24.30	n	n	n	y
2389	G010.8856+00.1221	18:09:07.98	-19:27:24.0	2.7	5500	19.70	y ^{4,11,14}	n	n	y
2434 ^Y	G012.8909+00.4938A	18:11:51.13	-17:31:21.1	2.4	20600	33.80	y ^{1,4,9,11,14}	y ⁷	y ¹³	y
2437	G012.0260-00.0317	18:12:01.88	-18:31:55.7	11.1	35000	110.80	n	n	n	y
2445 ^H	G012.1993-00.0342B	18:12:23.43	-18:22:51.0	12.0	143000	50.90	n ^e	Y	y ¹⁰	y
2489 ^H	G013.1840-00.1069A	18:14:38.98	-17:33:07.5	11.9	32000	54.40	n	n	n	y
2490	G012.9090-00.2607	18:14:39.56	-17:52:02.3	2.4	32000	36.70	y ^{4,9,11,14}	Y	y ¹⁰	y
2491	G013.3310-00.0407	18:14:41.80	-17:23:27.7	4.5	3700	54.70	n	Y	n	y
2512	G016.7122+01.3119	18:16:26.38	-13:46:24.4	2.1	1800	20.30	n	n	n	y
2529	G014.6087+00.0127	18:17:02.71	-16:14:28.0	2.6	4900	24.40	y ^{4,9,11,14}	y ¹²	Y	y
2535	G015.0939+00.1913	18:17:20.87	-15:43:45.9	2.9	1600	29.90	y ^{8,11,14}	Y	n	y
2536	G013.6562-00.5997	18:17:24.38	-17:22:14.8	4.1	14000	47.40	y ^{4,11,14}	y ^{7,12}	Y	y
2540	G014.0329-00.5155	18:17:50.63	-16:59:57.3	1.1	1000	20.30	n	n	n	y
2545	G018.3412+01.7681	18:17:58.11	-12:07:24.8	2.8	22000	33.10	y ^{4,6,11,14}	n ^f	n	y
2547	G016.9270+00.9599	18:18:08.62	-13:45:07.0	2.1	7600	20.90	y ^{4,8,11}	Y	Y	y
2577	G016.9512+00.7806	18:18:50.31	-13:48:53.9	2.4	945	24.90	n	n	n	y
2583 ^H	G017.0332+00.7476A	18:19:07.33	-13:45:23.6	2.4	2734	24.90	n ^e	n	n	y
2584	G010.8411-02.5919	18:19:12.09	-20:47:30.9	1.9	24000	12.30	y ^{4,6,9,11}	y ^{7,12}	Y	...
2586	G014.4335-00.6969	18:19:18.21	-16:43:56.1	1.1	1300	17.50	n	n	n	y
2591 ^Y	G017.4507+00.8118A	18:19:41.88	-13:21:35.4	2.1	2084	21.30	n	Y	Y	y
2611	G014.9958-00.6732	18:20:19.47	-16:13:29.8	2.0	13000	19.40	y ^{8,11}	Y	Y	y
2642	G015.1288-00.6717	18:20:34.60	-16:06:28.2	2.0	12000	19.00	n ^e	n	n	y
2645	G016.9261+00.2854	18:20:35.44	-14:04:13.9	2.4	1300	24.20	y ¹¹	n	n	y
2659	G016.7981+00.1264	18:20:55.28	-14:15:30.8	1.7	956	15.20	n	n	n	y
2690	G017.6380+00.1566	18:22:26.37	-13:30:12.0	2.2	100000	22.10	y ^{4,6,11,14}	n	n	y
2698 ^Y	G017.9642+00.0798A	18:23:20.94	-13:15:05.5	2.2	2835	22.60	y ¹¹	n	n	y
2716 ^H	G018.6608+00.0372A	18:24:50.24	-12:39:22.4	11.0	22300	81.10	y ^{11,14}	Y	y ¹⁰	y
2739	G018.3706-00.3818	18:25:48.36	-13:06:29.2	3.5	5200	44.60	n ^e	n	n	y
2757	G019.8922+00.1023	18:26:57.37	-11:32:09.6	3.4	3700	45.90	n ^e	n	n	y

Table 1—Continued

RMS ^a ID	MSX name	R.A. (J2000.0)	Decl. (J2000.0)	Distance (kpc)	L_{bol} (L_{\odot})	$V_{\text{sys}}^{\text{b}}$ (km s^{-1})	Detection ^c			MMB Coverage
							22 GHz	44 GHz	95 GHz	
2760	G018.8319-00.4788	18:27:02.34	-12:44:38.3	4.5	4300	65.20	n	Y	n	y
2785	G019.9386-00.2079	18:28:10.03	-11:38:21.8	4.2	3400	63.40	n	n	n	y
2788	G019.9224-00.2577	18:28:18.96	-11:40:36.7	4.3	3100	64.90	n ^e	Y	y ¹³	y
2799 ^Y	G020.7617-00.0638B	18:29:12.11	-10:50:36.2	11.8	62000	56.90	y ¹¹	Y	Y	y
2810	G016.8689-02.1552	18:29:24.23	-15:15:48.3	2.0	6600	18.60	y ^{1,4,6,11}	y ^{7,12}	y ²	...
2817	G028.5483+03.7649	18:30:01.36	-02:10:25.6	0.7	132	6.70	n	n	n	...
2821	G021.5624-00.0329	18:30:36.06	-10:07:11.0	9.7	48000	113.60	y ¹¹	n	n	y
2822 ^H	G021.3570-00.1795B	18:30:44.95	-10:22:12.6	10.5	47000	91.20	n	n	n	y
2837	G022.3554+00.0655	18:31:44.08	-09:22:18.5	4.9	11000	84.20	y ^{4,9,11}	Y	Y	y
2844	G023.3891+00.1851	18:33:14.32	-08:23:57.4	4.5	24000	75.50	n ^e	Y	Y	y
2846	G023.8176+00.3841	18:33:19.54	-07:55:37.8	4.5	3900	76.50	y ¹¹	Y	y ¹⁰	y
2853	G026.4207+01.6858	18:33:30.55	-05:01:02.0	2.9	19000	42.20	y ^{4,6,11}	n	n	y
2858 ^H	G024.0946+00.4565B	18:33:34.67	-07:38:49.0	5.2	2497	94.10	n	n	n	y
2879	G025.6498+01.0491	18:34:20.89	-05:59:42.5	3.0	41000	42.80	y ^{1,4,6,9,11}	y ¹²	Y	y
2881 ^H	G026.3819+01.4057A	18:34:25.67	-05:10:50.2	2.9	21400	42.10	y ^{4,6,11}	n	n	y
2901	G023.6566-00.1273	18:34:51.56	-08:18:21.6	3.2	10000	80.40	n	n	n	y
2920	G024.7320+00.1530	18:35:50.91	-07:13:27.2	7.7	12000	108.90	Y ^{11,d}	Y	n	y
2963 ^Y	G026.4958+00.7105A	18:37:07.30	-05:23:58.2	11.8	22300	48.60	n	Y	Y	y
2966 ^E	G025.4118+00.1052B	18:37:16.99	-06:38:24.3	5.2	10493	95.30	n	y ¹²	Y	y
2967	G024.6343-00.3233	18:37:22.68	-07:31:41.5	3.0	6800	42.80	n	n	n	y
2970 ^H	G025.3953+00.0336B	18:37:30.30	-06:41:17.8	16.3	310000	-13.00	y ^{8,11}	n	n	y
2978	G029.8129+02.2195	18:37:50.54	-01:45:37.5	3.0	1300	45.40	y ^{4,11}	n	n	...
2994	G026.2020+00.2262	18:38:18.51	-05:52:57.4	7.5	3600	112.40	n	n	n	y
3003 ^H	G025.4948-00.2990A	18:38:52.85	-06:45:07.8	n	n	n	y
3028 ^H	G026.5254-00.2667A	18:40:40.25	-05:49:12.9	7.5	9144	105.80	Y ^{11,d}	n	n	y
3032 ^H	G027.1852-00.0812B	18:41:13.26	-05:08:57.7	13.0	280000	25.80	y ^{4,11}	n	n	y
3044	G027.7571+00.0500	18:41:47.98	-04:34:52.9	5.4	13000	99.60	n	n	n	y
3049	G028.3373+00.1189	18:42:37.10	-04:02:02.1	4.6	7600	81.00	n ^f	Y	Y	y
3051	G028.2325+00.0394	18:42:42.50	-04:09:45.9	7.4	8600	107.10	n ^e	n	n	y
3056	G027.7954-00.2772	18:43:02.25	-04:41:48.8	3.1	5100	45.90	n	n	n	y
3075	G028.8621+00.0657	18:43:46.24	-03:35:29.2	7.4	94000	103.10	y ^{4,11}	Y	Y	y
3077 ^D	G028.3046-00.3871A	18:44:21.96	-04:17:39.5	10.0	191000	85.50	n ^e	n	n	y
3094	G030.9727+00.5620	18:45:51.68	-01:29:13.0	12.6	27000	23.70	y ¹¹	n	n	y
3099	G029.8620-00.0444	18:45:59.55	-02:45:06.5	4.9	28000	101.20	n	Y	n	y
3105	G029.8390-00.0980	18:46:08.44	-02:47:45.2	4.9	3300	99.20	n	n	n	y
3117 [†]	G030.2971+00.0549	18:46:25.79	-02:19:13.7	4.9	3300	108.10	n ^e	n	n	y
3119	G030.8185+00.2729	18:46:36.58	-01:45:22.4	4.9	8800	97.50	n	n	n	y
3126	G030.1981-00.1691	18:47:03.06	-02:30:36.1	4.9	30000	103.10	n	n	n	y
3145	G029.5904-00.6144	18:47:31.65	-03:15:13.8	4.4	2600	76.50	y ¹¹	n	n	y
3146 ^H	G030.9585+00.0862B	18:47:31.83	-01:42:59.6	11.7	70000	39.60	Y ^{4,11}	n	n	y
3155	G030.5942-00.1273	18:47:37.53	-02:08:19.6	4.9	2000	84.50	n	n	n	y
3158	G030.4117-00.2277	18:47:38.95	-02:20:51.8	4.9	2500	104.80	y ^{8,11}	Y	n	y
3186	G030.9959-00.0771	18:48:10.65	-01:45:25.3	4.9	1700	81.20	n ^e	Y	n	y
3187 ^H	G031.2803+00.0615A	18:48:12.38	-01:26:30.3	4.9	56000	109.00	y ¹¹	Y	Y	y
3205	G032.0451+00.0589	18:49:36.56	-00:45:45.4	4.9	24000	95.30	y ^{4,11}	Y	Y	y
3212	G032.0518-00.0902	18:50:09.25	-00:49:29.1	4.2	3400	70.20	n	n	n	y
3221 ^H	G032.9957+00.0415A	18:51:24.45	+00:04:34.0	9.2	34000	83.80	n ^e	y ¹²	n	y
3223	G033.3891+00.1989	18:51:33.82	+00:29:51.0	5.0	13000	85.30	n ^e	n	n	y
3236	G033.3933+00.0100	18:52:14.63	+00:24:52.6	7.0	17000	103.60	y ¹¹	Y	n	y
3241	G033.5237+00.0198	18:52:26.74	+00:32:08.9	7.0	13000	103.50	n	Y	Y	y

Table 1—Continued

RMS ^a ID	MSX name	R.A. (J2000.0)	Decl. (J2000.0)	Distance (kpc)	L_{bol} (L_{\odot})	$V_{\text{sys}}^{\text{b}}$ (km s^{-1})	Detection ^c			MMB Coverage
							22 GHz	44 GHz	95 GHz	
3254	G034.8211+00.3519	18:53:37.88	+01:50:30.5	3.5	24000	56.90	n ^e	n	n	y
3261	G034.0126-00.2832	18:54:25.05	+00:49:56.6	12.9	31000	11.80	n	n	n	y
3263	G034.0500-00.2977	18:54:32.29	+00:51:32.9	12.9	23000	11.50	n	n	n	y
3265	G035.3449+00.3474	18:54:36.14	+02:18:20.2	6.8	24000	94.30	n	n	n	y
3266	G034.7569+00.0247	18:54:40.72	+01:38:06.8	4.6	12000	76.90	n	n	n	y
3279	G035.8546+00.2663	18:55:49.27	+02:43:20.3	2.0	1600	29.20	n	n	n	y
3282 ^H	G040.5451+02.5961B	18:56:04.57	+07:57:29.2	2.3	40000	33.10	n ^f	n	n	...
3291	G034.7123-00.5946	18:56:48.26	+01:18:47.1	2.9	9700	44.50	n	n	n	y
3292 ^H	G036.9194+00.4825A	18:56:59.78	+03:46:03.9	15.8	26100	-30.50	Y ^{11,d}	n	n	y
3304	G037.4974+00.5301	18:57:53.37	+04:18:17.5	12.8	923	10.90	y ^{4,11}	Y	Y	y
3308	G035.1979-00.7427	18:58:12.99	+01:40:31.2	2.2	35000	33.70	y ^{4,6,11,h}	y ¹²	y ¹⁰	y
3314	G037.5536+00.2008	18:59:09.94	+04:12:15.6	6.7	120000	85.10	y ¹¹	Y	Y	y
3316 ^H	G037.3412-00.0600A	18:59:42.28	+03:53:49.1	9.8	25400	55.80	n	n	n	y
3319	G036.8780-00.4728	19:00:19.81	+03:17:42.9	3.8	5200	60.90	n ^e	n	n	y
3335 ^H	G038.1208-00.2262B	19:01:44.15	+04:30:37.7	6.6	10400	82.30	n	n	n	y
3336	G035.3778-01.6405	19:01:44.54	+01:25:39.6	3.3	5900	43.60	n	n	n	y
3360	G038.9365-00.4592	19:04:03.67	+05:07:53.2	2.8	1500	41.90	y ¹¹	Y	n	y
3371 ^D	G039.9284-00.3741A	19:05:35.27	+06:03:01.3	9.0	7713	60.00	n	n	n	y
3373	G040.2849-00.2378	19:05:45.66	+06:25:52.3	6.4	5300	72.40	Y ^{11,d}	n ^f	n	y
3381	G039.4943-00.9933	19:06:59.68	+05:22:53.4	3.5	8700	53.40	n	n	n	y
3382 ^Y	G042.0977+00.3521A	19:07:00.50	+08:18:44.1	10.9	62000	20.80	y ^{4,11}	n	n	y
3386 ^H	G042.0341+00.1905A	19:07:28.20	+08:10:53.2	11.1	27000	17.80	n	n	n	y
3390	G041.0780-00.6365	19:08:39.25	+06:57:07.7	6.3	3500	73.70	n	n	n	y
3402 ^H	G043.0786+00.0033A	19:10:05.01	+09:01:15.6	11.1	10600	14.40	n ^{e,f}	n	n	y
3414	G043.1635-00.0697A	19:10:30.28	+09:03:45.4	11.1	4900	4.40	n ^{e,f}	n	n	y
3427	G043.9956-00.0111	19:11:51.64	+09:49:40.4	6.0	21000	65.40	Y ^{11,d}	n	n	y
3429	G043.8152-00.1172	19:11:54.20	+09:37:12.7	3.3	795	46.90	y ¹¹	n	n	y
3436	G043.5216-00.6476	19:13:15.46	+09:06:48.9	8.1	1900	58.30	n	n	n	y
3446	G044.2836-00.5249	19:14:14.92	+09:50:43.5	6.0	9800	66.30	n ^e	n	n	y
3448 ^H	G045.4543+00.0600A	19:14:21.31	+11:09:11.7	7.3	152000	59.00	y ¹¹	n	n	y
3457	G045.1894-00.4387	19:15:39.00	+10:41:14.3	5.9	5600	67.30	n	n	n	y
3483	G050.0721+00.5591	19:21:24.82	+15:28:04.4	10.8	14000	-4.50	y ¹¹	Y	Y	y
3489	G049.2982-00.0582	19:22:09.43	+14:29:46.9	5.4	4300	59.30	n	n	n	y
3503 ^H	G048.9897-00.2992A	19:22:26.66	+14:06:46.2	5.4	45000	67.70	y ^{4,11}	Y	Y	y
3504	G049.2015-00.1876	19:22:26.55	+14:20:59.2	5.4	4800	64.90	n	n	n	y
3546	G049.5993-00.2488	19:23:26.61	+14:40:16.9	5.4	1800	56.90	y ¹¹	n	n	y
3550 [†]	G049.4227-00.3715	19:23:32.65	+14:27:28.5	5.4	25000	66.60	n ^{e,f}	n	n	y
3555 ^H	G049.4883-00.3545B	19:23:36.79	+14:31:16.4	5.4	10800	60.10	y ^{4,11}	y ^{7,12,h}	Y	y
3580	G050.7796+00.1520	19:24:17.41	+15:54:01.8	5.3	2900	42.30	n ^e	n	n	y
3585 ^H	G052.2025+00.7217A	19:24:59.84	+17:25:18.1	10.0	29000	0.80	y ¹¹	n	n	y
3586	G052.2078+00.6890	19:25:08.53	+17:24:47.4	9.8	13000	3.80	y ¹¹	Y	Y	y
3587 ^H	G050.2844-00.3925A	19:25:17.79	+15:12:24.5	9.3	190000	16.10	y ¹¹	n	n	y
3588	G049.0431-01.0787	19:25:22.24	+13:47:19.6	3.0	4000	38.70	y ^{6,11}	Y	Y	y
3593	G050.2213-00.6063	19:25:57.77	+15:02:59.6	3.3	13000	40.60	n	n	n	y
3597	G052.9217+00.4142	19:27:34.98	+17:54:38.0	5.1	7300	45.00	n ^e	n	n	y
3603 ^Y	G053.0366+00.1110A	19:28:55.65	+17:51:59.5	9.5	11900	4.80	y ¹¹	y ¹²	Y	y
3608	G053.1417+00.0705	19:29:17.59	+17:56:23.0	1.9	8700	21.70	y ¹¹	Y	y ¹³	y
3609 ^H	G051.4006-00.8893A	19:29:19.70	+15:57:05.5	5.2	5600	62.80	n	n	n	y
3611	G053.6185+00.0376	19:30:23.04	+18:20:26.6	7.9	19000	23.00	n	n	n	y
3621	G052.5405-00.9272	19:31:45.03	+16:55:59.1	5.1	4000	64.70	n	n	n	y

Table 1—Continued

RMS ^a ID	MSX name	R.A. (J2000.0)	Decl. (J2000.0)	Distance (kpc)	L_{bol} (L_{\odot})	$V_{\text{sys}}^{\text{b}}$ (km s^{-1})	Detection ^c			MMB Coverage
							22 GHz	44 GHz	95 GHz	
3625	G053.5343-00.7943	19:33:16.40	+17:52:04.8	5.0	7300	58.50	n	n	n	y
3635	G056.4120-00.0277	19:36:21.53	+20:45:17.9	9.3	22000	-4.40	n ^e	n	n	y
3641	G056.3694-00.6333	19:38:31.63	+20:25:18.7	5.9	8700	32.40	y ^{4,11}	n	n	y
3642	G058.7087+00.6607	19:38:36.83	+23:05:43.5	4.4	3300	30.90	n	n	n	y
3648 ^H	G057.5474-00.2717A	19:39:39.61	+21:37:31.7	8.3	39300	4.30	n	n	n	y
3659	G059.7831+00.0648	19:43:11.23	+23:44:03.6	2.2	22000	22.40	y ^{4,11}	y ¹²	y ²	y
3661	G059.9997+00.1167	19:43:27.78	+23:56:53.0	9.3	9000	-15.20	n	n	n	y
3663	G059.6403-00.1812	19:43:48.53	+23:29:17.9	2.2	1500	27.40	y ¹¹	Y	y ¹³	y
3671 ^H	G060.8828-00.1295B	19:46:20.14	+24:35:29.2	2.2	50000	21.70	n	n	n	...
3683	G063.1140+00.3416	19:49:32.11	+26:45:15.0	4.7	5500	20.00	y ^{4,6,11}	Y	Y	...
3712	G068.2040+00.2387	20:01:59.95	+31:03:10.3	9.0	7000	-35.50	n	n	n	...
3722	G071.8944+01.3107	20:07:04.79	+34:44:42.6	1.4	1500	11.60	n	n	n	...
3724	G073.0633+01.7958	20:08:10.08	+35:59:24.0	1.4	3500	0.60	y ^{4,11}	y ¹²	Y	...
3733 ^H	G072.2479+00.2617A	20:12:17.28	+34:28:11.0	11.3	10700	-71.00	n	n	n	...
3734	G077.5671+03.6911	20:12:33.70	+40:47:40.7	5.7	4500	-21.90	n	n	n	...
3735	G071.5219-00.3854	20:12:57.87	+33:30:26.8	1.4	1700	10.30	y ^{4,6,11}	Y	n	...
3739	G078.1224+03.6320	20:14:25.86	+41:13:36.3	1.4	4000	-3.90	y ^{1,4,6,11}	y ^{7,12}	Y	...
3741	G075.6014+01.6394	20:15:48.15	+38:01:31.2	11.2	8800	-77.50	n	n	n	...
3742	G073.6525+00.1944	20:16:21.96	+35:36:06.2	11.2	100000	-73.40	y ^{4,11}	n	n	...
3746	G072.5056-01.1708	20:18:44.19	+33:53:08.8	7.2	6100	-26.00	n	Y	n	...
3748 ^H	G078.4373+02.6584B	20:19:38.49	+40:56:33.7	1.4	12100	0.90	n	n	n	...
3749	G078.8699+02.7602	20:20:30.60	+41:21:26.6	1.4	6500	7.90	y ^{4,11}	y ¹²	Y	...
3752	G073.6952-00.9996	20:21:18.88	+34:57:50.9	7.4	17000	-31.30	n	n	n	...
3757	G077.8999+01.7678	20:21:55.01	+39:59:45.5	1.4	741	-2.50	n	n	n	...
3760	G079.1272+02.2782	20:23:23.83	+41:17:39.3	1.4	1600	-2.00	n	n	n	...
3761	G076.0902+00.1412	20:23:27.29	+37:34:53.9	1.4	1400	-0.10	y ^{4,d}	n	n	...
3764	G080.0251+02.6933	20:24:20.00	+42:16:01.8	1.4	751	5.20	n	n	n	...
3765 ^Y	G079.8855+02.5517B	20:24:31.68	+42:04:22.4	1.4	2440	5.90	n ^e	n	n	...
3766	G080.1710+02.7450	20:24:33.42	+42:24:58.2	1.4	1300	5.60	Y ^{6,11,d}	Y	n	...
3767	G078.7641+01.6862	20:24:51.66	+40:39:25.2	10.5	13000	-76.30	y ¹¹	n	n	...
3774	G078.3762+01.0191	20:26:32.33	+39:57:20.7	1.4	461	-0.90	n	n	n	...
3775	G078.4754+01.0421	20:26:44.44	+40:02:57.8	1.4	4300	-3.70	Y ^{11,d}	n	n	...
3796	G078.8867+00.7087	20:29:24.86	+40:11:19.4	3.3	200000	-6.00	y ^{1,4,6,11}	Y	Y	...
3808	G079.3398+00.3417	20:32:22.08	+40:20:17.1	1.4	1700	0.20	n	n	n	...
3816	G083.7071+03.2817	20:33:36.51	+45:35:44.0	1.4	3900	-3.60	y ¹¹	n	n	...
3830 ^H	G080.8282+00.5670A	20:36:07.53	+41:40:09.0	1.4	3979	11.50	n	n	n	...
3832	G080.8624+00.3827	20:37:00.93	+41:34:55.8	1.4	2000	-1.90	y ¹¹	Y	Y	...
3838	G081.8652+00.7800	20:38:35.36	+42:37:13.7	1.4	3600	9.40	y ^{1,4,6,11}	y ^{7,12}	y ²	...
3841	G081.7131+00.5792	20:38:57.19	+42:22:40.9	1.4	4900	-3.60	y ^{1,4,11}	y ¹²	y ²	...
3846	G081.7624+00.5916	20:39:03.72	+42:25:29.6	1.4	2600	-4.40	y ^{1,4,11}	y ^{7,12}	Y	...
3856	G084.3065+01.8933	20:41:58.51	+45:14:00.4	10.5	8200	-86.50	n	n	n	...
3859 ^H	G082.5682+00.4040A	20:42:33.76	+42:56:51.3	1.4	7600	-4.10	n	n	n	...
3865	G082.5828+00.2014	20:43:28.49	+42:50:01.8	1.4	654	11.00	y ¹¹	Y	Y	...
3866	G084.1940+01.4388	20:43:36.70	+44:51:54.2	1.4	2100	-1.80	y ¹¹	n	n	...
3878 ^H	G085.4102+00.0032A	20:54:14.36	+44:54:04.5	5.5	42000	-35.80	y ¹¹	n	n	...
3880	G084.9505-00.6910	20:55:32.47	+44:06:10.1	5.5	13000	-34.90	y ¹¹	n	n	...
3887	G090.2095+02.0405	21:03:41.76	+49:51:47.1	7.4	7600	-65.10	n	n	n	...
3892	G089.6368+00.1732	21:09:45.75	+48:10:58.1	6.5	26000	-54.60	n	n	n	...
3894	G095.0531+03.9724	21:15:55.63	+54:43:31.0	8.7	12000	-84.10	y ^{4,6,11}	Y	Y	...
3895	G093.1610+01.8687	21:17:14.17	+51:54:23.0	6.8	8800	-63.10	n ^e	n	n	...

Table 1—Continued

RMS ^a ID	MSX name	R.A. (J2000.0)	Decl. (J2000.0)	Distance (kpc)	L_{bol} (L_{\odot})	$V_{\text{sys}}^{\text{b}}$ (km s^{-1})	Detection ^c			MMB Coverage
							22 GHz	44 GHz	95 GHz	
3906	G094.3228-00.1671	21:31:45.11	+51:15:35.3	4.4	5700	-38.40	n	n	n	...
3910 ^Y	G097.5268+03.1837B	21:32:11.29	+55:53:39.9	7.0	84000	-70.00	y ^{1,4,11}	Y	Y	...
3911	G094.2615-00.4116	21:32:30.59	+51:02:16.0	5.2	9000	-46.60	y ^{4,6,11}	y ^{7,12}	n	...
3914	G094.4637-00.8043	21:35:09.11	+50:53:09.6	5.0	21000	-44.60	y ^{4,6,11}	n	n	...
3915 ^H	G096.4353+01.3233A	21:35:21.23	+53:47:12.0	7.0	18700	-68.90	n ^e	n	n	...
3916	G096.5438+01.3592	21:35:43.82	+53:53:09.3	7.0	18000	-69.40	n	n	n	...
3917	G094.6028-01.7966	21:39:58.25	+50:14:20.9	4.9	43000	-43.90	y ^{4,6,11}	n	n	...
3919 ^Y	G095.0026-01.5779A	21:40:57.34	+50:39:58.5	4.5	4546	-40.00	n ^e	n	n	...
3922	G097.9978+01.4688	21:42:43.19	+54:55:51.9	6.5	5000	-65.80	n	n	n	...
3927	G100.1685+02.0266	21:52:02.77	+56:44:59.7	6.0	8400	-62.40	n	n	n	...
3928	G100.2124+01.8829	21:52:57.15	+56:39:54.2	5.9	8300	-61.90	n ^e	n	n	...
3933	G101.2490+02.5764	21:55:45.55	+57:51:05.6	6.1	4300	-65.00	n	n	n	...
3935	G102.3533+03.6360	21:57:25.19	+59:21:56.6	8.4	110000	-88.60	y ^{4,11}	n	n	...
3936	G102.3340+03.6094	21:57:26.08	+59:19:54.1	8.3	6600	-87.50	y ¹¹	n	n	...
3939	G103.8744+01.8558	22:15:09.08	+58:49:07.8	1.6	6800	-18.30	n	n	n	...
3940	G100.3779-03.5784	22:16:10.35	+52:21:34.7	3.7	17000	-37.60	y ^{4,11}	n	n	...
3941 ^Y	G102.8051-00.7184B	22:19:09.11	+56:05:00.3	4.0	5900	-43.50	n ^e	n	n	...
3945	G103.8034+00.4062	22:20:46.17	+57:34:17.2	5.7	4200	-63.40	y ¹¹	n	n	...
3949	G105.5072+00.2294	22:32:23.85	+58:18:59.8	4.6	7000	-52.30	n	n	n	...
3958 ^Y	G108.5955+00.4935C	22:52:38.09	+60:01:01.1	4.3	9700	-51.20	y ^{1,4,6,11}	y ¹²	Y	...
3960 ^H	G107.6823-02.2423A	22:55:29.82	+57:09:24.9	4.7	8200	-55.10	n	n	n	...
3963	G109.8715+02.1156	22:56:17.98	+62:01:49.7	0.7	15000	-11.10	y ^{1,4,6,11}	Y	Y	...
3968	G108.7575-00.9863	22:58:47.25	+58:45:01.6	4.3	14000	-51.50	y ^{4,11}	n	n	...
3970	G109.0775-00.3524	22:58:59.08	+59:27:36.4	4.0	2400	-48.10	y ¹¹	n	n	...
3972	G108.4714-02.8176	23:02:32.07	+56:57:51.3	4.5	5100	-53.80	y ^{1,4,11}	n	n	...
3976	G110.0931-00.0641	23:05:25.16	+60:08:15.4	4.3	17000	-53.10	y ^{6,11}	y ¹²	Y	...
3980 ^Y	G111.5234+00.8004A	23:13:32.39	+61:29:06.2	2.6	6700	-58.60	y ¹¹	n ^f	n	...
3982	G111.5320+00.7593	23:13:43.91	+61:26:57.7	2.6	4600	-56.10	y ^{1,4,6,11}	y	y ²	...
3985	G111.5851+00.7976	23:14:01.71	+61:30:17.8	2.6	1800	-56.60	Y ^{11,d}	n	n	...
3986	G111.5671+00.7517	23:14:01.75	+61:27:19.8	2.6	23000	-57.20	y ¹¹	Y	Y	...
3991	G111.8904+00.9894	23:15:50.03	+61:47:39.7	2.6	6600	-48.50	Y ^{11,d}	n	n	...
3992 ^H	G111.2824-00.6639A	23:16:04.00	+60:02:00.6	3.5	48000	-44.10	y ^{4,6,11}	n	n	...
3996	G111.2552-00.7702	23:16:10.39	+59:55:28.2	3.5	11000	-44.70	y ^{1,4,6,11}	Y	Y	...
3998	G111.2348-01.2385	23:17:21.01	+59:28:48.0	4.4	42000	-54.40	y ^{4,6,11}	y ¹²	Y	...
3999	G110.8038-02.5649	23:17:52.26	+58:05:11.0	2.7	654	-34.60	n	n	n	...
4004	G114.0835+02.8568	23:28:27.76	+64:17:38.4	4.2	7100	-53.20	n	n	n	...
4365	G032.8205-00.3300	18:52:24.60	-00:14:57.7	4.7	10000	79.30	y ¹¹	Y	Y	y
4741 ^Y	G136.8283+01.0635B	02:49:04.04	+60:43:17.0	2.5	562	-34.30	n	n	n	...
4745	G173.4815+02.4459	05:39:13.02	+35:45:51.3	2.0	7600	-16.20	y ^{1,4,6,11}	y ^{7,12}	y ²	...
4747	G183.3485-00.5751	05:51:11.15	+25:46:16.4	2.0	3800	-9.40	y ⁶	y ¹²	Y	...
4748	G197.1387-03.0996	06:10:49.94	+12:32:45.2	3.4	1000	21.00	n	n	n	...
4751	G238.9590-01.6835	07:35:15.23	-23:48:45.9	7.2	1200	82.30	n	n	n	y
4888	G019.8817-00.5347	18:29:14.68	-11:50:23.6	3.3	4700	43.50	y ^{11,14}	Y	y ¹⁰	y
4905	G030.8786+00.0566	18:47:28.85	-01:48:07.1	4.9	2200	75.10	n	n	n	y
4910	G030.9726-00.1410	18:48:22.03	-01:48:30.3	4.9	2700	77.50	y ¹¹	Y	n	y
4924 ^H	G039.3880-00.1421B	19:03:45.15	+05:40:44.4	4.3	14400	66.30	n ^e	Y	y ¹⁰	y
4941	G059.8329+00.6729	19:40:59.32	+24:04:44.1	2.2	570	34.40	y ^{4,11}	y ¹²	Y	y
4952 [†]	G093.0166+02.4953	21:13:39.09	+52:14:05.1	n	n	n	...
4954	G100.0141+02.3591	21:49:38.26	+56:54:36.5	5.9	1300	-61.70	n	n	n	...

^aFor multiple RMS sources within a $20''$ radius, the superscript Y, H, D, and E indicate the type of nearby sources as YSO, HII region, Diffuse HII region and Evolved stars, respectively. Dagger symbol represents the single source finally classified with HII region, of which its type was YSO at the observation time.

^bThe systemic velocity from the RMS archives.

^cY: New detection, y: detection, n: non-detection

^dDetected in this survey but not detected in Urquhart et al. (2011).

^eDetected in Urquhart et al. (2011) but not detected in this survey.

^fMaser emission was detected by the first sidelobe.

^gAdopted distance from nearby known YSO, VV Mon (Testi et al. 1998).

^hMaser emission was detected not only by the main beam but also by the first sidelobe at different velocities.

References. — 1. Han et al. (1995), 2. Val'tts et al. (1995), 3. Han et al. (1998), 4. Valdetaro et al. (2001), 5. Kurtz et al. (2004), 6. Sunada et al. (2007), 7. Val'tts et al. (2007), 8. Urquhart et al. (2009), 9. Breen et al. (2011), 10. Chen et al. (2011), 11. Urquhart et al. (2011), 12. Bayandina et al. (2012), 13. Chen et al. (2012), 14. Titmarsh et al. (2014)

Table 2. Summary of Observations

Telescope	Maser Transition	Frequency (GHz)	FWHM (")	η_A	Velocity Resolution (km s ⁻¹)	Velocity Coverage (km s ⁻¹)	T _{sys} (K)	f^a (Jy K ⁻¹)
KVN 21m	H ₂ O 6 ₁₆ -5 ₂₃	22.235080	120	0.6	0.105	431	60–200	13.3
	CH ₃ OH 7 ₀ -6 ₁ A ⁺	44.069430	62	0.6	0.053	218	120–350	13.3
	CH ₃ OH 8 ₀ -7 ₁ A ⁺	95.169463	32	0.5	0.025	101	160–470	16.0
	HCO ⁺ J=1–0	89.188523	32	0.4 ^b	0.026	108	170–200	
TRAO 14m	¹³ CO J=1–0	110.201353	48	0.5 ^b	0.703	300	600–700	

^aThe conversion factor from T_A^{*} to flux density.

^bThe main-beam efficiency.

Table 3. Summary of Detections

Maser	Epoch	Number	Detection Rate (%)
22 GHz	2011	126	42
	2012	112	37
	Subtotal	135	45
44 GHz	2011	76	25
	2012	81	27
	Subtotal	83	28
95 GHz	2012	68	23
Any	Both	151	51

Table 4. Detected Maser Line Parameters

RMS ID	Maser	Epoch (yyymmdd)	Station ^a	V_p (km s ⁻¹)	S_p (Jy)	$\int S_\nu dv$ (Jy km s ⁻¹)	V_{min} (km s ⁻¹)	V_{max} (km s ⁻¹)	V_{range} (km s ⁻¹)	L_{maser} (L_\odot)	Notes ^b
4	22	20110326	YS	-43.00	6.4	4.7	-43.42	-42.58	0.84	8.55E-07	
7	22	20110324	YS	-83.03	3.6	1.7	-83.24	-82.82	0.42	1.26E-06	
		20120212	YS	-81.56	5.1	3.0	-81.56	-81.13	0.42	2.18E-06	
18	22	20110411	US	-52.96	4.1	2.9	-53.17	-52.54	0.63	1.12E-06	
35	22	20110322	YS	-39.04	1221.6	4519.8	-56.10	-24.71	31.39	4.19E-04	
		20120521	YS	-42.62	841.7	4096.1	-62.21	-25.56	36.66	3.80E-04	
	44	20110322	YS	-42.55	1.2	1.0	-42.55	-42.55	0.21	1.92E-07	
		20120521	YS	-42.55	2.2	5.2	-43.62	-40.64	2.98	9.50E-07	
	95	20120521	YS	-43.24	3.0	6.0	-43.63	-41.27	2.36	2.39E-06	
37	22	20110322	YS	-39.02	3432.2	12782.0	-56.29	-24.48	31.81	1.19E-03	
		20120212	YS	-42.39	4552.1	14832.7	-54.82	-25.11	29.70	1.38E-03	
46	22	20110327	YS	-65.93	13.5	7.6	-66.35	-65.51	0.84	7.02E-07	
		20121012	TN	-42.34	4.3	2.8	-42.55	-41.91	0.63	2.63E-07	
49	22	20110322	YS	-72.45	17.4	47.9	-80.66	-63.60	17.06	4.00E-05	
		20120214	YS	-69.08	24.2	70.1	-78.14	-64.02	14.11	5.85E-05	
53	22	20110323	YS	-45.88	6.8	3.8	-46.30	-45.67	0.63	8.99E-07	
		20120521	YS	-41.03	3.2	4.6	-46.30	-40.61	5.69	1.08E-06	
58	22	20110323	YS	-35.39	2.3	3.6	-35.39	-25.70	9.69	8.55E-07	
		20120214	YS	-22.75	9.7	7.1	-23.17	-22.12	1.05	1.68E-06	
61	22	20110322	YS	-31.84	2.5	1.5	-31.84	-31.42	0.42	1.99E-07	
63	22	20110411	US	-6.42	4.3	2.4	-6.63	-6.00	0.63	3.61E-08	
		20120216	YS	-7.26	11.4	7.7	-7.47	-6.84	0.63	1.14E-07	
84	22	20110327	YS	-15.96	6.6	6.0	-17.02	-12.80	4.21	5.00E-07	
		20120521	YS	-20.81	12.4	18.0	-21.23	-14.07	7.16	1.51E-06	
88	22	20110325	YS	-29.82	233.8	211.7	-30.87	-28.77	2.11	1.96E-05	
		20120301	YS	-30.03	216.0	194.4	-30.87	-26.03	4.85	1.80E-05	
91	22	20110331	YS	-5.50	135.8	297.1	-10.14	5.66	15.80	2.76E-05	
		20120310	YS	-0.87	234.5	335.3	-13.30	5.66	18.96	3.11E-05	
	44	20110331	YS	-3.34	6.2	8.2	-3.98	-1.64	2.34	1.51E-06	
		20120310	YS	-3.13	7.0	2.4	-3.34	-3.13	0.21	4.35E-07	
	95	20120310	YS	-3.33	5.8	5.5	-3.92	-2.74	1.18	2.16E-06	
106	22	20120320	YS	-19.57	1.8	0.4	-19.57	-19.57	0.21	3.57E-08	
113	22	20110412	US	-3.83	3.4	1.8	-4.04	-3.41	0.63	1.66E-07	
121	22	20110401	YS	7.21	53.3	84.6	-3.75	12.05	15.80	6.36E-06	
		20130430	YS	-3.11	24.8	45.5	-3.75	7.84	11.59	3.42E-06	
	44	20110401	YS	3.05	7.0	11.7	1.56	4.11	2.55	1.75E-06	
		20130430	YS	3.05	6.4	14.5	1.13	4.75	3.61	2.16E-06	
	95	20130430	YS	3.08	6.4	13.4	1.50	4.45	2.95	4.32E-06	
	6.7		MMB			444.0				1.00E-05	
125	22	20110402	YS	18.42	4.4	3.3	18.00	18.63	0.63	3.08E-07	
131	22	20110322	YS	6.03	394.3	671.7	-9.56	11.72	21.28	6.23E-05	
		20120215	YS	3.29	251.0	577.6	-0.29	15.30	15.59	5.36E-05	
	44	20110322	YS	7.35	5.9	7.1	6.50	7.98	1.49	1.30E-06	
		20120215	YS	7.35	6.7	5.6	6.92	8.41	1.49	1.03E-06	
	95	20120215	YS	7.18	4.4	11.6	5.21	9.54	4.33	4.61E-06	
	6.7		MMB			64.0				1.78E-06	
133	22	20110402	YS	17.90	5.7	2.4	17.69	18.11	0.42	2.23E-07	
	44	20110402	YS	16.48	3.4	2.3	16.48	17.33	0.85	4.28E-07	
		20130421	US	16.48	2.4	1.4	14.57	16.70	2.13	2.59E-07	
	95	20130421	US	16.47	5.9	7.5	13.32	17.65	4.33	2.97E-06	
135	22	20110324	YS	19.58	363.6	204.0	18.11	20.42	2.32	1.33E-04	
		20120215	YS	19.58	301.1	170.1	18.32	20.21	1.90	1.11E-04	
	6.7		MMB			16.0				3.12E-06	
145	22	20110402	YS	125.07	7.5	19.9	122.34	127.18	4.85	1.15E-05	D
		20121011	TN	125.71	8.6	30.0	121.70	127.81	6.11	1.74E-05	D
149	22	20110329	YS	-8.29	2.4	1.1	-8.29	-8.08	0.21	9.31E-09	
		20120310	YS	7.72	6.7	2.4	7.51	7.93	0.42	2.01E-08	
	44	20110329	YS	7.35	136.4	91.7	6.07	9.47	3.40	1.52E-06	
		20120310	YS	7.35	100.2	59.2	7.13	7.98	0.85	9.78E-07	
	95	20120310	YS	7.18	43.4	32.7	5.80	8.56	2.76	1.17E-06	
153	22	20110325	YS	45.53	10.0	14.1	44.26	47.42	3.16	7.22E-06	H
		20120215	YS	46.58	7.9	13.0	40.05	76.71	36.66	6.65E-06	
	44	20110325	YS	44.73	23.4	15.7	44.31	45.37	1.06	1.59E-05	
		20120215	YS	44.73	18.2	11.9	44.52	45.16	0.64	1.21E-05	
	95	20120215	YS	44.58	12.0	7.1	44.38	45.17	0.79	1.56E-05	
175	22	20110327	YS	27.82	7.2	14.7	24.87	30.56	5.69	1.65E-06	

Table 4—Continued

RMS ID	Maser	Epoch (yyymmdd)	Station ^a	V_p (km s ⁻¹)	S_p (Jy)	$\int S_\nu dv$ (Jy km s ⁻¹)	V_{\min} (km s ⁻¹)	V_{\max} (km s ⁻¹)	V_{range} (km s ⁻¹)	L_{maser} (L_\odot)	Notes ^b
189	22	20120303	YS	26.13	15.5	29.0	24.87	34.56	9.69	3.25E-06	
		20110325	YS	46.79	35.6	42.0	45.94	59.21	13.27	1.64E-05	
		20120215	YS	46.79	19.9	31.9	42.78	57.53	14.75	1.24E-05	
196	6.7		MMB			87.0				1.75E-06	
203	22	20110327	YS	42.07	25.9	58.4	37.44	60.40	22.96	2.17E-05	
		20121009	TN	41.65	80.0	116.5	39.54	59.98	20.44	4.32E-05	
2360	22	20110410	US	11.45	25.7	24.4	4.29	12.08	7.79	4.76E-06	
		20120606	YS	14.19	2.8	1.4	13.77	14.19	0.42	2.76E-07	
2389	22	20110321	YS	17.19	10.7	30.0	13.40	25.40	12.01	5.08E-06	
		20120621	YS	23.51	10.5	30.4	13.19	24.14	10.95	5.14E-06	
2434	22	20110321	YS	29.27	42.0	54.7	28.01	32.85	4.85	7.31E-06	
		20120605	YS	29.27	121.4	174.7	28.22	32.64	4.42	2.33E-05	
	44	20110321	YS	31.41	19.4	23.1	31.20	34.60	3.40	6.10E-06	
		20120605	YS	31.41	20.5	25.9	30.77	34.38	3.61	6.85E-06	
	95	20120605	YS	31.41	21.9	30.8	31.22	34.17	2.95	1.76E-05	
2437	6.7		MMB			114.0				9.76E-05	
2445	44	20110321	YS	52.65	3.2	5.2	49.03	52.86	3.83	3.42E-05	
		20130426	US	52.65	4.3	6.5	48.82	52.86	4.04	4.29E-05	
	95	20130426	US	49.40	4.0	7.5	48.81	52.94	4.13	1.07E-04	
	6.7		MMB			17.0				1.70E-05	
2490	22	20110322	YS	34.43	11.4	33.2	-8.34	60.13	68.47	4.43E-06	H
		20120618	YS	-7.91	15.8	40.1	-8.55	36.96	45.50	5.36E-06	H
	44	20110322	YS	36.60	10.8	27.0	35.75	40.00	4.25	7.15E-06	
		20120618	YS	36.38	9.6	23.4	35.75	39.79	4.04	6.19E-06	
	95	20120618	YS	36.37	9.3	18.6	35.38	39.52	4.13	1.06E-05	
2491	44	20110410	US	54.05	5.1	2.3	53.83	54.26	0.43	2.14E-06	
		20120621	YS	53.83	2.5	2.4	53.41	54.26	0.85	2.19E-06	
2529	22	20110322	YS	26.19	24.9	53.9	7.65	33.56	25.91	8.45E-06	
		20120605	YS	26.19	25.0	45.1	21.13	33.56	12.43	7.07E-06	
	44	20110322	YS	24.98	28.8	51.9	20.95	27.54	6.59	1.61E-05	
		20120605	YS	24.98	27.9	47.1	22.86	27.54	4.68	1.46E-05	
	95	20120605	YS	25.16	24.7	46.6	22.60	26.15	3.54	3.13E-05	
2535	22	20110411	US	27.99	20.3	45.0	-7.83	30.52	38.34	8.78E-06	H
		20130419	YS	28.20	17.2	32.7	-7.83	30.31	38.13	6.38E-06	H
	44	20130419	YS	30.36	3.5	1.4	30.15	30.36	0.21	5.42E-07	
	6.7		MMB			8.0				4.68E-07	
2536	22	20110322	YS	42.00	7.7	48.5	36.31	54.85	18.54	1.89E-05	
		20120605	YS	49.16	25.2	61.1	37.57	50.00	12.43	2.38E-05	
	44	20110322	YS	48.37	50.5	67.0	45.82	49.65	3.83	5.17E-05	
		20120605	YS	48.58	52.4	67.2	46.25	49.65	3.40	5.19E-05	
	95	20120605	YS	48.37	40.5	51.6	46.20	48.76	2.56	8.60E-05	
2545	22	20110322	YS	12.26	16.8	64.0	7.20	46.39	39.18	1.16E-05	
		20120613	YS	31.85	5.8	3.0	31.64	32.06	0.42	5.49E-07	
	6.7		MMB			49.0				2.67E-06	
2547	22	20110411	US	-70.93	128.4	364.2	-75.56	-60.60	14.96	3.73E-05	D
		20120620	YS	-65.45	945.0	2113.3	-71.98	-61.02	10.95	2.16E-04	D
	44	20110411	US	19.50	4.6	1.9	19.28	19.50	0.21	3.79E-07	
		20120620	YS	19.50	2.8	3.8	19.07	21.62	2.55	7.66E-07	
	95	20120620	YS	19.98	2.3	1.6	19.78	21.56	1.77	7.14E-07	
2584	22	20110321	YS	-82.03	75.1	246.2	-87.93	-78.66	9.27	2.06E-05	D
		20120605	YS	-69.39	4.8	14.1	-82.66	-68.34	14.33	1.18E-06	D
	44	20110321	YS	13.26	118.3	104.0	11.98	14.75	2.76	1.72E-05	
		20120605	YS	13.26	146.3	126.4	11.98	14.32	2.34	2.10E-05	
	95	20120605	YS	13.15	111.8	84.4	11.97	13.74	1.77	3.02E-05	
2591	44	20110412	US	20.96	14.0	6.5	20.53	21.17	0.64	1.31E-06	
		20120618	YS	20.96	8.2	3.6	20.75	21.17	0.43	7.39E-07	
	95	20120618	YS	20.90	5.4	2.1	20.70	21.10	0.39	9.29E-07	
2611	22	20110322	YS	21.90	29.8	102.6	-0.43	35.17	35.60	9.52E-06	
		20120623	YS	21.06	20.7	38.5	19.58	22.53	2.95	3.57E-06	
	44	20110322	YS	19.00	8.4	9.1	17.30	19.21	1.91	1.68E-06	
		20120623	YS	19.00	5.2	6.4	16.66	19.21	2.55	1.17E-06	
	95	20120623	YS	19.09	3.2	4.5	17.91	19.09	1.18	1.79E-06	
2645	22	20120612	YS	27.25	6.4	3.8	27.04	27.47	0.42	5.09E-07	
2690	22	20110322	YS	23.03	10.2	35.3	16.50	30.19	13.69	3.96E-06	
		20120613	YS	23.45	29.0	43.0	16.50	26.40	9.90	4.83E-06	
	6.7		MMB			5.9				1.98E-07	

Table 4—Continued

RMS ID	Maser	Epoch (yyymmdd)	Station ^a	V_p (km s ⁻¹)	S_p (Jy)	$\int S_\nu dv$ (Jy km s ⁻¹)	V_{min} (km s ⁻¹)	V_{max} (km s ⁻¹)	V_{range} (km s ⁻¹)	L_{maser} (L_\odot)	Notes ^b
2698	22	20110412	US	26.59	4.3	5.9	21.74	26.80	5.06	6.59E-07	
2716	22	20110322	YS	26.68	3.3	14.8	26.26	78.09	51.82	4.16E-05	H
		20130427	US	42.48	5.6	13.5	40.80	82.51	41.71	3.79E-05	H
	44	20110322	YS	79.18	5.6	12.2	78.55	82.16	3.61	6.80E-05	
		20130427	US	79.40	7.0	16.9	77.48	82.16	4.68	9.42E-05	
	95	20130427	US	80.28	4.0	9.6	78.11	82.05	3.94	1.16E-04	
2760	44	20110412	US	64.90	2.8	2.6	64.90	65.96	1.06	2.46E-06	
2788	44	20110412	US	64.02	25.1	44.6	61.26	65.72	4.46	3.79E-05	
		20120607	YS	64.45	22.5	36.9	61.90	65.51	3.61	3.13E-05	
	95	20120607	YS	64.01	14.6	25.8	62.43	65.19	2.76	4.73E-05	
2799	22	20110323	YS	59.61	49.8	70.0	55.81	60.87	5.06	2.26E-04	
		20120605	YS	59.82	19.9	37.4	55.81	60.45	4.63	1.21E-04	
	44	20110323	YS	55.83	5.7	12.1	54.98	58.60	3.61	7.73E-05	
		20120605	YS	56.05	6.0	7.4	55.83	57.75	1.91	4.75E-05	
	95	20120605	YS	56.33	7.9	11.3	55.93	57.51	1.58	1.57E-04	
2810	22	20110411	US	22.84	72.4	119.2	-1.18	25.79	26.97	1.11E-05	
		20120605	YS	19.47	77.3	141.2	-10.02	33.58	43.61	1.31E-05	
	44	20110411	US	17.62	126.3	293.6	13.58	29.10	15.52	5.39E-05	
		20120605	YS	17.62	113.8	250.4	14.65	22.51	7.87	4.60E-05	
	95	20120605	YS	17.48	55.5	142.0	16.30	21.42	5.12	5.64E-05	
2821	22	20120613	YS	114.13	7.8	3.1	113.92	114.55	0.63	6.69E-06	
	6.7		MMB			18.3				1.20E-05	
2837	22	20110323	YS	87.32	15.6	21.4	75.31	88.17	12.85	1.19E-05	
		20120605	YS	87.32	25.9	40.2	8.53	89.01	80.48	2.24E-05	H
	44	20110323	YS	84.00	49.9	29.5	82.51	84.42	1.91	3.25E-05	
		20120605	YS	84.00	57.1	30.8	83.15	84.42	1.28	3.39E-05	
	95	20120605	YS	83.89	42.9	22.8	83.69	84.28	0.59	5.42E-05	
2844	44	20110323	YS	77.72	5.5	3.2	76.23	77.72	1.49	2.98E-06	
		20120621	YS	77.72	7.2	5.0	76.23	77.93	1.70	4.65E-06	
	95	20120621	YS	77.78	9.5	4.1	76.21	77.78	1.58	8.20E-06	
	6.7		MMB			66.9				9.42E-06	
2846	22	20120621	YS	68.19	7.9	9.0	66.93	68.61	1.69	4.25E-06	
	44	20110413	US	75.38	9.3	14.7	71.34	78.36	7.02	1.37E-05	
		20120621	YS	75.38	7.5	11.1	71.56	75.60	4.04	1.03E-05	
	95	20120621	YS	75.03	2.6	8.1	72.66	77.39	4.73	1.63E-05	
2853	22	20110324	YS	58.95	5.5	6.1	58.53	60.00	1.47	1.20E-06	
	6.7		MMB			2.6				1.52E-07	
2879	22	20110323	YS	41.91	2573.3	2314.1	-14.55	67.40	81.95	4.83E-04	H
		20140521	TN	41.07	272.5	435.7	-12.02	67.40	79.42	9.10E-05	H
	44	20110323	YS	41.73	58.7	56.6	40.46	45.35	4.89	2.34E-05	
		20140521	TN	41.73	59.6	58.7	40.46	45.77	5.31	2.43E-05	
	95	20140521	TN	41.71	50.2	79.8	38.75	45.77	7.28	7.12E-05	
	6.7		MMB			48.7				3.05E-06	
2881	22	20120612	YS	40.73	13.0	9.8	40.10	41.15	1.05	1.91E-06	
2901	6.7		MMB			37.8				2.69E-06	
2920	22	20110323	YS	102.92	2.6	4.2	102.71	105.66	2.95	5.74E-06	
	44	20110323	YS	109.50	1.4	2.2	109.50	110.35	0.85	6.10E-06	
2963	44	20110324	YS	47.87	10.3	10.3	47.66	49.15	1.49	6.57E-05	
		20120611	YS	47.87	7.8	7.1	47.66	48.94	1.28	4.53E-05	
	95	20120611	YS	48.46	3.8	5.8	47.48	49.64	2.17	7.97E-05	
2966	44	20110413	US	95.33	10.7	14.1	94.91	97.46	2.55	1.75E-05	
		20120616	YS	95.33	9.8	10.3	94.70	96.40	1.70	1.27E-05	
	95	20120616	YS	95.38	7.9	8.9	95.18	97.15	1.97	2.38E-05	
2967	6.7		MMB			4.5				2.82E-07	
2970	22	20110322	YS	-15.88	16.4	23.6	-17.14	-10.19	6.95	1.46E-04	
		20120613	YS	-15.88	14.2	16.8	-17.14	-13.35	3.79	1.03E-04	
2978	22	20110414	US	56.74	5.1	6.4	56.32	60.53	4.21	1.33E-06	
3028	22	20110324	YS	109.29	3.7	3.5	108.24	109.71	1.47	4.53E-06	
	6.7		MMB			3.5				1.37E-06	
3032	22	20110324	YS	17.31	473.9	1737.1	12.89	64.29	51.40	6.81E-03	H
		20120616	YS	19.21	386.0	1333.7	14.99	50.81	35.81	5.23E-03	
3044	6.7		MMB			0.5				1.01E-07	
3049	44	20110324	YS	81.52	6.8	9.1	80.46	83.01	2.55	8.85E-06	
		20120611	YS	81.52	5.5	4.9	81.31	82.37	1.06	4.75E-06	
	95	20120611	YS	82.12	3.4	3.4	81.33	82.12	0.79	7.17E-06	
3075	22	20110325	YS	105.19	161.5	502.9	84.75	108.14	23.38	6.39E-04	

Table 4—Continued

RMS ID	Maser	Epoch (yyymmdd)	Station ^a	V_p (km s ⁻¹)	S_p (Jy)	$\int S_\nu dv$ (Jy km s ⁻¹)	V_{\min} (km s ⁻¹)	V_{\max} (km s ⁻¹)	V_{range} (km s ⁻¹)	L_{maser} (L_\odot)	Notes ^b
		20120605	YS	105.19	125.2	399.9	88.75	106.87	18.12	5.08E-04	
	44	20110325	YS	103.36	15.2	13.8	102.72	104.85	2.13	3.47E-05	
		20120605	YS	103.36	17.5	17.1	102.08	104.64	2.55	4.30E-05	
	95	20120605	YS	103.25	24.7	20.6	102.85	103.84	0.98	1.12E-04	
3077	6.7		MMB			54.7				3.80E-05	
3094	22	20110325	YS	27.65	3.2	6.4	14.38	30.81	16.43	2.37E-05	
	6.7		MMB			0.3				3.31E-07	
3099	44	20110325	YS	100.86	4.0	6.8	98.31	102.13	3.83	7.53E-06	
		20120614	YS	100.86	4.1	1.7	100.86	101.07	0.21	1.91E-06	
3119	6.7		MMB			2.2				3.67E-07	
3126	6.7		MMB			30.4				5.07E-06	
3145	22	20110413	US	80.97	5.7	4.1	80.55	81.39	0.84	1.83E-06	
		20130421	YS	74.65	6.8	4.8	74.23	75.07	0.84	2.17E-06	
3146	22	20110325	YS	39.02	22.8	59.0	-58.31	41.76	100.07	1.87E-04	H
		20130427	US	-53.26	11.0	75.6	-65.90	58.40	124.30	2.40E-04	H
3158	22	20110419	US	58.26	9.0	33.4	52.99	60.15	7.16	1.86E-05	D
		20120623	YS	51.94	12.4	38.5	48.57	111.56	62.99	2.14E-05	H
	44	20110414	US	104.87	9.3	21.8	102.11	107.00	4.89	2.41E-05	
		20120623	YS	104.66	5.3	11.9	102.11	106.79	4.68	1.31E-05	
3186	44	20110414	US	82.35	3.0	4.4	80.86	82.77	1.91	4.89E-06	
		20120612	YS	82.77	2.7	3.1	81.50	82.77	1.28	3.47E-06	
3187	22	20110325	YS	113.90	24.2	20.1	101.26	114.54	13.27	1.12E-05	
	44	20130426	US	106.74	10.1	28.7	104.21	113.06	8.85	1.60E-05	
		20110325	YS	109.12	13.8	39.5	105.72	111.67	5.95	4.36E-05	
		20130426	US	109.33	11.9	38.4	105.72	113.80	8.08	4.23E-05	
	95	20130426	US	109.25	10.4	38.5	104.92	111.62	6.69	9.18E-05	
	6.7		MMB			158.6				2.65E-05	
3205	22	20110325	YS	97.33	6.7	15.9	94.38	102.59	8.22	8.88E-06	
		20120606	YS	92.90	7.3	10.8	92.69	94.59	1.90	6.02E-06	
	44	20110325	YS	95.26	16.9	30.3	92.71	98.02	5.31	3.34E-05	
		20120606	YS	95.26	12.0	22.3	93.77	98.02	4.25	2.45E-05	
	95	20120606	YS	94.81	6.7	10.8	94.02	95.99	1.97	2.57E-05	
	6.7		MMB			139.1				2.32E-05	
3221	44	20110325	YS	83.22	4.7	3.5	82.58	83.43	0.85	1.37E-05	
		20120623	YS	83.22	5.6	3.7	82.58	83.43	0.85	1.43E-05	
3236	22	20110326	YS	98.06	2.3	3.4	74.04	98.06	24.02	3.91E-06	
	44	20110326	YS	103.17	2.5	2.2	103.17	104.24	1.06	5.05E-06	
		20120606	YS	103.17	2.3	2.5	103.17	104.02	0.85	5.54E-06	
	6.7		MMB			35.4				1.21E-05	
3241	44	20110414	US	104.87	3.7	1.4	104.87	105.08	0.21	3.08E-06	
		20120623	YS	104.87	3.8	1.6	104.66	105.08	0.43	3.54E-06	
	95	20120623	YS	105.26	1.1	0.2	105.07	105.07	0.20	1.04E-06	
3266	6.7		MMB			0.8				1.18E-07	
3292	22	20110323	YS	-30.80	5.1	6.2	-31.86	-30.17	1.69	3.59E-05	
	6.7		MMB			0.4				6.94E-07	
3304	22	20110326	YS	11.32	49.5	169.5	-5.54	27.75	33.29	6.44E-04	
		20130421	YS	11.53	47.3	159.7	-14.18	27.33	41.50	6.07E-04	
	44	20130421	YS	12.44	3.0	1.0	12.22	12.44	0.21	7.76E-06	
	95	20130421	YS	12.16	2.6	4.0	9.99	12.94	2.95	6.57E-05	
3308	22	20110322	YS	23.30	75.9	58.6	22.67	23.72	1.05	6.58E-06	
		20120518	YS	20.77	13.2	8.0	20.35	20.98	0.63	8.95E-07	
	44	20110322	YS	34.93	27.2	58.0	31.75	36.85	5.10	1.29E-05	
		20120518	YS	34.93	23.2	50.0	30.26	36.00	5.74	1.11E-05	
	95	20120518	YS	34.98	18.6	50.4	29.47	37.34	7.88	2.42E-05	
3314	22	20110326	YS	84.37	128.1	138.9	83.74	89.43	5.69	1.45E-04	
		20130427	US	86.06	18.5	17.4	83.53	86.48	2.95	1.81E-05	
	44	20110326	YS	86.55	3.9	5.5	85.48	87.19	1.70	1.13E-05	
		20130427	US	86.33	3.6	4.8	85.06	86.97	1.91	9.91E-06	
	95	20130427	US	85.27	3.4	6.1	83.89	87.04	3.15	2.71E-05	
	6.7		MMB			8.4				2.62E-06	
3335	6.7		MMB			7.0				2.12E-06	
3360	22	20110326	YS	66.99	5.1	3.8	66.14	67.20	1.05	6.90E-07	
	44	20110326	YS	42.18	3.8	0.8	42.18	42.18	0.21	2.94E-07	
		20121010	TN	42.40	2.9	1.2	42.18	42.40	0.21	4.25E-07	
3373	22	20110412	US	73.36	35.2	84.8	59.24	76.10	16.85	8.06E-05	
		20120521	YS	73.78	48.8	98.3	70.83	86.84	16.01	9.34E-05	

Table 4—Continued

RMS ID	Maser	Epoch (yyymmdd)	Station ^a	V_p (km s ⁻¹)	S_p (Jy)	$\int S_\nu dv$ (Jy km s ⁻¹)	V_{min} (km s ⁻¹)	V_{max} (km s ⁻¹)	V_{range} (km s ⁻¹)	L_{maser} (L_\odot)	Notes ^b	
3382	22	20110402	YS	17.86	5.3	19.6	10.27	25.02	14.75	5.41E-05		
		20120611	YS	23.12	3.9	2.4	23.12	23.54	0.42	6.60E-06		
3386	6.7		MMB			27.2				2.33E-05		
3427	22	20110402	YS	83.43	3.2	3.0	82.80	83.85	1.05	2.54E-06		
3429	22	20110415	US	41.07	265.2	477.2	35.17	49.29	14.11	1.21E-04		
		20120521	YS	41.07	200.6	370.1	33.28	49.71	16.43	9.35E-05		
3448	22	20110414	US	51.56	17.3	22.3	19.54	51.99	32.44	2.76E-05	H	
		20120520	YS	51.35	12.5	11.7	50.51	52.20	1.69	1.45E-05		
3483	22	20110331	YS	-7.94	3.0	2.1	-8.36	-6.88	1.47	5.75E-06		
		20110331	YS	-4.33	2.9	2.0	-4.33	-3.69	0.64	1.07E-05		
		20130421	YS	-4.33	4.0	1.5	-4.97	-4.33	0.64	7.94E-06		
3503	95	20130421	YS	-4.47	2.7	1.6	-5.07	-4.47	0.59	1.86E-05		
		20110414	US	65.53	63.5	136.8	30.98	68.06	37.08	9.25E-05	H	
		20120520	YS	66.38	57.1	106.4	64.27	68.69	4.42	7.19E-05		
		20110414	US	66.41	105.7	129.9	65.13	70.02	4.89	1.74E-04		
3546	22	20120520	YS	66.41	80.3	101.4	65.13	69.60	4.46	1.36E-04		
		20120520	YS	66.41	36.3	84.4	65.03	70.15	5.12	2.44E-04		
		20110416	US	58.69	9.7	23.7	40.78	68.17	27.39	1.60E-05		
3555	6.7	20120512	YS	58.06	18.4	20.7	55.32	59.53	4.21	1.40E-05		
			MMB			66.9					1.36E-05	
3580	22	20110416	US	50.90	1652.5	14673.1	-42.64	145.49	188.13	9.92E-03	H	
		20120519	YS	57.01	3623.0	10923.7	-79.93	150.75	230.68	7.39E-03	H	
		20110416	US	60.04	30.5	62.2	54.08	66.63	12.54	8.33E-05		
		20120519	YS	60.04	21.8	43.8	55.36	66.63	11.27	5.86E-05		
		20120519	YS	60.03	10.9	25.1	58.84	66.52	7.68	7.26E-05		
3585	6.7		MMB			2.9				5.66E-07		
		20110329	YS	-3.93	1.6	1.3	-5.20	-3.93	1.26	3.10E-06		
3586	22		MMB			3.9				2.71E-06		
		20110324	YS	-7.09	11.8	26.8	-8.78	4.28	13.06	5.97E-05		
		20110324	YS	6.67	4.6	9.2	2.21	6.89	4.68	4.06E-05		
3587	95	20121011	TN	6.67	4.5	6.7	2.42	6.89	4.46	2.97E-05		
		20121011	TN	6.74	2.0	3.7	4.77	7.13	2.36	3.53E-05		
		20110331	YS	-44.71	4.2	20.6	-52.51	19.54	72.05	4.14E-05	D	
3588	22	20120502	YS	10.48	6.7	21.4	-47.24	10.48	57.72	4.29E-05	H	
		20110415	US	39.65	3.4	6.5	29.54	44.07	14.54	1.36E-06		
		20130422	YS	42.18	2.6	1.4	41.97	42.18	0.21	2.97E-07		
		20110415	US	39.28	7.7	7.3	38.01	40.13	2.13	3.00E-06		
		20130422	YS	39.28	5.7	5.1	38.43	39.71	1.28	2.11E-06		
3597	6.7	20130422	YS	39.27	1.9	0.6	39.07	39.27	0.20	4.95E-07		
			MMB			52.4					3.28E-06	
3603	22		MMB			4.5				8.14E-07		
		20110416	US	0.26	1.8	0.8	0.26	0.26	0.21	1.63E-06		
3608	44	20121011	TN	3.21	6.9	4.3	2.79	3.63	0.84	8.98E-06		
		20110416	US	5.58	6.1	12.8	3.03	6.65	3.61	5.29E-05		
		20121011	TN	6.22	4.5	10.5	3.03	6.86	3.83	4.37E-05		
		20121011	TN	5.37	3.1	6.9	3.60	6.94	3.35	6.15E-05		
		20120513	YS	23.79	3.3	0.7	23.58	23.58	0.21	5.89E-08		
3611	6.7	20110415	US	21.95	19.9	21.4	18.12	22.37	4.25	3.55E-06		
		20120513	YS	21.95	16.6	16.7	19.40	26.84	7.44	2.77E-06		
		20120513	YS	21.98	13.4	14.3	20.60	22.96	2.36	5.13E-06		
3641	22		MMB			0.6				1.51E-08		
			MMB			3.6					1.56E-06	
3659	22	20110413	US	40.72	418.5	539.2	38.19	41.77	3.58	4.35E-04	H	
		20120509	YS	40.30	10.3	14.8	-95.37	72.95	168.33	1.20E-05	H	
		20110416	US	26.72	93.7	260.1	15.97	33.04	17.06	2.92E-05		
		20121011	TN	10.08	39.3	145.0	6.92	32.62	25.70	1.63E-05		
		20110416	US	22.56	20.3	18.7	20.86	23.62	2.76	4.17E-06		
3663	22	20121011	TN	22.56	19.7	16.3	21.71	24.05	2.34	3.63E-06		
		20121011	TN	22.57	14.5	15.6	20.60	23.75	3.15	7.47E-06		
			MMB			27.0					9.08E-07	
		20110412	US	28.03	25.9	40.6	24.45	38.56	14.11	4.56E-06		
		20120623	YS	25.92	13.1	24.3	24.02	41.93	17.91	2.73E-06		
3683	22	20110412	US	27.23	3.1	4.4	26.38	28.72	2.34	9.86E-07		
		20120623	YS	27.23	6.6	9.3	26.17	28.72	2.55	2.07E-06		
		20120623	YS	26.69	1.8	1.4	25.90	26.69	0.79	6.64E-07		
3683	22	20110411	US	1.94	1.7	3.2	1.94	2.78	0.84	1.66E-06		

Table 4—Continued

RMS ID	Maser	Epoch (yyymmdd)	Station ^a	V_p (km s ⁻¹)	S_p (Jy)	$\int S_\nu dv$ (Jy km s ⁻¹)	V_{\min} (km s ⁻¹)	V_{\max} (km s ⁻¹)	V_{range} (km s ⁻¹)	L_{maser} (L_\odot)	Notes ^b
3724	44	20110411	US	21.19	11.4	19.0	19.27	21.40	2.13	1.93E-05	
		20120317	YS	21.19	4.0	5.4	18.85	21.19	2.34	5.43E-06	
	95	20120317	YS	21.04	6.7	8.7	19.27	21.43	2.17	1.90E-05	
	22	20121011	TN	19.13	19.4	17.8	18.29	23.56	5.27	8.07E-07	
	44	20110414	US	0.12	12.7	9.3	-0.73	0.76	1.49	8.34E-07	
3735		20121011	TN	0.22	11.3	6.8	-0.20	0.65	0.85	6.10E-07	
	95	20121011	TN	0.08	8.0	6.8	-0.51	0.87	1.38	1.31E-06	
	22	20110413	US	14.28	4.8	3.9	14.07	15.96	1.90	1.76E-07	
3739		20130422	YS	14.07	30.0	27.2	13.22	14.91	1.69	1.24E-06	
	44	20130422	YS	9.68	1.4	0.7	9.68	9.90	0.21	5.93E-08	
	22	20110412	US	-5.60	22.8	31.1	-17.19	-3.71	13.48	1.41E-06	
3742	44	20110412	US	-3.23	11.2	18.6	-4.50	-1.74	2.76	1.67E-06	
		20120311	YS	-3.23	10.7	3.3	-3.44	-3.23	0.21	2.96E-07	
	95	20120311	YS	-3.23	13.9	24.5	-4.81	-0.08	4.73	4.76E-06	
3746	22	20110330	YS	-76.24	52.5	96.5	-92.04	-70.98	21.07	2.81E-04	
		20120318	YS	-76.24	73.3	107.0	-93.10	-70.98	22.12	3.11E-04	
	44	20110413	US	-26.59	3.6	1.4	-26.80	-26.59	0.21	3.38E-06	
3749		20130422	YS	-26.59	3.0	1.1	-26.80	-26.59	0.21	2.73E-06	
	22	20110416	US	1.66	73.3	118.8	-2.55	17.04	19.59	5.40E-06	
		20121010	TN	15.57	265.7	328.3	1.66	17.25	15.59	1.49E-05	
3761	44	20110416	US	8.88	40.1	17.1	8.46	9.31	0.85	1.54E-06	
		20121010	TN	8.88	48.0	20.5	8.46	9.31	0.85	1.84E-06	
	95	20121010	TN	8.87	38.6	21.5	8.08	9.85	1.77	4.18E-06	
3766	22	20110414	US	6.79	1.7	0.7	6.79	6.79	0.21	3.31E-08	
		20120318	YS	0.62	9.8	9.1	0.19	3.35	3.16	4.12E-07	
	22	20110416	US	-25.68	5.0	6.6	-26.53	-24.84	1.69	3.01E-07	D
3767		20120317	YS	4.23	1.2	0.3	4.02	4.02	0.21	1.16E-08	
	44	20110416	US	4.91	2.5	2.0	4.91	5.55	0.64	1.76E-07	
		20121012	TN	5.55	1.9	0.7	5.12	5.55	0.43	6.64E-08	
3775	22	20120419	YS	-70.51	9.5	8.7	-73.88	-69.03	4.85	2.23E-05	
		20110416	US	8.71	6.1	6.3	8.08	9.35	1.26	2.85E-07	
		20120318	YS	10.40	14.9	8.7	9.98	10.82	0.84	3.94E-07	
3796	22	20110323	YS	-9.18	74.9	193.1	-29.19	-3.49	25.70	4.88E-05	
		20121012	TN	-23.92	115.2	444.7	-31.51	11.26	42.77	1.12E-04	
	44	20121012	TN	-5.97	3.5	0.7	-5.97	-5.97	0.21	3.70E-07	
3816	95	20121012	TN	-6.32	2.5	1.8	-6.71	-5.92	0.79	1.95E-06	
	22	20110413	US	-4.57	8.1	8.7	-7.10	-4.15	2.95	3.95E-07	
		20120317	YS	-4.36	27.7	24.6	-6.25	-3.94	2.32	1.12E-06	
3832	22	20110415	US	-3.39	15.3	10.4	-4.02	-3.18	0.84	4.72E-07	
		20130421	YS	-2.97	34.9	30.5	-3.60	6.51	10.11	1.39E-06	
	44	20110415	US	-2.08	4.5	2.5	-2.29	-1.87	0.43	2.24E-07	
3838		20130421	YS	-2.93	3.9	3.8	-2.93	-2.08	0.85	3.46E-07	
	95	20130421	YS	-2.22	4.0	4.5	-3.00	-0.64	2.36	8.81E-07	
	22	20110411	US	10.42	3540.6	5874.2	-11.07	20.11	31.18	2.67E-04	
3841		20121010	TN	15.05	463.0	1328.3	-11.70	22.00	33.71	6.04E-05	
	44	20110411	US	8.77	12.9	27.6	6.43	10.90	4.46	2.49E-06	
		20121010	TN	8.77	13.6	23.5	6.22	10.68	4.46	2.11E-06	
3846	95	20121010	TN	8.89	6.8	22.0	5.94	12.63	6.69	4.27E-06	
	22	20110415	US	-4.53	809.4	1635.8	-10.64	31.71	42.34	7.44E-05	H
		20121012	TN	0.72	128.9	390.2	-19.93	7.04	26.97	1.77E-05	
3865	44	20110415	US	-0.01	242.9	268.2	-5.75	0.84	6.59	2.41E-05	
		20121012	TN	-0.04	218.0	248.9	-9.18	1.45	10.63	2.24E-05	
	95	20121012	TN	0.31	52.7	59.9	-5.59	0.90	6.50	1.16E-05	
3866	22	20110416	US	10.45	18.6	66.3	4.97	11.51	6.53	3.01E-06	
		20120321	YS	3.50	7.0	12.5	0.76	3.92	3.16	5.66E-07	
	44	20110416	US	-3.18	30.1	43.5	-5.52	-2.33	3.19	3.92E-06	
3878		20120321	YS	-3.18	24.5	43.1	-5.94	1.50	7.44	3.88E-06	
	95	20120321	YS	-3.24	10.8	31.7	-7.18	6.21	13.39	6.17E-06	
	22	20110411	US	28.48	6.3	19.9	-12.60	29.11	41.71	9.03E-07	
3878		20121011	TN	28.69	8.5	15.0	27.64	34.59	6.95	6.82E-07	
	44	20110411	US	10.41	252.5	157.2	9.77	11.26	1.49	1.41E-05	
		20121011	TN	10.41	236.5	149.1	9.77	11.26	1.49	1.34E-05	
3878	95	20121011	TN	10.29	146.9	100.1	9.50	12.26	2.76	1.95E-05	
	22	20110412	US	3.25	63.6	111.3	0.30	6.20	5.90	5.06E-06	
		20120317	YS	0.09	43.0	55.4	-0.96	3.25	4.21	2.52E-06	
3878	22	20110326	YS	-33.45	87.6	129.9	-38.08	-18.07	20.01	9.12E-05	

Table 4—Continued

RMS ID	Maser	Epoch (yyymmdd)	Station ^a	V_p (km s ⁻¹)	S_p (Jy)	$\int S_\nu dv$ (Jy km s ⁻¹)	V_{min} (km s ⁻¹)	V_{max} (km s ⁻¹)	V_{range} (km s ⁻¹)	L_{maser} (L_\odot)	Notes ^b
3880	22	20120310	YS	-33.66	63.7	77.8	-38.29	-16.17	22.12	5.46E-05	
		20110322	YS	-41.33	3.7	1.4	-41.54	-41.11	0.42	9.67E-07	
3894	22	20110326	YS	-87.05	10.9	16.8	-88.53	-80.73	7.79	2.95E-05	
		20130418	TN	-85.60	6.6	3.5	-85.80	-85.21	0.59	6.06E-06	
	44	20110326	YS	-85.54	9.1	4.1	-85.75	-85.33	0.43	1.42E-05	
		20130418	TN	-85.54	6.7	3.7	-87.88	-84.48	3.40	1.30E-05	
	95	20130418	TN	-85.60	6.6	3.5	-85.80	-85.21	0.59	2.59E-05	
3910	22	20110330	YS	-77.56	411.8	867.7	-99.68	-60.70	38.97	9.86E-04	
		20120419	YS	-77.14	87.4	388.6	-107.89	-64.71	43.19	4.42E-04	H
	44	20120419	YS	-68.85	2.7	1.1	-69.07	-68.85	0.21	2.50E-06	
	95	20120419	YS	-68.95	1.1	1.9	-70.52	-68.16	2.36	9.42E-06	
3911	22	20110323	YS	-75.04	6.5	6.2	-76.09	-74.61	1.47	3.86E-06	D
		20120303	YS	-65.77	3.4	1.6	-65.98	-65.34	0.63	9.85E-07	
	44	20121011	TN	-47.60	1.1	0.5	-47.60	-47.60	0.21	5.97E-07	
3914	22	20110322	YS	-40.39	3.2	4.8	-45.45	-40.18	5.27	2.80E-06	
		20120301	YS	-47.77	2.9	1.1	-47.98	-47.77	0.21	6.22E-07	
3917	22	20110322	YS	-54.54	124.9	202.8	-56.22	-40.00	16.22	1.13E-04	
		20120216	YS	-53.70	17.4	22.4	-54.33	-40.63	13.69	1.25E-05	
3935	22	20110325	YS	-85.55	7.0	8.1	-87.23	-85.12	2.11	1.33E-05	
		20120420	YS	-86.39	19.0	15.8	-92.92	-85.55	7.37	2.59E-05	
3936	22	20110326	YS	-60.22	1.8	6.0	-70.75	-60.22	10.53	9.52E-06	H
		20130429	YS	-10.08	3.2	6.0	-65.70	-9.45	56.25	9.52E-06	D
3940	22	20110326	YS	-28.76	94.4	133.7	-44.98	-27.70	17.27	4.25E-05	
		20120215	YS	-35.08	26.7	37.8	-41.40	-34.45	6.95	1.20E-05	
3945	22	20110410	US	-56.02	4.5	11.4	-67.61	-54.76	12.85	8.59E-06	
		20130430	YS	-57.29	2.8	2.8	-69.71	-57.07	12.64	2.10E-06	
3958	22	20110410	US	-96.39	11.7	25.8	-109.45	-91.75	17.70	1.11E-05	D
	44	20110410	US	-51.89	4.4	9.1	-53.17	-48.49	4.68	7.76E-06	
		20130430	YS	-51.89	4.2	7.4	-52.74	-49.34	3.40	6.31E-06	
	95	20130430	YS	-51.82	3.6	6.0	-52.80	-50.04	2.76	1.10E-05	
3963	22	20110410	US	-9.52	730.5	1548.5	-44.07	29.24	73.31	1.76E-05	H
		20121010	TN	-9.73	1084.3	2754.7	-41.12	31.14	72.26	3.13E-05	H
	44	20110410	US	-13.07	5.8	4.0	-13.70	-11.58	2.13	8.97E-08	
		20121010	TN	-13.07	6.1	2.6	-13.28	-13.07	0.21	5.75E-08	
	95	20121010	TN	-10.34	1.6	3.4	-11.91	-9.55	2.36	1.64E-07	
3968	22	20110322	YS	-49.85	57.0	51.8	-50.48	-48.80	1.69	2.22E-05	
		20120303	YS	-49.85	70.3	47.2	-50.48	-26.47	24.02	2.02E-05	
3970	22	20110410	US	-52.83	3.7	2.5	-53.25	-52.62	0.63	9.35E-07	
		20120316	YS	-47.77	2.5	4.5	-54.30	-47.56	6.74	1.67E-06	
3972	22	20110410	US	-60.96	78.1	209.6	-69.81	-50.00	19.80	9.84E-05	
		20120310	YS	-55.27	25.1	84.7	-66.22	-50.00	16.22	3.98E-05	
3976	22	20110403	YS	-54.89	3.9	22.9	-73.43	-31.51	41.92	9.81E-06	
		20120311	YS	-57.42	34.3	50.1	-62.90	-38.04	24.86	2.15E-05	
	44	20110403	YS	-54.43	25.7	15.3	-54.85	-53.79	1.06	1.30E-05	
		20120311	YS	-54.43	13.7	5.5	-54.64	-54.43	0.21	4.65E-06	
	95	20120311	YS	-54.50	7.1	3.8	-54.70	-53.91	0.79	6.90E-06	
3980	22	20110323	YS	-75.17	19.2	57.8	-78.33	-51.57	26.75	9.07E-06	
		20121012	TN	-58.11	6.4	13.9	-70.32	-57.89	12.43	2.18E-06	
3982	22	20110403	YS	-56.66	30.5	186.0	-78.57	-35.60	42.98	2.92E-05	H
		20120216	YS	-54.35	37.5	173.2	-76.68	-7.58	69.10	2.72E-05	
	44	20110403	YS	-57.24	41.9	91.3	-59.37	-51.93	7.44	2.83E-05	
		20120216	YS	-57.24	26.0	53.1	-57.88	-52.99	4.89	1.65E-05	
	95	20120216	YS	-53.49	10.9	41.4	-58.61	-52.90	5.71	2.77E-05	
3985	22	20110403	YS	-48.18	8.9	5.3	-48.60	-47.97	0.63	8.27E-07	
		20120216	YS	-48.39	6.6	4.3	-48.60	-47.97	0.63	6.82E-07	
3986	22	20110323	YS	-72.26	114.4	250.9	-77.53	-49.72	27.81	3.93E-05	
		20121012	TN	-69.95	123.5	127.7	-72.47	-53.51	18.96	2.00E-05	
	44	20110323	YS	-57.68	15.5	18.1	-58.32	-55.98	2.34	5.62E-06	
		20121012	TN	-57.68	12.7	18.3	-58.32	-55.76	2.55	5.69E-06	
	95	20121012	TN	-57.62	12.9	18.6	-58.60	-55.26	3.35	1.24E-05	
3991	22	20110403	YS	-93.47	5.0	8.1	-93.68	-39.75	53.93	1.27E-06	H
		20121011	TN	-50.70	7.8	19.7	-51.75	-39.33	12.43	3.09E-06	
3992	22	20110322	YS	-43.36	5.0	2.6	-43.78	-43.15	0.63	7.30E-07	
		20120612	YS	-44.21	9.6	11.9	-46.52	-43.78	2.74	3.39E-06	
3996	22	20110331	YS	-47.12	90.4	108.6	-53.02	-39.33	13.69	3.09E-05	
		20130430	YS	-47.12	33.9	59.7	-58.50	-39.96	18.54	1.70E-05	

Table 4—Continued

RMS ID	Maser	Epoch (yyymmdd)	Station ^a	V_p (km s ⁻¹)	S_p (Jy)	$\int S_\nu dv$ (Jy km s ⁻¹)	V_{\min} (km s ⁻¹)	V_{\max} (km s ⁻¹)	V_{range} (km s ⁻¹)	L_{maser} (L_\odot)	Notes ^b
3998	44	20110331	YS	-45.82	2.8	3.9	-45.82	-44.12	1.70	2.19E-06	
		20130430	YS	-45.60	1.3	1.1	-45.60	-45.39	0.21	6.00E-07	
	95	20130430	YS	-44.53	2.2	3.9	-46.50	-43.94	2.56	4.78E-06	
	22	20110322	YS	-53.24	32.6	60.3	-54.29	-41.87	12.43	2.71E-05	
		20121010	TN	-51.35	54.0	85.0	-60.40	-50.08	10.32	3.82E-05	
4365	44	20110322	YS	-52.75	6.9	5.4	-54.88	-52.54	2.34	4.77E-06	
		20121010	TN	-52.75	5.5	4.3	-54.88	-52.54	2.34	3.84E-06	
	95	20121010	TN	-54.82	4.2	3.5	-54.82	-52.46	2.36	6.68E-06	
	22	20110325	YS	79.31	0.8	1.9	77.62	79.31	1.69	9.67E-07	
		20120613	YS	73.41	9.0	8.5	73.20	78.89	5.69	4.37E-06	
4745	44	20110325	YS	79.77	5.7	8.9	78.28	81.47	3.19	9.05E-06	
		20120613	YS	79.98	5.0	9.3	78.28	82.11	3.83	9.42E-06	
	95	20120613	YS	79.89	2.8	1.8	79.50	79.89	0.39	3.88E-06	
	22	20110326	YS	-19.89	238.7	331.0	-21.99	-15.04	6.95	3.07E-05	
		20120303	YS	-21.78	123.4	222.6	-22.63	-14.62	8.01	2.07E-05	
4747	44	20110326	YS	-16.68	29.2	33.6	-19.23	-14.55	4.68	6.18E-06	
		20120303	YS	-16.68	31.2	32.3	-18.80	-14.98	3.83	5.94E-06	
	95	20120303	YS	-16.82	19.6	23.5	-18.78	-14.65	4.13	9.32E-06	
	22	20110329	YS	-10.98	40.4	21.6	-11.61	-10.56	1.05	2.01E-06	
		20120303	YS	-10.98	14.2	6.9	-11.40	-10.77	0.63	6.38E-07	
4888	44	20110329	YS	-10.30	6.4	2.5	-10.52	-10.09	0.43	4.63E-07	
		20120303	YS	-10.30	8.2	3.2	-10.30	-10.09	0.21	5.89E-07	
	95	20120303	YS	-10.21	6.7	4.1	-10.80	-10.02	0.79	1.61E-06	
	22	20110322	YS	33.46	52.2	98.0	8.18	47.79	39.61	2.48E-05	H
		20120605	YS	34.51	38.6	169.5	13.45	62.32	48.88	4.28E-05	H
4910	44	20110322	YS	43.62	31.0	50.9	41.28	45.32	4.04	2.54E-05	
		20120605	YS	43.62	31.9	44.9	42.56	44.90	2.34	2.25E-05	
	95	20120605	YS	43.09	64.8	117.6	41.12	46.04	4.92	1.27E-04	
	22	20120619	YS	71.77	3.9	2.7	71.56	71.99	0.42	1.48E-06	
	44	20120619	YS	76.87	1.9	0.8	76.87	76.87	0.21	9.07E-07	
4924	6.7		MMB			23.8				3.97E-06	
	44	20110410	US	66.38	3.7	4.4	65.32	66.81	1.49	3.73E-06	
		20120607	YS	66.60	2.5	4.9	64.05	66.60	2.55	4.14E-06	
4941	95	20120607	YS	66.37	5.7	3.2	65.58	66.37	0.79	5.95E-06	
	22	20110411	US	35.77	4.4	3.8	34.93	35.77	0.84	4.26E-07	
		20130422	YS	36.82	10.2	18.9	35.14	40.40	5.27	2.12E-06	
	44	20110411	US	35.20	8.1	2.9	34.98	35.20	0.21	6.43E-07	
		20130422	YS	35.20	4.7	1.6	34.98	35.20	0.21	3.54E-07	
	95	20130422	YS	35.16	2.8	3.7	33.78	35.36	1.58	1.77E-06	

^aYS, US, and TN are the KVN Yonsei, Ulsan, and Tamna stations, respectively. MMB is the MMB survey of 6.7 GHz class II CH₃OH masers.

^bD: H₂O maser with a dominant shifted feature at that epoch, H: presence of H₂O maser emission with high-velocity(>30 km s⁻¹) component

Table 5. Statistics of Maser Line Parameters

Maser	Number	S_p (Jy)				V_{rel} (km s $^{-1}$)				V_{range} (km s $^{-1}$)			
		mean	median	min	max	mean	median	min	max	mean	median	min	max
1st Epoch													
22	126	156.6 \pm 525.5	13.5	0.8	3540.6	-3.73 \pm 18.63	-0.93	-94.33	78.47	17.37 \pm 24.21	12.01	0.21	188.13
44	76	24.9 \pm 46.0	9.1	1.2	252.5	0.02 \pm 1.05	-0.05	-2.39	3.59	2.92 \pm 2.60	2.34	0.21	15.52
2nd Epoch													
22	112	144.4 \pm 563.6	17.2	1.2	4552.1	-2.69 \pm 20.05	-0.11	-92.86	79.11	19.70 \pm 32.59	9.69	0.21	230.68
44	81	21.5 \pm 41.6	6.7	1.1	236.5	0.05 \pm 1.06	-0.05	-2.39	3.56	2.54 \pm 2.41	2.13	0.21	11.27
95	68	16.2 \pm 25.0	6.7	1.1	146.9	0.09 \pm 1.08	-0.02	-2.39	3.91	2.96 \pm 2.31	2.36	0.20	13.39
Either Epoch													
22	135	150.9 \pm 542.6	15.5	0.8	4552.1	-3.24 \pm 19.28	-0.89	-94.33	79.11	18.46 \pm 28.42	9.90	0.21	230.68
44	83	23.1 \pm 43.7	7.0	1.1	252.5	0.03 \pm 1.05	-0.05	-2.39	3.59	2.72 \pm 2.50	2.34	0.21	15.52
95	68	16.2 \pm 25.0	6.7	1.1	146.9	0.09 \pm 1.08	-0.02	-2.39	3.91	2.96 \pm 2.31	2.36	0.20	13.39
MMB Survey Area													
2nd Epoch													
22	54	130.3 \pm 506.1	15.8	2.6	3623.0	-7.52 \pm 19.65	-1.70	-92.86	7.90	25.47 \pm 42.98	10.95	0.21	230.68
44	51	13.1 \pm 16.5	6.4	1.9	80.3	0.13 \pm 1.00	0.03	-2.39	2.87	2.73 \pm 2.26	2.34	0.21	11.27
95	45	12.3 \pm 14.7	6.4	1.1	64.8	0.04 \pm 1.02	0.03	-2.39	2.94	2.80 \pm 2.06	2.56	0.20	7.88
6.7	38	48.7 \pm 90.2	18.6	0.9	517.3	-0.40 \pm 4.70	-0.90	-12.00	7.70	7.80 \pm 4.72	6.80	0.90	17.00

Note. — Upper : Maser sources for KVN observations
 Lower : Maser sources combining the current work with 6.7 GHz in an region covered with MMB survey

Table 6. Dominant Shifted H₂O Maser Source Candidates

RMS ID	¹³ CO ^a J=1-0	HCO ⁺ ^a J=1-0	Note ^b
145	n	–	R
2547	n	–	B
2584	n	–	B
2716	y	y	N
3158	y	n	B
3360	y	y	N
3587	n	–	B
3766	n	–	B
3911	n	–	B
3936	n ^c	–	R
3958	n	–	B

^aThe presence of molecular line emission associated with the dominant blue- or redshifted H₂O maser feature candidates.

^bB: dominant blueshifted, R: dominant redshifted, N: no dominant maser emission

^cThe ¹³CO J=2-1 line data from the JCMT archives.